



Vinyl-Ester (VE) Cure Characterization Via Direct Current Sensors

by Bruce K. Fink, Mahendra B. Dorairaj, and
John W. Gillespie, Jr.

ARL-TR-2441

March 2001

Approved for public release; distribution is unlimited.

20010404 108

The findings in this report are not to be construed as an official Department of the Army position unless so designated by other authorized documents.

Citation of manufacturer's or trade names does not constitute an official endorsement or approval of the use thereof.

Destroy this report when it is no longer needed. Do not return it to the originator.

Army Research Laboratory

Aberdeen Proving Ground, MD 21005-5069

ARL-TR-2441

March 2001

Vinyl-Ester (VE) Cure Characterization Via Direct Current Sensors

Bruce K. Fink

Weapons and Materials Research Directorate, ARL

Mahendra B. Dorairaj and John W. Gillespie, Jr.

University of Delaware

Approved for public release; distribution is unlimited.

Abstract

High-performance thermosetting composites typically consist of a high-modulus fibrous material embedded in a thermosetting polymer matrix. The behavior of the resulting composite depends on the properties of the reinforcement, the interphase, and the matrix. Vinyl-ester (VE) resins are relatively low-cost matrix resins used in liquid molding of large structures such as contiguous vehicle hulls. In liquid-molding processes, quality-control sensors can ensure resin impregnation of the preform and cure of the resin after infiltration. For these purposes, SMARTweave (SW), based on direct current (DC) sensing, is used as an in-situ flow-front detection and cure-monitoring system. SW measures change in the ionic conductivity with cure, which can then be related to the material properties like viscosity and degree of cure. This enables in-situ measurement of degree of cure and viscosity development during cure from SW measurements. This report builds on previous modeling work that assumed a direct dependence of DC resistance on the resin viscosity, limiting the use of such models beyond gelation. This report presents a continuum model based on free volume theory to describe ionic conductivity through gelation to vitrification.

Contents

List of Figures	vii
List of Tables	xi
1. Introduction and Background	1
1.1 Motivation.....	1
1.2 Objectives	1
1.3 The SMARTweave System.....	2
1.4 Previous Work on Ionic Conductivity Modeling.....	6
1.4.1 Review of England's Model [4]	7
1.4.2 The Need for a Continuum Model.....	9
1.5 Report Overview.....	9
1.6 Section Summary	13
2. Experimental Methods	14
2.1 Introduction	14
2.2 Materials.....	14
2.2.1 Background on VE Resins	14
2.2.1.1 VE Resin Systems	14
2.2.1.2 Free Radical Chain Growth Copolymerization.....	15
2.2.2 Resin Compositions	17
2.3 Viscosity Experiments.....	17
2.3.1 Sample Preparation.....	17
2.3.2 Instrumentation.....	18
2.4 SW Experiments.....	18
2.5 Dielectric Cure Monitoring.....	20
2.6 FTIR Experiments	21
2.6.1 Instrumentation and Sample Preparation	21
2.6.2 IR Spectra of VE.....	22
2.7 DSC Experiments.....	23

2.8	DMA Experiments	25
2.9	Liquid Chromatography	25
2.9.1	Sample Preparation	26
2.9.2	HPLC Instrumentation	26
2.10	Atomic Force Microscopy (AFM)	26
2.10.1	Background	27
2.10.2	Instrumentation and Sample Preparation	28
2.11	Section Summary	28
3.	Cure Kinetics of VE Resins	30
3.1	Introduction	30
3.2	Cure Kinetics Using FTIR	30
3.3	Effect of Styrene Concentration	32
3.4	Effect of Temperature	34
3.5	Autocatalytic Kinetics Model Parameters	36
3.6	Section Summary	36
4.	Cure Monitoring of VE Resin	38
4.1	Introduction	38
4.2	SW Cure Data	38
4.2.1	Effect of Styrene	38
4.2.2	Effect of Temperature	42
4.3	Dielectric Cure Monitoring	43
4.3.1	Effect of Styrene	44
4.3.2	Effect of Temperature	46
4.4	Section Summary	46
5.	Characterization of Microgels	50
5.1	Introduction	50
5.2	Background	51
5.3	Results	52
5.3.1	Comparison of Microgel Growth Kinetics with SW Data	52
5.3.2	Separation of Microgels	54
5.3.3	AFM Analysis of Microgels	57

5.4	Percolation Model.....	57
5.4.1	Modeling Approach.....	59
5.4.2	Percolation-Based Continuum Model	61
5.4.2.1	Conductivity Model	61
5.4.2.2	Viscosity Model	63
5.5	Summary	64
6.	Mathematical Model of the Ionic Conductivity Behavior	65
6.1	Introduction	65
6.2	Free Volume Model	66
6.2.1	Background.....	66
6.2.2	Theory	67
6.2.3	Conductivity Model.....	68
6.2.4	Viscosity Model.....	71
6.3	Predictive Capability of the Free Volume Model.....	75
6.3.1	Conductivity Model.....	77
6.3.2	Viscosity Model.....	77
6.4	Section Summary	79
7.	Conclusions and Future Work	80
7.1	Introduction	80
7.2	Conclusions.....	80
7.3	Summary of Free Volume Methodology	81
7.4	Recommendations for Further Research.....	82
7.4.1	Fundamental Understanding of T_g - α Relationship	82
7.4.2	Positron Annihilation Studies	82
8.	References	83
Appendix A.	Dielectric Cure Monitoring	89
A.1	Basis of Dielectric Behavior.....	89
A.2	Dielectric Measurements for On-line Cure Monitoring.....	90
A.2.1	Ionic Resistivity	90
A.2.2	Dielectric Constant and Dielectric Loss.....	91

Appendix B. Calculation of the Volume Fraction of Microgels	93
Appendix C. Determination of L/A Ratio of Single Node Test Cell (SNTC)-3	95
Appendix D. Doping Results	99
D.1 Introduction	99
D.2 Cure Monitoring	99
D.3 Cure Kinetics	100
Appendix E. Percolation Model	103
E.1 Introduction	103
E.2 Theory	103
E.3 Percolation and Conduction	105
E.4 Evidence of Percolation in VE system	106
Appendix F. Analyzing Diffusion in the Pregel and Postgel Stage	109
F.1 Pregel Stage	109
F.2 Postgel Stage	110
Appendix G. Differential Scanning Calorimeter (DSC)-Based Free Volume Modeling	113
G.1 Introduction	113
G.2 Cure Kinetic Model	113
G.3 T_g - α Model	113
G.4 Conductivity Model	114
G.5 Viscosity Model	114
Distribution List	119
Report Documentation Page	139

List of Figures

Figure 1. Schematic illustration of an SW system and its components.....	3
Figure 2. SW system in operation.	3
Figure 3. Experimental setup of SW sensors.....	4
Figure 4. Circuit diagram of a single node cell.	5
Figure 5. Typical SW signal of a curing resin mixture.	6
Figure 6. Schematic representation of England's model [4].....	8
Figure 7. Schematic of continuum model.....	11
Figure 8. Chemical structure of VE and styrene monomers.	16
Figure 9. Schematic illustration of a Brookfield viscometer and small sample adapter.....	19
Figure 10. Typical viscosity profile of a curing VE resin.....	19
Figure 11. SNTC-3 single node test cell.	20
Figure 12. Typical dielectric signal of a curing VE sample.	21
Figure 13. FTIR experimental setup.....	22
Figure 14. FTIR spectra of VE825 at the beginning of cure at 40 °C cure temperature.....	23
Figure 15. Degree of conversion of VE 411-C-50 at 30 °C as obtained from PIRSA.....	24
Figure 16. Schematic illustration of DMA setup.....	25
Figure 17. Schematic illustration of HPLC experimental setup.....	27
Figure 18. AFM micrograph of microgels in VE 411-C-50 at a cure temperature of 70 °C [21].	28
Figure 19. Block diagram for tapping mode operation.	29
Figure 20. Typical profiles of VE and styrene double-bond conversion.....	31
Figure 21. Fractional conversion of VE double bonds in Derakane 441-400 cured at 40 °C.	33
Figure 22. Fractional conversion of styrene double bond in Derakane 441-400 cured at 40 °C.....	33
Figure 23. Fractional conversion of VE double bonds in Derakane 411-C-50 cured at isothermal temperatures of 30°, 40°, and 50 °C.	35

Figure 24. Fractional conversion of styrene double bonds in Derakane 411-C-50 cured at isothermal temperatures of 30°, 40°, and 50 °C.....	35
Figure 25. SW behavior of Derakane 441-440 cured at 40 °C.....	40
Figure 26. Initial DC signal vs. styrene concentration in Derakane 441-400.	40
Figure 27. Initial viscosity vs. styrene concentration in Derakane 441-400.	41
Figure 28. Viscosity development in Derakane 441-400 cured at 40 °C.....	41
Figure 29. Fractional double-bond conversion vs. styrene concentration in Derakane 441-400 at DC signal cutoff.	42
Figure 30. Glass transition temperature vs. styrene concentration for Derakane 441-400 resin.....	43
Figure 31. SW signal vs. time for Derakane 411-C-50 at different isothermal cure temperatures.....	43
Figure 32. Viscosity development in Derakane 411-C-50 at different isothermal cure temperatures.....	44
Figure 33. Effect of styrene on Derakane 441-400 cured at 40 °C using dielectric cure monitoring at (a) 28 weight-percent styrene, and (b) 47 weight-percent styrene concentration.....	45
Figure 34. Dielectric cure monitoring of Derakane 411-C-50 at isothermal temperatures of (a) 30°, (b) 40°, and (c) 50 °C.....	47
Figure 35. Ionic conductivity from dielectric measurements on Derakane 411-C-50 at 30 °C isothermal cure temperature.....	48
Figure 36. Comparison of SW behavior of ionic conductivity with dielectric behavior of Derakane 411-C-50 at 30 °C cure temperature.	48
Figure 37. Illustration of cross-linking polymerization (a) at beginning, (b) initiation, (c) reaction in progress, and (d) possible gelation schemes.	52
Figure 38. Influence of microgels on SW behavior of 411-C-50 for (a) 30° and (b) 40 °C, respectively.....	53
Figure 39. DLS data showing influence of microgels on SW response of 441-400 at (a) 28% and (b) 57% styrene.	54
Figure 40. HPLC response (in μ V) of pure styrene.....	55
Figure 41. HPLC response (in μ V) of pure unreacted VE825 with 28 weight-percent styrene.....	55
Figure 42. HPLC response (in μ V) of fractionated microgels.	56
Figure 43. FTIR spectra of VE825 (a) at the beginning of cure and (b) at 9 min at 40 °C cure temperature.....	56
Figure 44. FTIR spectra of fractionated microgels formed in the first 9 min of isothermal cure of VE825 at 40 °C.	57

Figure 45. AFM pictures of microgels as observed on a fractured surface of 411-C-50 sample cured at an isothermal temperature of 40 °C.	58
Figure 46. AFM pictures of microgels as observed on a fractured surface of 411-C-50 sample cured at an isothermal temperature of 50 °C.	58
Figure 47. 2-D percolation behavior of a continuous conducting medium [41].	60
Figure 48. 2-D percolation behavior modeling using resistor network [40].	60
Figure 49. 3-D percolation modeling using non-zero resistor values [35].	60
Figure 50. Development of resistor network model for curing VE resin at (a) time $t=0$, (b) time $t=t_1$, and (c) time $t=SW$ cutoff. The left side illustrates different stages of cure and the right side illustrates equivalent resistor network.	61
Figure 51. Normalized DC signal vs. microgel volume fraction of Derakane 411-D-50 at different isothermal cure temperatures.	62
Figure 52. Normalized DC signal vs. microgel volume fraction of Derakane 441-400 at different styrene concentrations.	62
Figure 53. Experimental vs. theoretical fluidity of Derakane 411-C-50 at isothermal cure temperature of 30 °C.	64
Figure 54. SW behavior prediction using free volume theory at 30 °C. (Degree of conversion obtained using FTIR.)	71
Figure 55. SW behavior prediction using free volume theory at 40 °C. (Degree of conversion obtained using FTIR.)	71
Figure 56. Viscosity prediction using free volume theory at 30 °C. (Degree of conversion obtained using FTIR.)	72
Figure 57. Viscosity prediction using free volume theory at 40 °C. (Degree of conversion obtained using FTIR.)	73
Figure 58. Schematic of viscosity and cure sensing using SMARTweave signal as the model input.	73
Figure 59. T_g (K) development with cure time as predicted by the free volume model.	74
Figure 60. Degree of cure prediction from SW data at 30 °C using free volume theory.	74
Figure 61. Degree of cure prediction from SW data at 40 °C using free volume theory.	75
Figure 62. Effect of deviation of ionic conductivity on degree of cure prediction from the free volume model at 40 °C for 411-C-50.	76
Figure 63. Effect of deviation of ionic conductivity on viscosity prediction from the free volume model at 40 °C for 411-C-50.	76

Figure 64. Free volume modeling of ionic conductivity using average WLF parameters.....	78
Figure 65. Free volume modeling of viscosity using average WLF parameters.....	78
Figure C-1. SNTC-3 single node test cell.....	95
Figure C-2. Circuit diagram of a single node cell.....	96
Figure C-3. Experimental cell for conductivity studies.....	96
Figure D-1. Comparison of SW response of TI-doped 411-C-50 against TA- doped and undoped 411-C-50 at an isothermal cure temperature of 40 °C.....	100
Figure D-2. SW response of undoped 411-C-50 at an isothermal cure temperature of 40 °C.....	100
Figure D-3. Degree of conversion comparison between doped and undoped resin at 40 °C isothermal cure temperature.....	101
Figure E-1. Illustration of increasing volume contribution of the microgels with cure.....	104
Figure E-2. Normalized DC signal vs. microgel volume fraction of Derakane 411-C-50 at different isothermal cure temperatures.....	106
Figure E-3. Normalized DC signal vs. microgel volume fraction of Derakane 411-C-50 at different isothermal cure temperatures.....	107
Figure G-2. SMARTweave (SW) behavior prediction using free volume theory at 30 °C.....	115
Figure G-3. SW behavior prediction using free volume theory at 40 °C.....	115
Figure G-4. Viscosity prediction using free volume theory at 30 °C.....	116
Figure G-5. Viscosity prediction using free volume theory at 40 °C.....	116
Figure G-6. Schematic of viscosity and cure sensing using SW signal as the model input.....	117
Figure G-7. Degree of cure prediction from SW data using free volume theory at 30 °C.....	117
Figure G-8. Degree of cure prediction from SW data using free volume theory at 40 °C.....	118

List of Tables

Table 1. List of compositions of the reacting resin mixture used in this study.	12
Table 2. Autocatalytic parameters for the degree of conversion as observed using DSC.....	24
Table 3. Tapping mode specifications.	29
Table 4. Kinetic parameters corresponding to VE 411-C-50 FTIR data.....	37
Table 5. Autocatalytic parameters for FTIR data of VE 441-400 cured at 40 °C. ...	37
Table 6. DMA results for Derakane 411-C-50.....	44
Table 7. Maximum conversion of 411-C-50 from DC and AC cure monitoring....	49
Table 8. Maximum conversion of 441-400 from DC and AC cure monitoring.....	49
Table 9. T_g - α model parameters for 411-C-50 corresponding to DSC.	69
Table 10. T_g - α parameters for Venditti's relationship for 411-C-50 corresponding to FTIR.....	70
Table 11. WLF Parameters for conductivity model.....	70
Table 12. WLF parameters for viscosity modeling.....	72
 Table E-1. Percolation thresholds.....	 105
 Table G-1. T_g - α model parameters.....	 113
Table G-2. WLF parameters for conductivity model.....	114
Table G-3. WLF parameters for viscosity modeling.....	116

INTENTIONALLY LEFT BLANK.

1. Introduction and Background

1.1 Motivation

High-performance thermosetting composite materials typically consist of a high-modulus fibrous-reinforcing material embedded in a thermosetting polymer matrix. The behavior of the resulting composite depends on the properties of the reinforcement, interphase, and the matrix [1]. Vinyl-ester (VE) resins are one of the most important matrix resins used in liquid-molding processes such as resin-transfer molding (RTM), vacuum-assisted RTM (VARTM), and Seemann's composite resin-infusion molding process (SCRIMP) [2]. These processes have proven to be cost-effective methods for room temperature near net-shape manufacturing of large composite structures for naval, infrastructure, and military systems. Consequently, there is an increased demand to improve the quality and to further reduce the cost of manufacturing. In liquid molding processes, quality control requires sensors to ensure resin impregnation of the preform and cure of resin after infiltration. To address these needs, research laboratories have begun to develop and refine new sensor technologies for flow and cure monitoring. In this work, the focus is on the study of neat VE resin using two such monitoring systems. One is based on direct current (DC) sensing known as SMARTweave (SW). SW is a patented system developed jointly by the U.S. Army Research Laboratory (ARL) and the University of Delaware Center for Composite Materials (UD-CCM). The other method is the more commonly used dielectric monitoring, which is based on alternating current (AC). A structured attempt is made to study the various parameters relevant to cure kinetics and to obtain an insight into the structure of cured VE resins. This work also attempts to model, characterize, and relate ionic conductivity, viscosity and degree of cure to sensor response.

1.2 Objectives

The purpose of this research is to investigate how the SW signal can be utilized to in-situ monitor the viscosity and cure of a reacting polymer. Previous studies toward this direction have been successful only up to the gel point of the resin [3, 4]. A primary reason is limitation due to these models' assumed dependence of ionic conductivity on the macroscopic viscosity. This poses problems since the macroscopic viscosity rapidly increases to infinity at gelation. However, the ionic mobility continues resulting in continuation of an observed SW signal. This necessitates the use of a different model, one that does not exhibit a direct dependency on the macroscopic viscosity. Another concern specific to VE resin systems is that there is an offset between the time when the viscosity reaches a

minima and when the ionic conductivity reaches a maximum, thereby introducing inaccuracies in the previous models adopted for VE.

The objectives of this work are to:

- Develop a theoretical understanding of the ionic conductivity of the reacting VE resins, based on the molecular events such as network formation, homopolymerization of the individual monomers, and molecular mobility.
- Develop a continuum model for ionic conductivity that extends through gelation to vitrification.
- Monitor viscosity and degree of conversion in composite liquid molding processes as a function of ionic conductivity using DC-based sensors.

1.3 The SMARTweave System

SMARTweave (Sensors Mounted as Roving Threads) (SW) was developed and patented in 1990 by ARL [3] as a flow front detection system and is well suited for use in conjunction with liquid molding processes. Figure 1 shows the basic components of an SW system, while Figure 2 shows an actual photograph of the system in operation. The flow front is obtained by sensing the changes in DC conductivity of the overlapping grid of insulated conductors embedded in the preform prior to injection molding as shown in Figure 3. One set of the grid serves as the excitation leads and the orthogonal set laid out in the parallel plane serves as the sense leads. The presence of resin at a node is detected by the step change in conductivity upon resin arrival. Continued monitoring of the conductivity provides information about the cure behavior of the resin at a point. SW offers a specific advantage over the conventional alternating current sensors by allowing for use of a large array of sensors in multiple planes (multiplexing) enabling a three-dimensional (3-D) visualization of flow fronts and cure from the DC signal.

The underlying principle behind the SW system is that when a resin is injected into the preform carrying the SW sensors, the resin acts as the conducting medium between the sensors. Therefore, the signal obtained from the SW sensor is sensitive to the resin conductivity providing insight into the material properties that affect the ionic conductivity. Owing to its low conductivity, the resin acts as a resistor and, under an applied voltage, current is induced in a circuit containing a sense resistor (R_s). Prior to the arrival of the resin between the sensing grids, the resistance between them is infinite. Upon the infiltration of the resin between the sensing planes, a step change in resistance to a finite value occurs. Subsequent data reduction enables flow visualization and the identification of defects such as dry spots. The distribution of the orthogonal sets of sensing and excitation leads ensures that defects do not exceed the area of

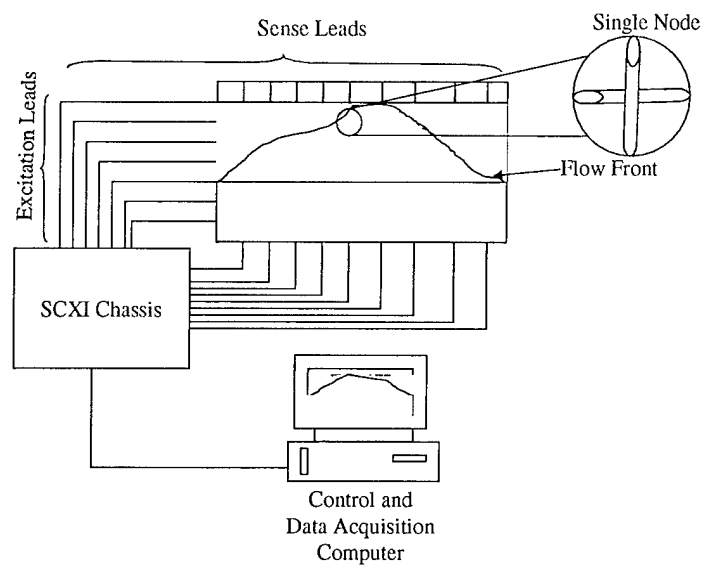


Figure 1. Schematic illustration of an SW system and its components.

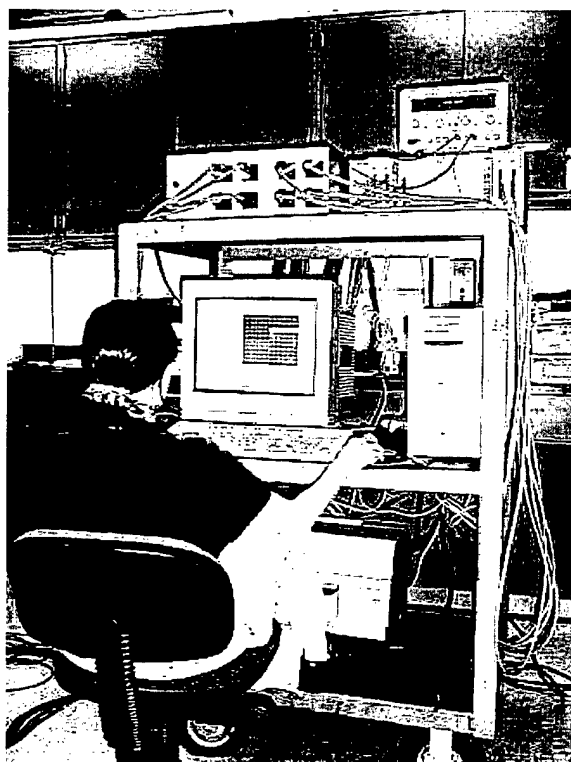


Figure 2. SW system in operation.

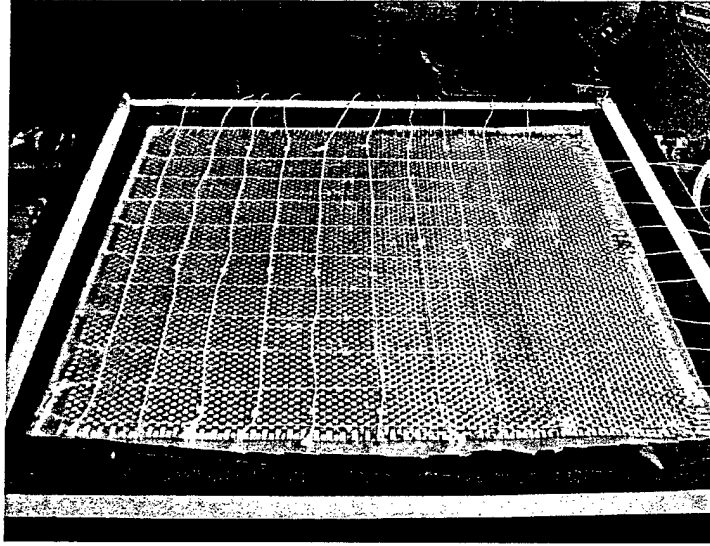


Figure 3. Experimental setup of SW sensors.

individual squares formed by the sensor grid. One can customize and design the placement of these sensor grids to ensure that the maximum defect size is less than the actual defect size permissible for a specific application. SW can become an integral part of quality assurance/quality control for flow and cure monitoring and defect detection for VARTM parts.

The SW system used in this study represents a fourth generation system developed at the University of Delaware. The system basically consists of a National Instruments SCXI chassis and multiplexer and a computer for data storage and display. A voltage difference of 10 V is applied between the excitation and the sense leads. The present system is capable of monitoring 64×64 single nodes. Only one excitation lead is active at any point of time and the SCXI chassis monitors the sense leads for the induced current. Figure 4 shows a schematic circuit diagram of a SW at the point of crossover between an excitation lead and a sense lead. For the single node experiments performed in this study, a 10 V applied voltage and a $10 \text{ M}\Omega$ sense resistor, R_s , were typically used. The measured voltage, $V_m(t)$, and sense resistance can be used to calculate the junction resistance, $R_j(t)$, by:

$$R_j(t) = (10/V_m(t))R_s - R_s \quad (1)$$

and

$$\sigma = L/(R_j(t)A), \quad (2)$$

where σ is the ionic conductivity, L is the separation distance between the electrodes, and A is the area of the electrodes available for ionic conduction.

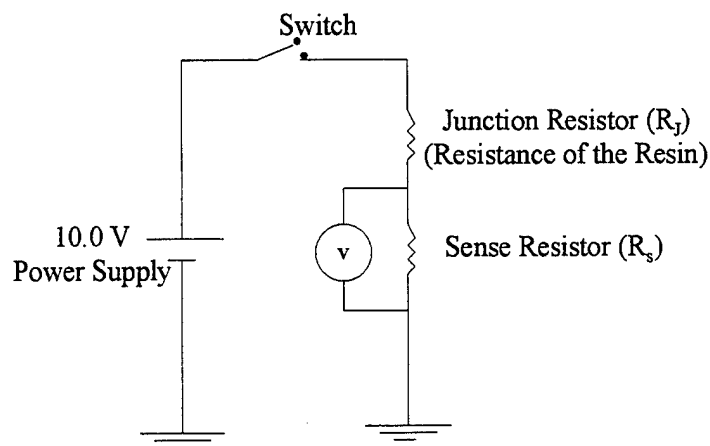


Figure 4. Circuit diagram of a single node cell.

The junction resistance is the resistance of the resin infiltrating the fiber preform. During a test run, in the presence of the resin between the sense plane and the excitation plane, a voltage is created across R_s . Changes in $R_j(t)$ are then recorded as changes in $V_m(t)$ by the SW National Instruments-based Labview software. A detailed explanation of the working of SW and its application to commercial projects is discussed elsewhere [4]. A typical SW signal obtained during a single node test is shown in Figure 5. Point A corresponds to the point along the time scale when the resin reaches the node under consideration. Following the arrival of the resin, the junction resistance undergoes a step change from a value of infinity to a finite value as marked by the point B. The region between points B and C is when the reaction starts to occur. As the reaction proceeds, the exothermic nature of the reaction increases the local temperature, forcing resin viscosity to decrease, resulting in the increase in the DC signal between point C and D. Subsequently, the viscosity of the resin continues to increase due to cross linking and network formation. This forces the viscosity to rapidly increase to infinity corresponding to the onset of gelation. This phenomenon is reflected on the DC signal as a pronounced decrease in the observed voltage value represented by the curves inflection at point E. The reactive mixture eventually reaches a glassy state (vitrification) thereby severely restricting molecular mobility at point F. Vitrification is said to have occurred when the glass transition temperature, T_g , equals the cure temperature, T . This results in the DC signal tapering off to zero, represented by point G. This is designated as the "cutoff point" for the sensor.

SW vs. Dielectric Cure Monitoring. One of the widely used online cure monitoring methods is AC sensing or dielectric cure monitoring. A comprehensive review of AC sensing is presented in Appendix A. Dielectric cure monitoring presents multiple problems in the areas of isolating ionic

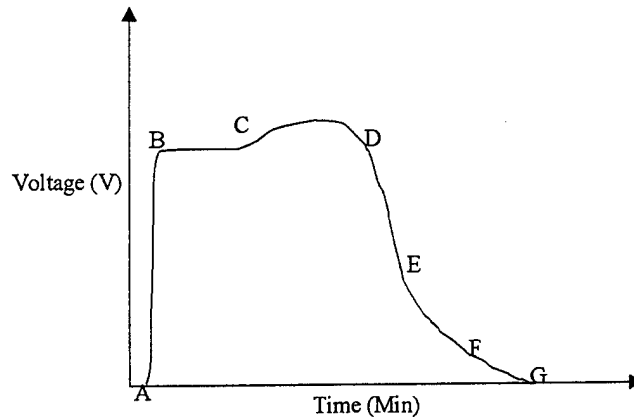


Figure 5. Typical SW signal of a curing resin mixture.

conductivity from dipolar contributions and obtaining relaxation time and experimental results in the right set of frequencies.

The mathematical steps involved in extracting ionic conductivity are cumbersome and involves numerous approximations, limiting its use. Dielectric sensors are point sensors, providing information at specific locations in the parts. The cost of dielectric sensors can be prohibitive for monitoring a large number of locations during processing.

SW, on the other hand, offers a simpler yet effective alternative to dielectric cure monitoring. The DC signal obtained from SW provides a reliable representation of the ionic conductivity without any intermediate computational steps involved. SW offers the advantage of cost-effective multiplexing with the current University of Delaware system capable of handling 4096 nodes. SW accomplishes multiple goals of intelligent processing and control of large parts and identification of defects. SW has been used on large bridge components at an average cost of \$0.20/sensor including placement and materials costs.

Owing to the multiple advantages inherent to the SW system, this work is based extensively on DC behavior to model the relevant processing parameters. However, every attempt has been made to compare dielectric response and to identify the advantages and disadvantages of each approach.

1.4 Previous Work on Ionic Conductivity Modeling

While use of a DC-applied voltage for tracking the flow front during liquid molding processes was patented by ARL in 1990 [3], little fundamental research has been done on this issue [3, 5-7]. Kikuchi et al. investigated the sensing of the resin flow during molding processes using a modified SW system [8]. This system suffered from a low signal-to-noise (S/N) ratio and there was no attempt

made to measure viscosity and degree of conversion based on the SW data. Schwab et al. [9] used a novel parallel plate design consisting of individual sensors mounted in an RTM tool and proposed a theoretical model to relate sensor output to material behavior. The theoretical model developed by Schwab et al. was the basis on which England [4] developed a model of DC conductivity, which could predict the sensor response as a function of macroscopic viscosity changes and degree of cure.

1.4.1 Review of England's Model [4]

Figure 6 schematically represents the different modules adopted by England [4] to model the DC conductivity signal as an in-situ sensing tool to predict the macroscopic viscosity and degree of cure as obtained from Fourier-transform infrared (FTIR). As a means of quantifying the concentration of the conducting ions in the resin system, England used an organic salt as a dopant. About 0.1 weight-percent of tetrabutyl ammonium acetate (TA) was used in all of this experimental work. The previously mentioned concentration of TA, being far greater than that of other contaminant ions inherent in the resin system, presents a useful way of controlling the concentration of conducting ions present in the system for modeling purposes.

England adopted Equation 3 for ionic conductivity modeling:

$$R_j(t) = 6\pi\eta(t)L/A(\sum_i C_i Q_i^2 / r_i) \quad (3)$$

where $R_j(t)$ is the junction resistance of the resin at time t , C_i is the ionic concentration in ions per cubic meter, Q_i is the charge carried per ion, r_i is the radius of the ion in meters, $\eta(t)$ is the viscosity of the resin at a given time t , and L is the separation distance between the electrodes and A is the area of cross section of the electrodes "visible" to the ions.

For resin systems doped with TA, the model inputs were $\eta(t)$, L , A and C_i . The characterization of model inputs can be found elsewhere [4]. During cure, the separation distance, L , is no longer the shortest distance between the electrodes. The network formation impedes the motion of ions in a linear path, forcing them to travel increasingly tortuous paths to reach the electrodes. This increases the separation distance with cure. For purposes of simplicity, the tortuosity effect was neglected by England.

Module I of Figure 6 deals with developing resistance (R) vs. viscosity (η) relationship. This is accomplished by assuming that during cure the remaining parameters in equation 3 do not undergo a change except for R and η . Therefore, one can relate these two parameters as:

$$\eta(t) = \eta_o(T) * R_j(t)/R_o, \quad (4)$$

where $\eta_o(T)$ is the initial viscosity at temperature, T , and R_o is the initial resistance of the resin system at $t = 0$.

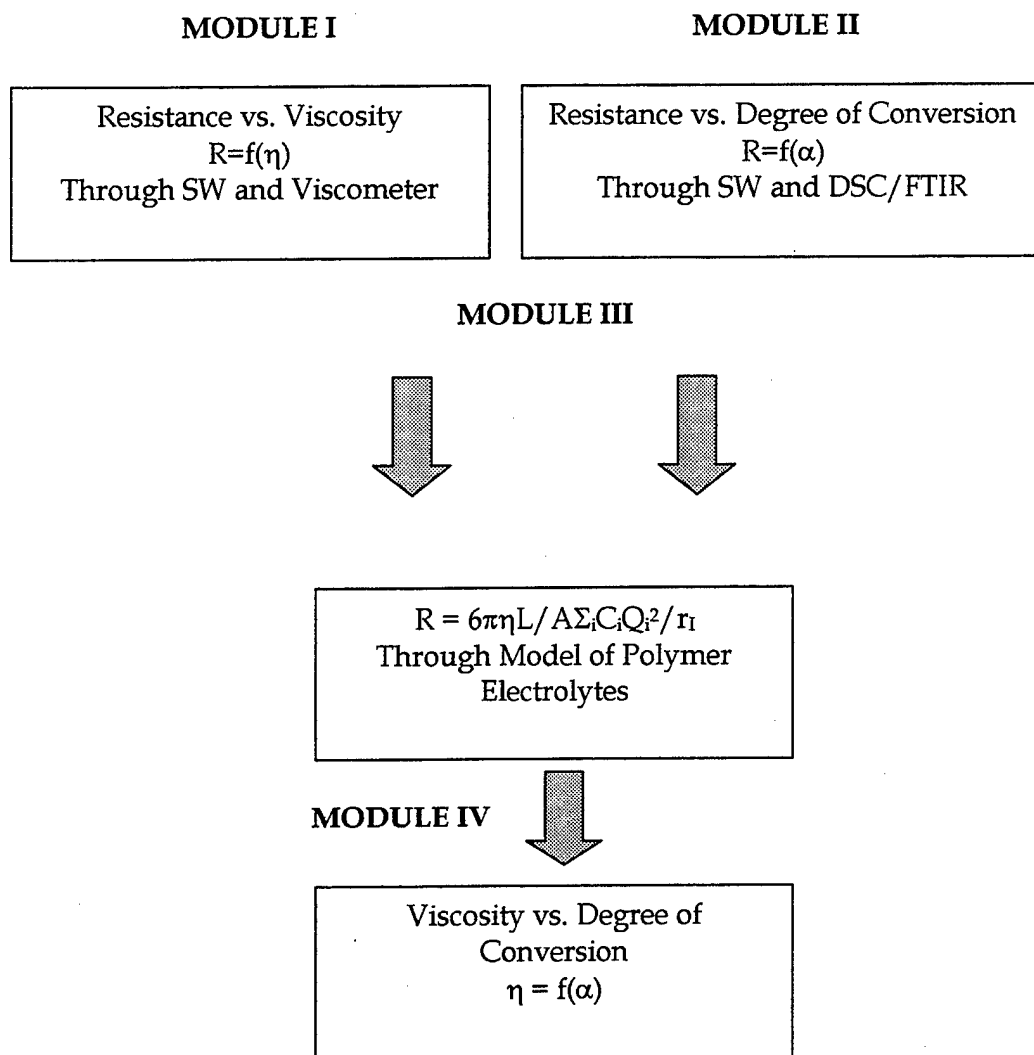


Figure 6. Schematic representation of England's model [4].

Module II deals with deriving a resistance, R , vs. degree of cure, α , relationship. This was accomplished by way of curve fitting experimental α vs. R data. A typical equation derived for cure temperature of 40 °C is given as

$$V(\alpha_{\text{Total}})_{40\text{C}} = 1.07 - 0.11\alpha_{\text{Total}} + 4.18 \times 10^{-3}\alpha_{\text{Total}}^2 - 6.66 \times 10^{-5}\alpha_{\text{Total}}^3. \quad (5)$$

Module III attempts to relate degree of cure and macroscopic viscosity through resistance, R , which acts as the common parameter linking the two. Module IV presents the degree of cure, α , vs. macroscopic viscosity, η , relationship as

$$\eta(\alpha, T) = [12R_s\eta_o(T)/V(\alpha, T)R_o] - [R_s\eta_o(T)/R_o]. \quad (6)$$

Degree of cure observations were carried out by England using FTIR. This proves to be a superior technique as compared to differential scanning

calorimeter (DSC), since FTIR enables the estimation of individual degree of cure of VE and styrene monomers. A knowledge of the degree of conversion of monomers is used extensively in this research work to draw insight into the network formation during cure.

England's model [4] was successful in predicting material properties like viscosity and degree of cure until gelation. Section 1.4.2 discusses the need for a continuum model—one that would allow modeling ionic conductivity beyond gelation until vitrification.

1.4.2 The Need for a Continuum Model

The model presented by England [4] is valid until the point of gelation and fails to accurately model the conductivity behavior beyond gelation due to the assumptions implicit in the model itself. A direct dependence of ionic resistivity on viscosity (Module I) is questionable for VE systems based on experimental observation where there is an offset between the time at which the viscosity reaches a minimum to when the ionic conductivity reaches a maximum. Module II of the above model relies on an empirical relationship to model DC resistivity and the degree of cure. It is therefore desirable to develop a fundamental model for relating the two. The model also fails to take into consideration molecular events like change in polymer chain length and change in number-average and weight-average molecular weights with the degree of conversion. This necessitates the exploration of a "continuum model" that could accurately describe the viscosity and SW behavior through gelation to vitrification.

1.5 Report Overview

A thorough understanding of the cure kinetics, network formation and their relationship to ionic conductivity behavior is essential for the development of a continuum model to accurately describe the observed SW behavior. In this work, an attempt has been made to characterize the relevant parameters influencing the conductivity behavior of curing VE. From previous work, it is known that cure temperature and styrene concentration play a significant role in the cure kinetics and, hence, on the observed DC conductivity [4, 10]. Preliminary investigation also revealed a decrease in DC voltage coinciding with the growth of VE microgels. This indicates a possible link between the two events. The modeling approach would therefore have to take into account the following possible mechanisms that could be either individually or synergistically responsible for the observed DC conductivity profile:

- Development of cross-links and network formation during cure, which might be responsible for restricting ionic mobility.

- The tortuosity introduced by the presence of microgels. Since ionic conductivity is inversely proportional to the path length, L , traveled by the ion, an increase in the size and number of microgels would result in higher tortuosities and decreased ionic conductivity as cure proceeds.

A series of systematic experimental results were conducted in this study to identify the most important mechanisms governing ionic conductivity. For simplicity, ionic conduction through the microgels are neglected, i.e., the microgels are assumed to be of negligible conductivity compared to the resin surrounding it. Also, the previously mentioned effects are considered only on an individual basis and the synergetic effects are not considered. Based on the experimental work, two different models, one based on the percolation theory and the other based on the free volume theory, were proposed. The percolation theory takes into account the effect of microgels on ionic conductivity, while the free volume-based model takes into account the network development during cure. A comprehensive analysis of the two models revealed that the free volume-based model is superior. Figure 7 gives a schematic representation of the different steps involved in the development of the continuum models. Cure kinetics measurements and DC sensing of cure were used to investigate the dependence of degree of cure on isothermal cure temperature and initial concentration of the styrene monomers in the reacting resin mixture.

In the case of the free volume model, the degree of conversion obtained is related to the development of glass transition temperature, T_g , using the Venditti's relationship as follows [11, 12]:

$$\ln(T_g) = ((1 - \alpha)\ln(T_g) + (C_{pr})\alpha\ln(T_g^\infty)) / ((1 - \alpha) + (C_{pr}) \alpha), \quad (7)$$

where T_g is the glass transition temperature, α is the total degree of cure, C_{pr} is the model parameter, and T_g^∞ is the ultimate T_g .

The glass transition temperature is then used as the input parameter for determining ionic conductivity σ and viscosity η using the free volume theory

as:

$$\log(\sigma_T / \sigma_{T_g}) = C_1(T - T_g) / ((C_2 + C_3 T_g) + (T - T_g)) \quad (8)$$

and

$$\log(\eta_T / \eta_{T_g}) = C_1(T - T_g) / ((C_2 + C_3 T_g) + (T - T_g)). \quad (9)$$

By making use of the glass transition temperature, T_g , as the common link between ionic conductivity, viscosity and the degree of cure, it becomes possible to in-situ "sense" the material behavior like viscosity and degree of cure using DC sensing. In this approach, microgels do not directly influence ionic conductivity.

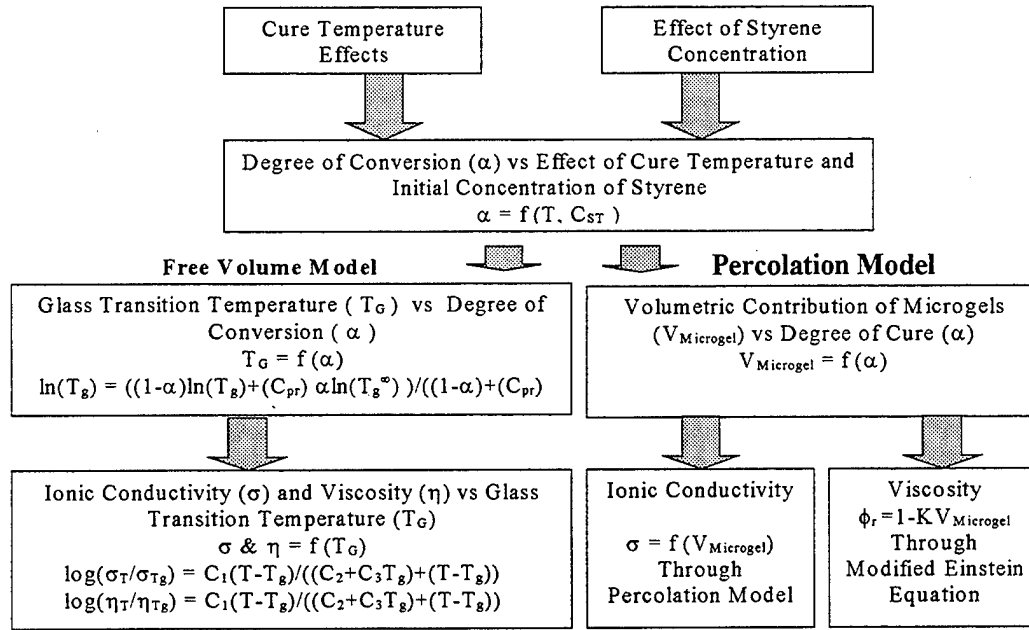


Figure 7. Schematic of continuum model.

In the case of the percolation-based model, the degree of conversion is related to the volumetric contribution of microgels as shown in Appendix B. The ionic conductivity development plotted against the volumetric contribution of microgels is compared to the classical percolation-based conductivity profiles. The viscosity modeling is accomplished through the modified Einstein equation:

$$\phi_r = 1 - KC, \quad (10)$$

where K is a constant in the range of 2.35 and 2.60, C is the volume concentration of spherical particles (i.e., microgels), and ϕ_r is the apparent fluidity. Therefore, by using the volumetric contribution of the microgels as the common factor, the percolation model relates ionic conductivity to both viscosity and degree of conversion during cure.

The main experimental techniques and materials used in this work are discussed in section 2. The experimental procedures and the data analysis techniques are also presented in this section. This section also draws a relationship between the different experimental techniques and their importance in the schema of continuum model. Table 1 presents the different resin systems and the various compositions of the reaction mixture used in this research work.

The cure kinetics of the resin systems studied are presented in section 3. FTIR spectroscopic techniques and DSC were employed to obtain the conversion kinetics of both the VE monomer and the styrene monomer in the given VE resin systems. This section quantifies the influence of temperature and styrene concentration on the curing of the VE resin system.

Table 1. List of compositions of the reacting resin mixture used in this study.

Experiment	VE Resin 411-C-50 ^a	VE Resin 441-400 ^b	VE Resin 825 ^c
Cure kinetics	0.2 weight-percent CoNap ^d 2 weight-percent Trigonox ^e	0.2 weight-percent CoNap 1 weight-percent Trigonox	0.2 weight-percent CoNap 1 weight-percent Trigonox
Viscosity	0.2 weight-percent CoNap 2 weight-percent Trigonox	0.2 weight-percent CoNap 1 weight-percent Trigonox	—
Cure Monitoring	0.2 weight-percent CoNap 2 weight-percent Trigonox	0.2 weight-percent CoNap 1 weight-percent Trigonox	—
DLS (microgel size)	0.2 weight-percent CoNap 2 weight-percent Trigonox	0.2 weight-percent CoNap 1 weight-percent Trigonox	—
Microgel Separation	—	—	0.1 weight-percent CoNap 0.5 weight-percent Trigonox

^aDow Derakane 411-C-50.

^bDow Derakane 441-400.

^cIn-house synthesized VE825.

^dCoNap = cobalt naphthenate accelerator.

^eTrigonox = AZCO Trigonox 239 initiator.

The cure monitoring efforts using SW and dielectric techniques are presented in section 4. Changes in the conductivity behavior are correlated to molecular events.

Section 5 addresses the presence of inhomogeneties (microgels) in the curing sample. A comprehensive set of data corresponding to the characterization of microgels has been presented and an explanation of the role of these microgels in cure kinetics and, hence, in conductivity behavior, has been explored. Section 5 also explores the feasibility of a continuum model based solely on the volume fraction of the microgels. This modeling approach assumes that all reaction contributes only to the formation of microgels, which are surrounded by unreacted resin mixture. An ionic conductivity model based on the percolation

theory and a viscosity model based on the modified Einstein's relationship are used to investigate the effectiveness of the assumption in describing the experimental observation. A large discrepancy between model predictions and experimental data suggested a need for a better model, one that would take into account the network formation outside the microgels during cure.

A mathematical model based on the molecular events identified in this experimental work is presented in section 6. This free volume-based model satisfies the requirements of a continuum model and describes the observed conductivity behavior through gelation until vitrification. Based on the experimental results generated, the free volume-based continuum model was adopted successfully for ionic conductivity modeling. The free volume model extends the ability to sense material properties like viscosity and degree of cure using the observed DC conductivity.

Section 7 presents a discussion of the work accomplished and possible areas for further research.

1.6 Section Summary

This section established the motivation and significance for a continuum model to predict degree of conversion and viscosity. In summary, this research work contributes the following information over and above the existing body of knowledge regarding DC-cure monitoring:

- Identification of the conducting system;
- Establishment of a relationship between cure-related molecular events and observed DC signal;
- Establishment of the role of microgels in gelation and hence on DC signal;
- Advantages and disadvantages of DC- and AC-cure sensing techniques;
- Development of a continuum model to predict ionic conductivity, viscosity, and degree of conversion; and
- Establishment of a fundamental theory to enable sensing of viscosity and degree of conversion through DC-cure monitoring such as SW.

2. Experimental Methods

2.1 Introduction

Seven experimental techniques were used in this work to support the development of the continuum model presented in Figure 7. The viscosity changes during the cure reaction were obtained using a Brookfield viscometer. The changes in DC conductivity with cure were sensed using an ARL SW system. Dielectric cure monitoring was carried out using a Micromet manufactured dielectrometer. The degree of conversion of the VE and styrene double bonds were monitored using FTIR spectroscopy in the infrared (IR) DSC. Glass transition temperature measurements were accomplished using dynamic mechanical analysis (DMA). Liquid chromatography using Hewlett-Packard manufactured chromatographs was performed to determine the effectiveness of microgel separation. The chemical composition of the microgels were then analyzed using FTIR spectroscopy. Atomic force microscopy (AFM) was performed on cured samples to determine the equilibrium size of the microgels. This section gives the details on all the experimental methods and sample preparation techniques. The materials used in this study are also discussed.

2.2 Materials

This research focuses primarily on ionic conductivity in VE resin systems. Section 2.2.1 provides a brief description of the VE resin system, while section 2.2.2 discusses specific VE resin systems used in this research work.

2.2.1 Background on VE Resins

A brief description of VE resin systems is given in section 2.2.1.1 and the chemistry of free-radical chain growth copolymerization is discussed in section 2.2.1.2.

2.2.1.1 VE Resin Systems

VE resins fall under the category of thermosetting resin systems. These resin systems are characterized by polyfunctional monomeric systems, which upon reaction form cross-links which result in a network structure that cannot be made to flow upon heating. The phenomenon of formation of a cross-linked network due to the reaction between the monomers present in the resin system is known as "curing." As the conversion of the monomers increase, the number of cross-links also increases, leading to the tightening of the resulting network. With conversion, a number of resin properties changes (e.g., the glass transition

temperature, T_g , increases with an increase in the degree of conversion). There are two distinct points of interest associated with the curing process: gelation and vitrification. Gelation of a resin system can be defined as the formation of network structure of macroscopic dimensions so as to occupy the entire volume of the resin system (i.e., the formation of an infinite network) [13]. This is associated with macroscopic viscosity of the resin system exponentially reaching infinity. Vitrification occurs when the glass transition temperature equals the cure temperature. Physically and macroscopically, a resin system is said to have vitrified when the material begins to solidify to a glassy state. At the molecular level, vitrification puts a severe restraint on the molecular motion severely curtailing the advancement of the cure reaction. In free-radical polymerization such as in VE resin systems, T_g exceeds cure temperatures at very low degrees of conversion.

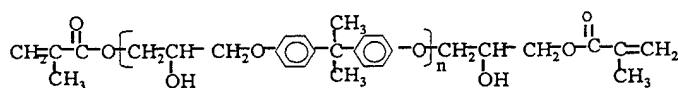
VE resin systems are essentially composed of VE monomers and styrene monomers apart from other additional chemical species such as inhibitors, stabilizers, etc., which are generally proprietary to the individual manufacturers. VE monomers are additional products of various epoxide resins and ethylenically unsaturated monocarboxylic acids such as acrylic or methacrylic acids. At this stage in the synthesis of VE resins, one ends up with the presence of chloride (Cl^-) ions in the resin. Traditionally, these chloride ions are considered to be responsible for the observed dielectric and ionic conductivity behavior in epoxy resins. Therefore, one could safely conclude that in undoped VE resins, the observed DC conductivity is the result of contribution from these chloride ions.

Styrene monomers are usually added to reduce the room temperature viscosity of the mixture. In most of the commercial resins, the concentration of the styrene is restricted between 30% and 55% by weight. Figure 8 shows the chemical structure of both the VE monomer and the styrene monomer. As shown in Figure 8, the VE monomer has two reactive end groups whereas the styrene monomer has only one reactive end group. This essentially means that of the two, only VE monomers can act as the cross-links and the conversion of

VE monomers is a measure of the degree of cross-linking in the final resulting network. The conversion of styrene monomers results in linear chain extensions. Hence, the degree of conversion of the styrene monomers is a measure of the approximate distance between the cross-links.

2.2.1.2 Free Radical Chain Growth Copolymerization

The VE resin system reacts through a free-radical co-polymerization. Mechanism of such a reaction is explained in detail in other literature [14]. A brief summary of the three main steps are:



Vinyl Ester



Styrene

Figure 8. Chemical structure of VE and styrene monomers.

- initiation involving two reactions: formation of the initiator radical (R) and addition of the initiator radical to a monomer;
- propagation of a monomer radical to another monomer molecule; and
- termination of all growing chains due to lack of mobility of unreacted monomers.

Possible initiators for a free-radical polymerization include peroxides and hydroperoxides, azo compounds, redox initiators, and photoinitiators [14]. In the current study, an organic hydroperoxide was used as the initiator. The main characteristics of the initiator material are that it should be fairly stable at room temperature, and simultaneously, to ensure practical reaction rates, it should be able to decompose fairly rapidly at reaction temperatures.

Primary radicals are formed through thermal decomposition of the peroxides. The addition of the monomers to the growing polymer chain results in the propagation stage of the polymerization reaction with continued propagation of the radical to the new monomer site. It is a common practice to add accelerators or promoters such as cobalt naphthenate (CoNap) to raise the decomposition rate of the initiator at low temperatures such as those used in our reactions which typically were between 30° and 50 °C.

Three types of VE resins were used in this study: (1) Derakane 411-C-50, (2) Derakane 441-400, and (3) an in-house synthesized VE825. The type of initiator used in the system was Trigonox 239A, purchased from AZKO. This initiator contained 45 weight-percent carboxylic ester, 45 weight-percent cumyl hydroperoxide, and 10 weight-percent cumyl acid. CoNap containing 6 weight-percent cobalt, was used as an accelerator to induce the decomposition of the initiator at low-curing temperatures. Styrene of 99% purity, purchased from Aldrich Chemicals, was used for diluting the VE system. Benzoquinone, which is an inhibitor for the free-radical reactions, was used to stop the reactions where required in case of reactions used to study microgel compositions. Benzoquinone was supplied by Aldrich Chemicals.

2.2.2 Resin Compositions

Two commercial VE resins were used in this work, namely Dow Derakane 441-400 and Derakane 411-C-50. For experimental techniques involving the separation of microgels and subsequent characterization, a specialized polymer designated VE825, developed in-house, was used. The previously mentioned commercial resins were both supplied by Dow Chemical Company. From the ^1H nuclear magnetic resonance (NMR) spectroscopy, it was determined by Dua [10, 15] that the value of the n -repeat group in Derakane 441-400 is approximately 1.66. The average molecular weight of the VE monomer in the resin was determined to be 700. The styrene content in the resin system was established to be 28% by weight. Using the same NMR technique, the n -repeat unit in 411-C-50 was determined to be 2.39, the average molecular weight was established to be 908, and the styrene content was determined as 45% by weight.

Derakane 411-C-50 was used to study the effect of temperature on kinetics, rheological changes and the modeling of the conductivity behavior. This resin is used widely in most of the liquid molding processes due to its lower viscosity, which facilitates resin infusion. Also, the longer-gelation time characteristic of this resin, makes it the ideal candidate for studying the reaction kinetics and viscosity changes in the pregel stage. Derakane 441-400 was primarily used to understand the effect of dilution with styrene on the cure kinetics of the VE resin system. As mentioned above, Derakane 441-400 contains only 28 weight-percent of styrene and, hence, is much more suitable for studying the effects of dilution up to 57 weight-percent of styrene, which is the practical upper limit for most of the commercial VE resin systems used in the composite industry. VE825 resin was also used for studying the effect of dilution with styrene. VE825 offers the unique advantage of offering the ability to be diluted with styrene, since this resin system is free of styrene monomers. The monodispersed nature of the VE monomers in VE825 is taken advantage of in the studies involving the microgel separation due to the fact that the effectiveness and ease of separation of the microgels is augmented.

2.3 Viscosity Experiments

Measurement of viscosity during cure is used as an effective tool to identify the onset of gelation. It is also used in this research as a benchmark to compare the sensitivity of DC monitoring to gelation. The effectiveness of the continuum model as an in-situ cure monitoring tool is based on its ability to accurately predict the experimentally observed viscosity profile during cure.

2.3.1 Sample Preparation

The samples were prepared by adding the desired quantities of the reaction mixture in the proper order, i.e., VE resin system followed by styrene (if

required), followed by CoNap. The prepared sample was then equilibrated to the desired temperature at which the viscosity characteristic needs to be studied, e.g., $T = 40\text{ }^{\circ}\text{C}$. Once the system was equilibrated to the desired temperature, a calculated amount of Trigonox was mixed to the resin system to start the reaction. About 10 mL (stipulated by the Brookfield Viscometer manual [16]) of the reaction mixture was then introduced into the cylindrical jacketed container of the Brookfield viscometer. The reaction was allowed to proceed within the cylinder and the viscosity changes were measured at fixed-time intervals.

2.3.2 Instrumentation

Viscosity experiments were performed on a Brookfield Model LVDV II+ digital viscometer. Sample temperature was controlled with the help of a Brookfield small sample adapter and Brookfield water bath/circulator model TC-200. The basic components are shown in Figure 9. The viscometer essentially consists of a fixed outer cylinder and a spindle that rotates at a constant angular velocity. The spindle is connected to a torque spring, which measures the frictional resistance generated by the resin inside the sample container. The viscosity is then calculated by the viscometer. In the experiments, care was taken to maintain the angular velocities at 20 rpm, since the accuracy of the resulting values were heavily compromised below 20 rpm, due to the limitations on torque measurements [16]. A typical viscosity profile is given in Figure 10. Point A in the figure corresponds to the initial viscosity of the reacting mixture. On further reaction, the exothermic nature of the reaction forces the temperature of the reacting mixture to increase thereby decreasing the viscosity between points A and B. With further cure, cross linking and network formation results in an exponential increase in the observed macroscopic viscosity resulting in gelation at point C.

2.4 SW Experiments

SW experiments form the core of this research effort as a way of providing in-situ DC-cure monitoring information. The continuum model strives to relate the observed SW signal to material properties like viscosity and degree of cure.

A batch of VE resin system was prepared as described before in section 2.3.1. The prepared resin batch was allowed to equilibrate in an oil bath. Once equilibrated, the sample was then transferred to the Single Node Test Cell (SNTC)-3 type of SW cell [4]. A typical SNTC-3 single node test cell is shown in Figure 11. A detailed explanation of the specifications of SNTC-3 is given in Appendix C. Throughout the reaction, care was taken to maintain the reaction temperature at the desired set value. The change in DC conductivity with resin cure was recorded and stored in a computer running the SW system. A

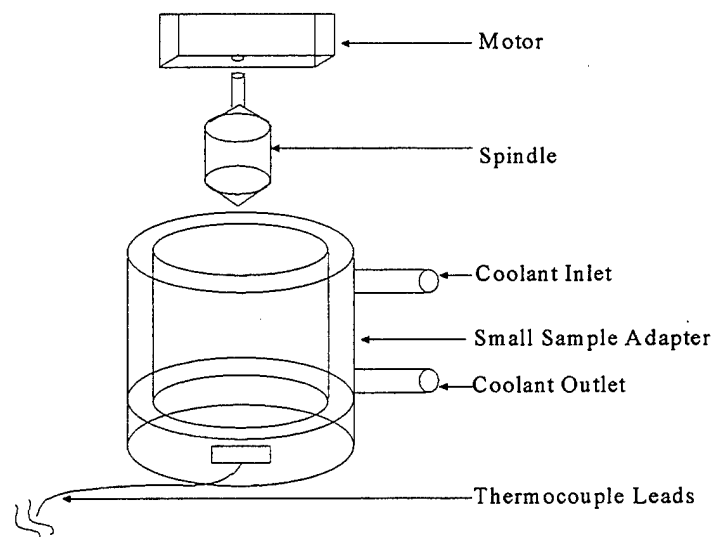


Figure 9. Schematic illustration of a Brookfield viscometer and small sample adapter.

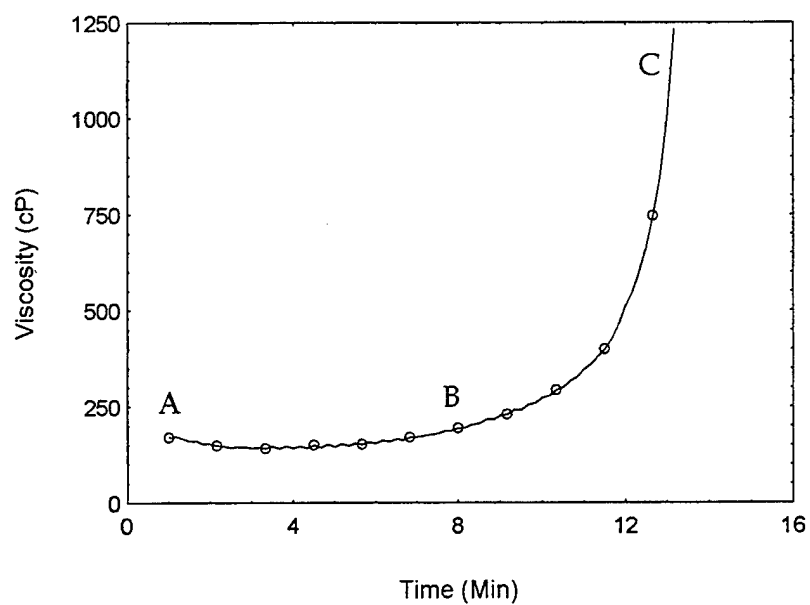


Figure 10. Typical viscosity profile of a curing VE resin.

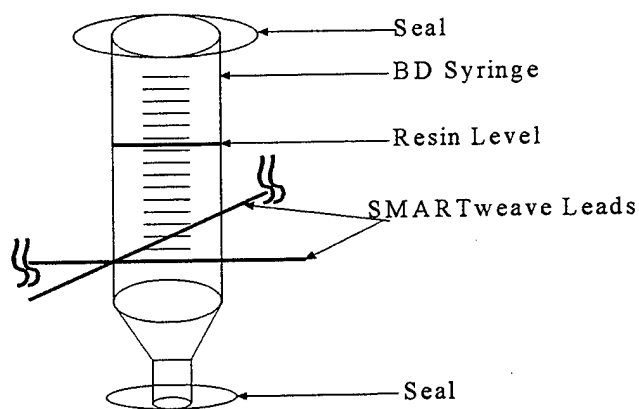


Figure 11. SNTC-3 single node test cell.

description of the SW apparatus and its working has been discussed in section 1.3. A detailed overview is discussed elsewhere [4, 17-20]. A typical SW profile generated using SNTC along with relevant explanations are presented in section 1.3.

2.5 Dielectric Cure Monitoring

Dielectric sensing has conventionally been used for in-situ cure monitoring. Therefore, in order to benchmark the performance of DC sensing as a cure monitoring tool, it is essential to compare and contrast the sensitivity of both these tools to the cure related events such as gelation and vitrification.

The resin system was prepared as discussed in section 2.3.1 and was then equilibrated using an oil bath. The cure initiation was achieved by introducing the calculated amount of Trigonox into the mixture. The reaction was run isothermally at the desired set temperature maintained by the oil bath. The data concerning changes in the dielectric behavior were collected and stored in a computer running the dielectrometer.

The dielectric experiments were all carried out using a Eumetric 100A dielectrometer, manufactured by Micromet Instruments, Inc. The Eumetric 100A interface hardware was preset at midconductivity mode and all experiments were performed using a 2-in tool mount sensor. The A/D ratio of the tool mount sensor used has been predetermined to be 40, where A is the surface area of the electrode and D is the separation distance between the electrodes.

ve411c50temp30

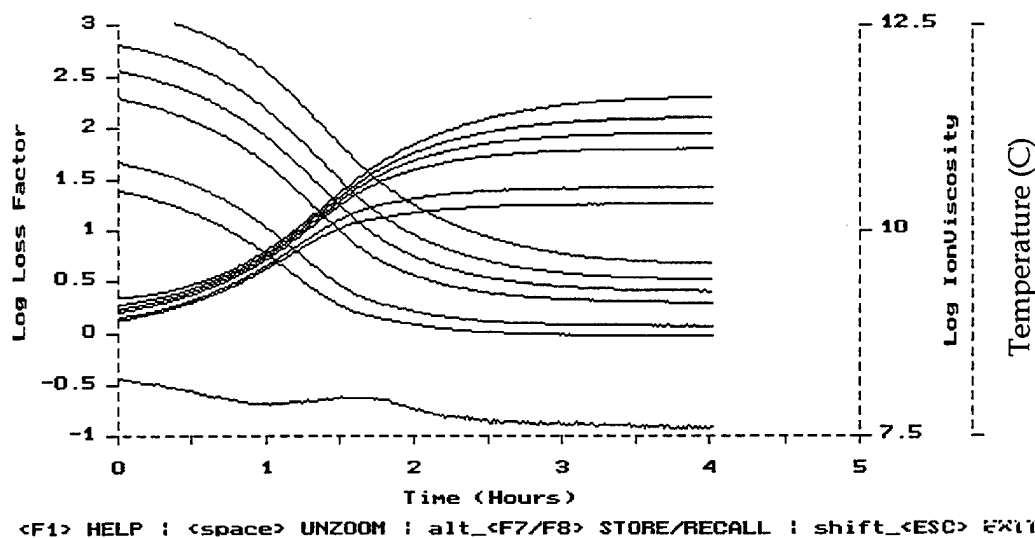


Figure 12. Typical dielectric signal of a curing VE sample.

The dielectric measurements were performed at seven different frequency modes to collect information on the rate of change of log loss factor and log ionic viscosity with cure. A review on the dielectric technique and the relevant parameters is presented in Appendix A. A typical dielectric profile is shown in Figure 12.

2.6 FTIR Experiments

FTIR measurements yield degree of conversion of monomers with time, thereby enabling one to relate cure events like gelation and vitrification to the extent of cure. The experimental data are also used extensively, in the modeling effort to analyze volumetric contribution of the microgels, in the latter stages of this research work. Section 6 deals with the effectiveness of a continuum model to predict the degree of cure profiles over a wide range of temperatures.

2.6.1 Instrumentation and Sample Preparation

Cure monitoring studies involving a study of the degree of conversion of VE double bonds and styrene double bonds were performed using a Nicolet 20 DXB FTIR spectrometer in the transmission mode working in the IR region of the spectrum. A batch of the resin system was prepared as described in section 2.3.1 and then the calculated amount of Trigonox was introduced. A drop of the reacting mixture was then placed in between two NaCl transparent crystal plates supplied by International Crystal Labs. A 0.025-mm Teflon spacer was used to regulate the sample thickness between the crystal plates. The crystal plates were equilibrated prior to the introduction of the resin mixture and the reaction was

allowed to proceed at the desired temperature in an isothermal mode. The crystals containing the sample between them was then placed in a sample holder housed in an assembly consisting of an aluminum block containing two 100-W cartridge heaters. A constant temperature was maintained through regulation by a thermocouple and a temperature controller. Figure 13 shows a typical cell design used in the FTIR spectroscopy studies.

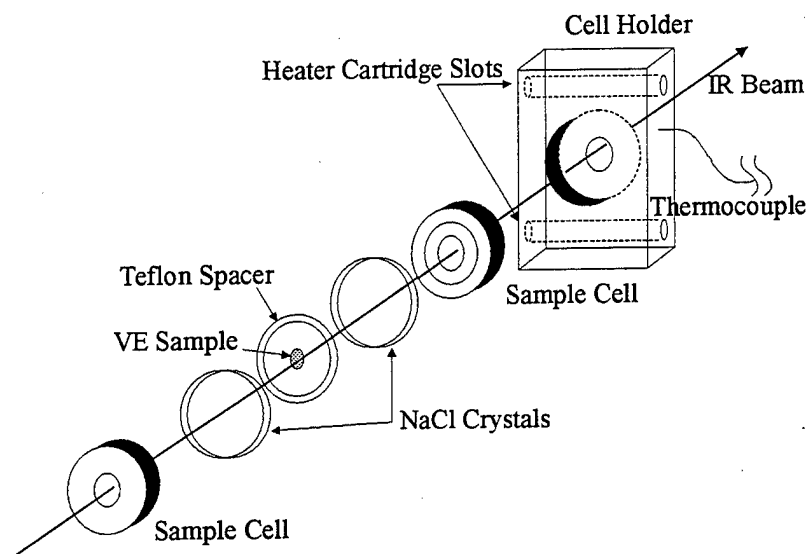


Figure 13. FTIR experimental setup.

2.6.2 IR Spectra of VE

FTIR spectroscopy is a characterization method that can be used to determine the degree of conversion of VE and styrene monomers of a curing resin system. In transmission mode FTIR, a beam of IR light is transmitted through the sample contained between the NaCl plates and the absorbance of laser light as it passes through the sample is measured. The amount of absorbed laser light, at characteristic wavelengths, is a measure of the increase or decrease of the concentration of those bonds that dissipate energy at those corresponding wavelengths [21].

The characteristic wavelengths of VE and styrene monomers are 945 cm^{-1} and 910 cm^{-1} , respectively. The absorbances of IR at these wavelengths result from the vibration and dissipation of energy by the carbon-carbon double bonds along the backbones of the monomers under consideration. With the proceeding of the cure, these double bonds break and are integrated into cross-links. This is reflected as the depletion in the C=C double bonds, which decreases the

absorbance at the characteristic wavelengths of 945 cm^{-1} and 910 cm^{-1} . Absorbance is normalized (to compensate the error introduced by way of evaporation of styrene and cure shrinkage) by a set of reference peaks. The reference peak for VE is set at 830 cm^{-1} and at 700 cm^{-1} for styrene. These reference peaks correspond to C-H bonds along the carbon backbone of the VE and styrene monomers [22].

Equations 11 and 12 were used to calculate normalized fractional conversion of VE and styrene double bonds from FTIR absorption data respectively:

$$\alpha_{\text{VE}}(t) = 1 - (\text{ABS}(t)_{945\text{cm}^{-1}} / \text{ABS}(t=0)_{945\text{cm}^{-1}})(\text{ABS}(t=0)_{830\text{cm}^{-1}} / \text{ABS}(t)_{830\text{cm}^{-1}}), \quad (11)$$

$$\alpha_{\text{ST}}(t) = 1 - (\text{ABS}(t)_{910\text{cm}^{-1}} / \text{ABS}(t=0)_{910\text{cm}^{-1}})(\text{ABS}(t=0)_{700\text{cm}^{-1}} / \text{ABS}(t)_{700\text{cm}^{-1}}), \quad (12)$$

where α is the fractional conversion of double bonds associated with each monomer at time t and ABS is the absorption intensity of the peaks. The magnitudes of the relevant absorbance peaks were measured taking into consideration slight shifts in peak locations and baselines. Figure 14 shows an FTIR spectra of VE resin at cure time t .

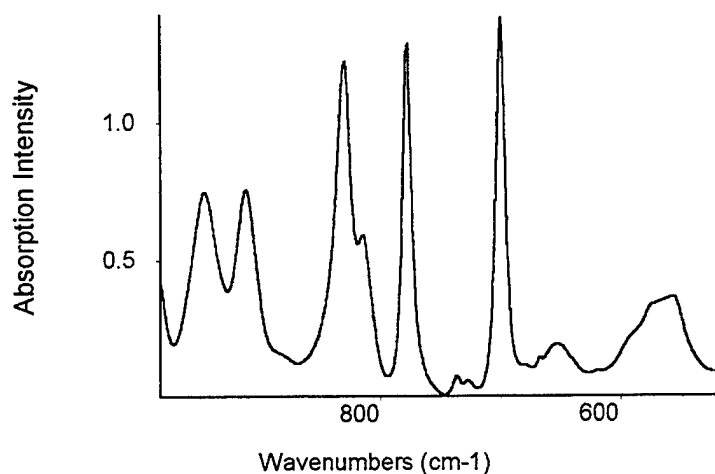


Figure 14. FTIR spectra of VE825 at the beginning of cure at $40\text{ }^{\circ}\text{C}$ cure temperature.

2.7 DSC Experiments

DSC experiments are used in this work to complement the FTIR results on the cure kinetics. While FTIR is a handy tool to measure the individual monomers' degree of conversion, DSC provides the total degree of conversion for the reacting mixture. DSC measurements are used in the T_g - α model developed by Stone [11], required for the continuum model developed in section 6.

Autocatalytic models have traditionally been used for modeling the cure kinetics of thermosets. In this study, an autocatalytic equation of the form given in

equation 13 was used to describe the cure rate of VE resin 411-C-50 as studied using the DSC technique:

$$d\alpha/dt = (K_1 + K_2\alpha^m)(\alpha_{\max} - \alpha)^n. \quad (13)$$

Stone [11] has explored the reaction order ($m + n$) for isothermal cures of VE 411-C-50. Kinetic parameters for the often used second order autocatalytic model are given in Table 2:

Table 2. Autocatalytic parameters for the degree of conversion as observed using DSC.

Cure Temp (°C)	K ₁ (1/min)	K ₂ (1/min)	M	n	Corr. Coeff.
20	0.0003 + 0.0001	0.01 + 0.002	1.075 + 0.015	0.925 + 0.015	0.9949
30	0.0012 + 0.0001	0.1273 + 0.070	1.038 + 0.004	0.962 + 0.004	0.9900
40	0.0035 + 0.0001	0.1694 + 0.002	1.037 + 0.009	0.963 + 0.009	0.9895

This study used cure simulation software, PIRSA [23], that incorporated the previously mentioned kinetic parameters to obtain degree of cure for isothermal runs of 20°, 30°, and 40 °C. A typical profile of the curing resin mixture generated using PIRSA is shown in Figure 15.

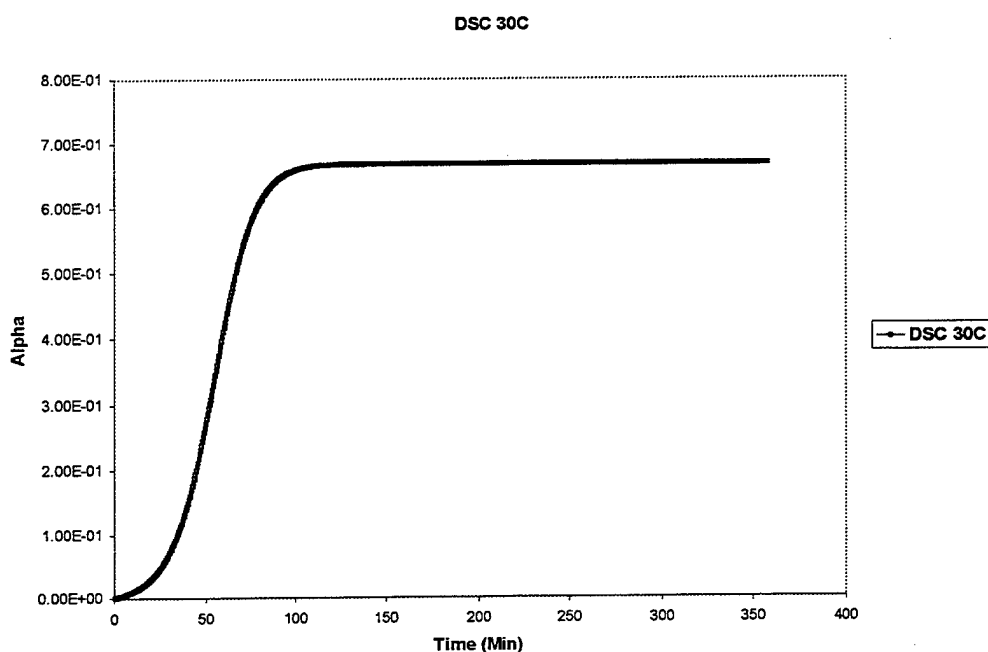


Figure 15. Degree of conversion of VE 411-C-50 at 30 °C as obtained from PIRSA.

2.8 DMA Experiments

DMA measurements yield information on the glass transition temperature T_g of the cured resin mixture. A knowledge of T_g is used in section 4 to relate the development of network structure to the observed SW behavior.

Sample Preparation and Instrumentation. Resin mixtures prepared as described in section 2.3.1 were cured as plaques on aluminum sheets at the desired cure temperature. Rectangular samples of dimensions 0.125 in \times 0.25 in \times 2.5 in were prepared from the cured plaques for DMA analysis. The DMA experiments were carried out using a 983A type dynamic mechanical analyzer at fixed frequency. All experiments were started at 25 °C and the samples were ramped to 200 °C at 2 °C/min to maintain thermal equilibrium. A schematic representation of the experimental set up is shown in Figure 16.

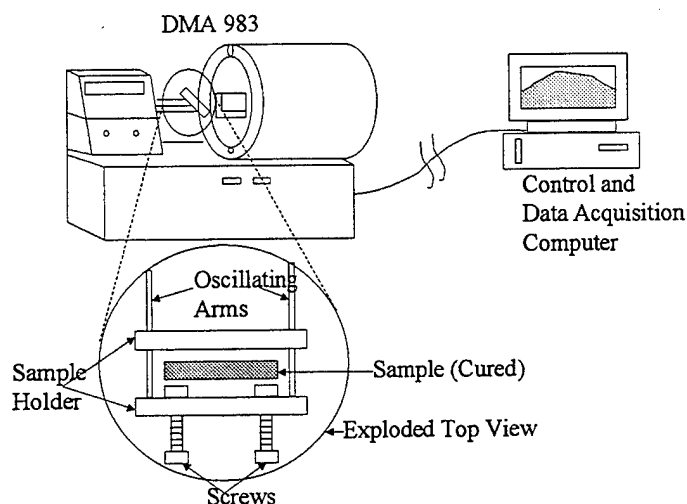


Figure 16. Schematic illustration of DMA setup.

2.9 Liquid Chromatography

Liquid chromatography was used in this research work to ascertain the effectiveness of the removal of unreacted VE and styrene monomers from the reacted high molecular weight component, namely microgels. The microgels were removed from the reacting mixture to characterize their chemical composition. Since contamination by unreacted VE and styrene monomers could introduce inaccuracies, it became essential to monitor the effectiveness of the "fractionation process" using liquid chromatography.

2.9.1 Sample Preparation

A batch of VE825 was mixed with 28 weight-percent styrene to obtain the VE resin system for liquid chromatographic analysis of the microgels. The VE resin system was equilibrated to 40 °C prior to the addition of CoNap and Trigonox. The choice of low styrene content in the resin sample was based on preliminary work where microgel separation was unsuccessful due to the presence of excess unreacted styrene monomers. Very low gelation times were experienced with this resin system at normal concentrations of 0.2 weight-percent CoNap and 2 weight-percent Trigonox. Consequently, lower and lower concentrations of CoNap and Trigonox were tried until a combination of 0.1 weight-percent CoNap and 0.5 weight-percent Trigonox yielded an acceptable time to gelation of 10 min at a 40 °C isothermal cure temperature.

Once the reaction was initiated, the reaction was allowed to proceed for 9 min at which time the reaction was stopped by the addition of 0.25 weight-percent benzoquinone. Care was taken to introduce the same volume of benzoquinone mixture as that of the reacting mixture with continuous vigorous shaking. The terminated mixture was then dissolved in an equal volume of tetrahydrofuran (THF) followed by reprecipitation by the addition of methanol. This stage presents multiple problems in that if excess volume of methanol was added, a large fraction of the unreacted monomers also were precipitated; on the other hand, a shortage of methanol addition results in no precipitation at all.

This procedure was repeated on the precipitate for 10 cycles. The final precipitate was then placed in a vacuum chamber for a period of 24 hr to remove any remaining traces of unreacted styrene monomer. Ten milligrams of the final sample was then dissolved in 10 mL of high-performance liquid chromatography (HPLC)-grade THF to prepare the experimental sample for HPLC analysis.

2.9.2 HPLC Instrumentation

A schematic illustration of the liquid chromatography instrumentation setup is shown in Figure 17. A syringe setup is used for introducing 20 mL of the sample solution and size variations between different chemical species in the injected sample are sensed and output as different peaks on a voltage versus time plot, with larger molecular species appearing earlier along the time axis.

2.10 Atomic Force Microscopy (AFM)

AFM was used to verify the presence of microgels in the reacted resin mixtures. Similar work on high temperature resin mixtures have shown the presence of these spherical entities. However, since reaction kinetics are dependent on temperature, it becomes essential to identify the presence of microgels in low-

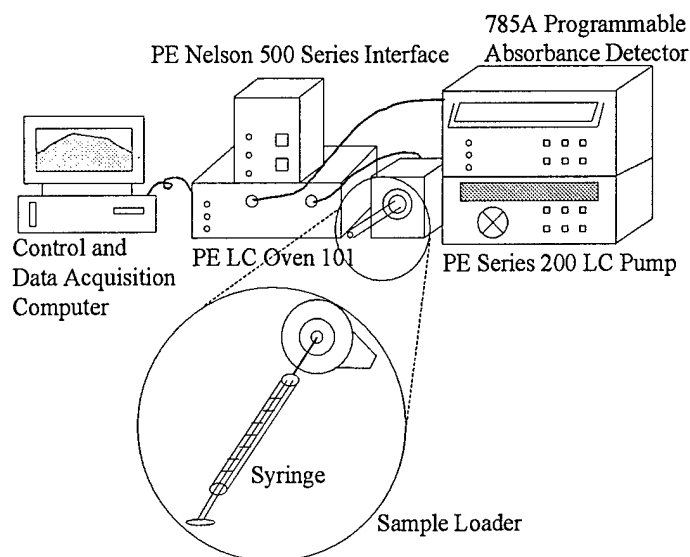


Figure 17. Schematic illustration of HPLC experimental setup.

temperature systems. AFM results were also used to identify the range of microgel sizes that were used in the parametric study presented in section 5 to ascertain the role of microgels on ionic conduction and gelation.

2.10.1 Background

Tapping mode imaging is a key advance in AFM for soft, adhesive, or fragile samples. This technique allows high-resolution topographic imaging of sample surfaces that are easily damaged. In conventional contact mode AFM, the probe tip is simply dragged across the surface and the resulting image is a topographical map of the surface. The serious drawback, however, is that the dragging motion of the tip, combined with the adhesive forces between the tip and the surface, can cause substantial damage to both the sample and the probe tip, besides causing artifacts in the image data. Tapping mode imaging, overcomes the limitations of the conventional scanning modes by alternately placing the tip in contact with the surface to provide high resolution and then lifting the tip off the surface to avoid dragging the tip across the surface. Tapping mode imaging is implemented in ambient air by oscillating the cantilever assembly at or near the cantilever's resonant frequency using a piezoelectric crystal. The piezo motion causes the cantilever to oscillate with a high amplitude when the tip is not in contact with the surface. The oscillating tip is then lowered toward the surface, until it begins to lightly touch or tap the surface. During scanning, the vertically oscillating tip alternately contacts the surface and lifts off, generally at a frequency of 50,000 to 500,000 cycles per second. As the oscillating cantilever begins to intermittently contact the surface,

the oscillation amplitude is reduced. The reduction in amplitude is used to identify and measure surface features. Figure 18 shows an AFM micrograph of VE 411-C-50 cured at an isothermal temperature of 70 °C obtained by Brill and Palmese [21].



Figure 18. AFM micrograph of microgels in VE 411-C-50 at a cure temperature of 70 °C [21].

2.10.2 Instrumentation and Sample Preparation

The AFM experiments were all performed under tapping mode imaging. The specifications under which these experiments were performed are given in Table 3. Figure 19 gives a schematic representation of the instrumental setup. The heart of the AFM instrument setup is the Dimension 3000 scanning probe microscope interfaced and controlled through the computer.

The drive amplitude and frequency adjustments were automatically accomplished using software control and motorized sample approach, which brought the cantilever into tapping mode operation at the lowest possible tracking force. The samples used in these experiments were prepared as plaques cured at isothermal temperatures of 30°, 40°, and 50 °C, respectively.

2.11 Section Summary

Sections 2.2–2.10 presented an overview of the different materials and experimental techniques employed in this research work. As explained in their respective sections, each experimental technique provides valuable insight into cure-related processes on which the continuum model builds. Sections 3–6 describe how these experimental techniques are used to obtain information corresponding to the different modules presented in Figure 7.

Table 3. Tapping mode specifications.

Drive Frequency Range	10 kHz–1MHz
Drive Voltage Range	0–20 V
Drive Amplitude and Frequency Adjustment	Software Controlled
Detector	RMS to DC Amplitude Detector
Cantilevers	Etched Silicon Cantilevers 60–400 kHz Resonant Frequencies
Tip-Sample Approach	Motorized Sample Approach

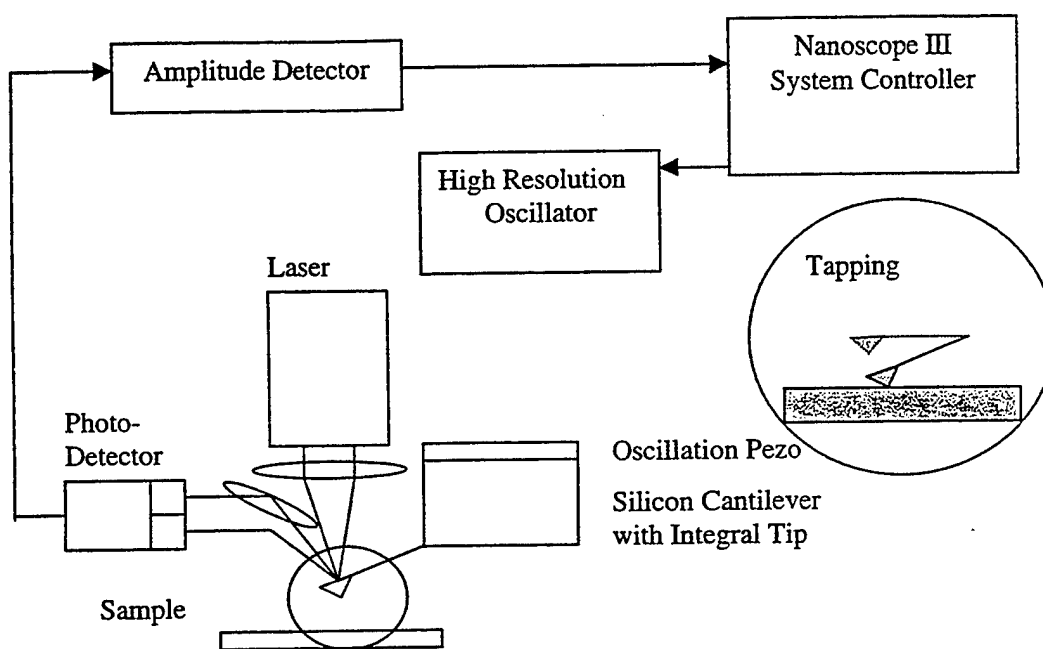


Figure 19. Block diagram for tapping mode operation.

3. Cure Kinetics of VE Resins

3.1 Introduction

A thorough understanding of the SW signal or that of any other cure monitoring technique, requires a comprehensive understanding of the molecular events associated with curing. This section analyzes some of the parameters that must be considered to develop the continuum model for ionic conductivity. As presented in Figure 7, cure kinetic studies are the first step in the development of the model. Using the experimental techniques described in section 2, it becomes possible to understand the effects of initial concentration of styrene and cure temperature on the cure processes and their relationship to ionic conductivity.

Thermal analysis using DSC has been used extensively by other researchers in both isothermal and nonisothermal mode to study the cure kinetics of the resin. However, DSC suffers from a disadvantage of not being able to yield any information regarding the degree of conversion of the individual components (i.e., VE and styrene) in the reacting mixture. Since the objective of this research work was to obtain as much information as possible regarding the individual components, FTIR was employed to obtain the degree of conversions of VE and styrene individually.

In this work, emphasis has been placed on understanding the effects of styrene concentration, temperature and molecular weight on cure kinetics. A thorough understanding of the previously mentioned factors is an important prerequisite in developing the conductivity model described in Figure 7.

3.2 Cure Kinetics Using FTIR

Figure 20 shows typical FTIR data of the degree of conversion of VE double bonds and styrene double bonds with time. The degree of conversion is expressed here as the percentage ratio between the number of double bonds consumed and the initial number of double bonds. Therefore, care should be taken in comparing the conversion data between different species and for different FTIR runs. As mentioned before, VE has two reactive double bonds whereas styrene has just one. When a double bond reacts, it could be the first double bond of a new VE monomer or it could be the second double bond of an already reacted and, hence, bound to the network VE, monomer. In short, the double bond conversion of the VE monomer is not the same as the double conversion obtained from FTIR. Figure 20 shows three distinct regions.

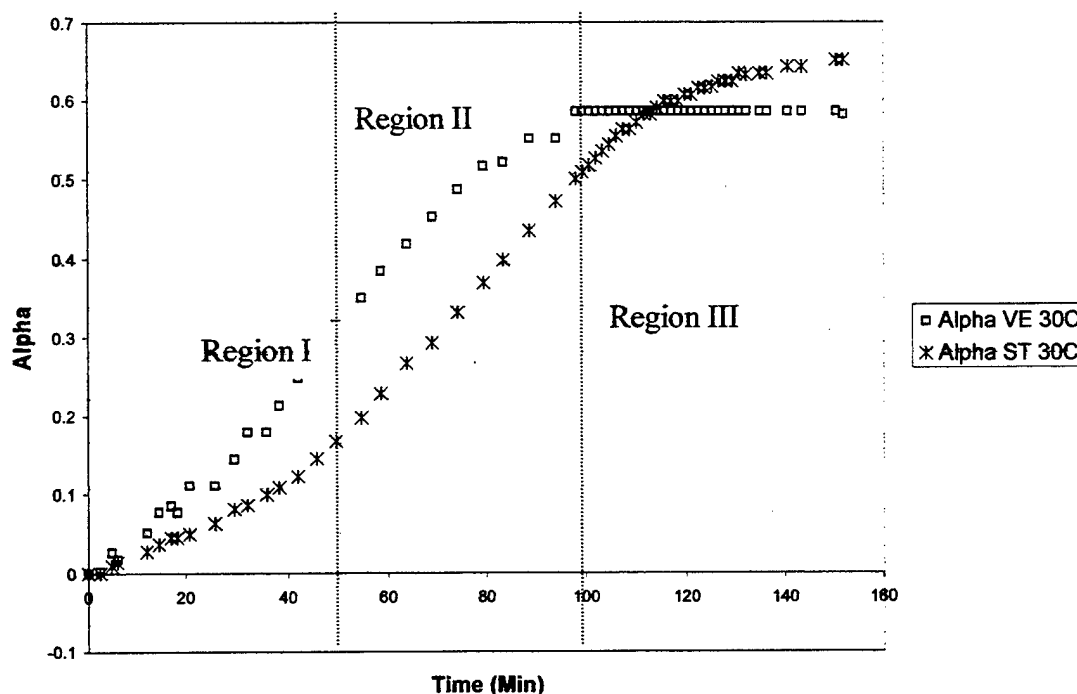


Figure 20. Typical profiles of VE and styrene double-bond conversion.

It should be noted however that the boundaries of these three regions are not definitive and they are likely to be quite diffuse. In Regions I and II, the conversion of the VE double bonds is greater than the conversion of the styrene double bonds. In Region III, VE plateaus can be seen, while styrene conversion continues and eventually exceeds the final VE conversion. In Region I, the reaction kinetics are determined by the reactivity ratios of VE and styrene. The higher conversion of VE suggests that the VE double bonds have a higher affinity to react with the free radicals as compared to the styrene double bonds [10, 15]. In Region II, due to gelation, the bimolecular termination rate is lowered due to the decrease in mobility of the growing radical species. The hindered bimolecular termination results in an increase in the concentration of the free radicals and accelerates the reaction. This effect is termed the Trommsdorf effect [24, 25]. In Region III, the diffusional limitations play a significant role. With the onset of vitrification, the serious restrictions placed on the molecular mobility is said to be the reason for the final conversion not being able to reach 100% [24, 25]. The higher final conversion of the styrene double bond suggests that since styrene is a smaller molecule compared to the VE monomer, it would be better able to diffuse to reactive sites.

An important feature of many free-radical, chain-growth, cross-linking copolymerization systems is the formation of localized, highly cross-linked, submicron size regions called microgels [26, 27]. These microgels are in the range of 100–150 nm in diameter and come into existence in the sea of VE resin,

almost instantaneously (as compared to the time scale of the curing process) [28]. With the proceeding of cure, the number of microgels in the reacting mixture increases with time, as opposed to the classical nucleation theory, where nucleation occurs simultaneously and the nucleated sites grow in size with time. Consequently, microgel formation is highly heterogeneous in nature. Another important factor that is believed to strongly affect the cure behavior of VE resins is the phase separation of the macromolecules from the unreacted monomers. Based on theoretical thermodynamic calculations, Palmese [28] and Ziaee [29] suggested that there is a high probability of phase separation in VE resins due to enthalpic contributions.

3.3 Effect of Styrene Concentration

Figures 21 and 22 show the effect of styrene concentration on the fractional conversions of VE and styrene double bonds for Derakane 441-400. The reactions were performed at 28%, 37%, 47% and 57% by weight of styrene. Owing to better temperature control available at 40 °C, all the reactions were conducted isothermally at 40 °C with 1.0 weight-percent Trigonox and 0.2 weight-percent CoNap. From the observation of Figures 21 and 22, it is clear that the initial conversion of VE double bonds decreases with an increase in the styrene concentration as is the case of styrene double-bond conversion. The same effect was observed by researchers working with DSC on similar systems [24]. The initial decrease in the VE conversion can be explained based on the fact that with increasing concentration of styrene, the VE concentration decreases leaving fewer VE double bonds to participate in the cure reaction. Dua [10] argues that the seemingly strange decrease in the reaction rate with an increase in the styrene content is due to the fact that the reactivity ratio of the VE monomers is higher than that of the styrene monomer. Therefore, the VE monomers react faster with the primary free radicals to give VE chain radicals which, in turn, react with the styrene monomers. This phenomenon explains why an increase in the styrene conversion with increasing VE concentration is observed, or conversely, why the styrene conversion decreases with increasing styrene content in the reacting mixture.

Lee and Lee [30] and Dua [10] have observed the formation of polystyrene during the latter stages of the cure and at higher styrene concentrations (47% and 57%). They attribute the formation of this homopolymer to the phenomenon of phase separation. Two phases are said to form during the course of copolymerization. The first phase essentially is the copolymer network swelled by the unreacted VE monomer and, perhaps, residual styrene monomers. The second phase essentially is made of unreacted styrene. It is hypothesized that even though copolymerization stops in the first phase due to vitrification of that phase, the homopolymerization continues in the styrene-rich second phase.

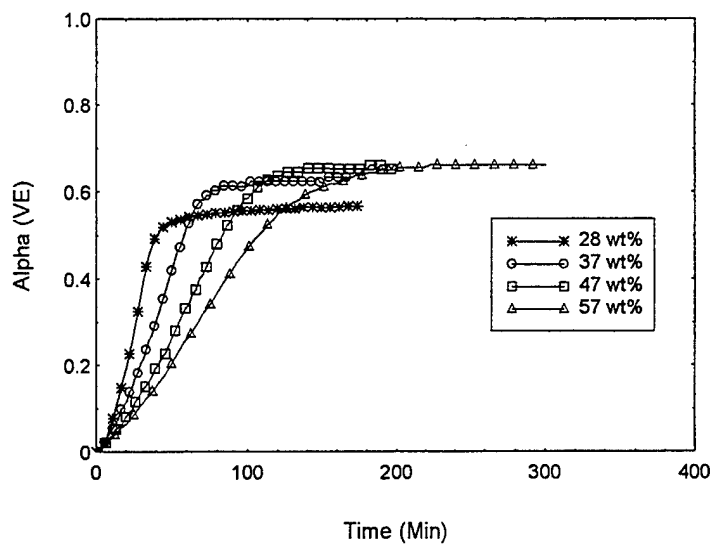


Figure 21. Fractional conversion of VE double bonds in Derakane 441-400 cured at 40 °C.

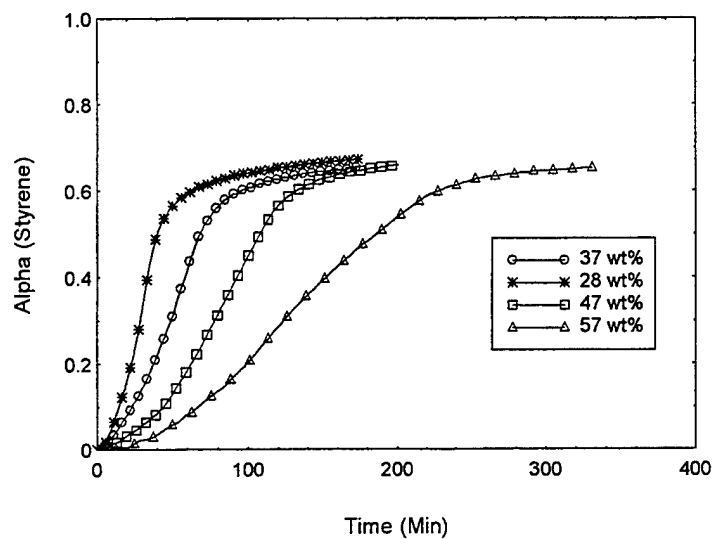


Figure 22. Fractional conversion of styrene double bond in Derakane 441-400 cured at 40 °C.

Dua [10] hypothesized that the copolymerization reaction could result in the formation of the microgels which are responsible for trapping a large number of the pendant VE double bonds due to the compactness of the microgel structure. The microgels are rich in VE and are surrounded by the styrene-rich region.

From Figures 21 and 22, it becomes apparent that the final conversion of the VE double bonds increases with the increase in styrene concentration, whereas in the case of styrene double-bond conversion, there seems to be no significant change in the final fractional conversion with styrene concentration. Similar results have been reported by Dua [10] and Brill and Palmese [21] for the same resin system. They argue that with an increase in the concentration of styrene, more styrene gets incorporated in the network leading to loosely networked structure. In other words, it leads to a structure with lower cross-linking density. This basically facilitates better mobility of the VE monomers enabling them to reach the reactive sites, hence, a higher final fractional conversion is achieved. The seemingly contradictory constant final fractional conversion of styrene is explained by the fact that the methacrylate groups of VE reacts faster and reach their maximum conversion much earlier than styrene (see Figures 21 and 22). This results in the onset of vitrification. The vitrified system may not allow the free diffusion of the styrene monomer to reactive sites thereby sealing them off, leading to almost the same final conversion for styrene monomers. It is argued that the phenomenon of phase separation becomes a significant factor in case of styrene concentrations beyond 47 weight-percent leading to the formation of VE rich and styrene rich phases. Due to the phase separation, the effect of increased styrene concentration is not really felt by the VE monomers that are copolymerizing in the other phase thereby resulting in the same final fractional conversion of VE monomers irrespective of styrene concentration beyond 47 weight-percent. The previously mentioned hypotheses are verified for accuracy using DC cure monitoring and DMA in section 4.2. The experimental results show that for 37- and 47-weight-percent styrene systems, the cross-link density is higher than for 28- and 57-weight-percent styrene systems. This indicates that an increase in the initial concentration of styrene in the reacting mixture does not necessarily result in a loose network, suggesting various degrees of homopolymerization between the resin mixtures under consideration.

3.4 Effect of Temperature

Figures 23 and 24 show the effect of temperature on the cure kinetics of Derakane 411-C-50. CoNap at 0.2 weight-percent was used along with 2-weight-percent Trigonox to initiate the reaction. From Figures 23 and 24, it is apparent that the reaction rates and the final conversion for both VE and styrene monomers increases with an increase in the reaction temperature. This can be explained by the fact that the additional thermal energy enables higher diffusion of these monomers so that more monomers are able to reach the reactive sites at higher temperatures. Another observation is that the final conversion of styrene is higher than that of the corresponding VE monomer. As described in section 3.2, styrene monomers are better able to overcome the diffusional limitations

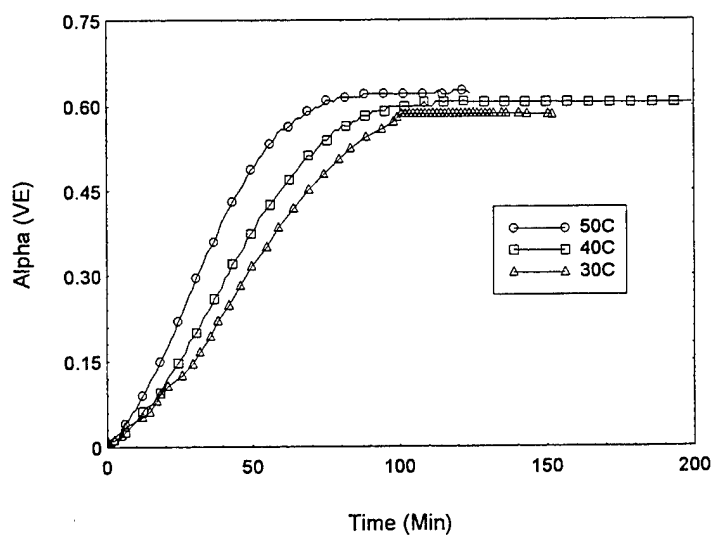


Figure 23. Fractional conversion of VE double bonds in Derakane 411-C-50 cured at isothermal temperatures of 30°, 40°, and 50 °C.

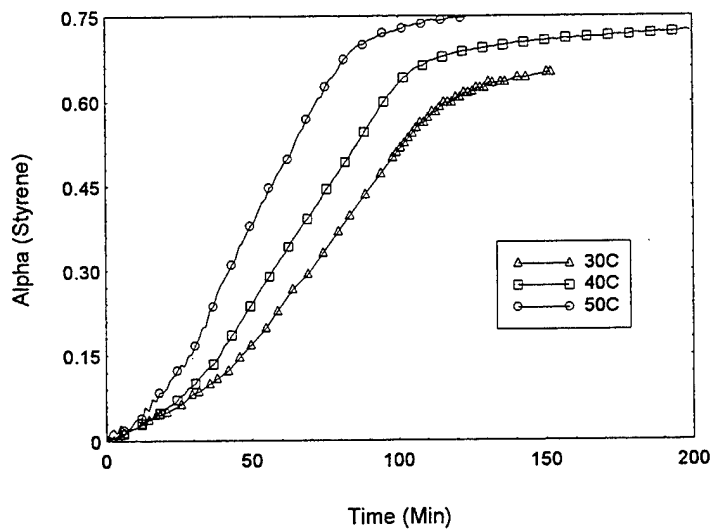


Figure 24. Fractional conversion of styrene double bonds in Derakane 411-C-50 cured at isothermal temperatures of 30°, 40°, and 50 °C.

imposed by network formation due to their relatively smaller size; the styrene monomers also exhibit higher final conversion. This, combined with the fact that one observes change in styrene fractional conversion long after the VE fractional conversion levels off, suggests polystyrene formation and hence a possibility of phase separation. Section 4 deals with the effect of temperature on the DC signal and how different aspects of the cure kinetics of Derakane 411-C-50 such as

development of cross-link density, formation of homopolymerised microgels and molecular mobility contribute towards the development of the continuum model presented in sections 5 and 6.

On comparison of the final fractional conversion of monomer double bonds of Derakane 441-400 (diluted to 47% styrene) maintained at 40 °C to that of Derakane 411-C-50 at 40 °C, one observes a higher VE fractional conversion in the case of 441-400 as compared to 411-C-50. As discussed previously, the VE monomers in 441-400 are of lower molecular weight as compared to those in 411-C-50 and hence exhibit higher mobility. However, the final fractional conversion of the styrene monomer in both cases is roughly the same owing to the fact that the styrene monomers are much smaller entities and the network structure does not restrict their mobility in both the cases. As will be discussed in section 4, the T_g value for 411-C-50 is much lower than that of 441-400, partly due to the higher fractional conversion of VE monomers.

3.5 Autocatalytic Kinetics Model Parameters

Autocatalytic kinetic models are widely used for fitting the experimental cure kinetic data for a number of VE and unsaturated polyester resins. For low temperature isothermal cure kinetics, the following relationship is widely used [30, 31]:

$$d\alpha/dt = (K_1 + K_2\alpha^m)(\alpha_{\max} - \alpha)^{2-m}, \quad (14)$$

where α is the fractional conversion at time t , α_{\max} is the maximum degree of conversion at that isothermal cure temperature, K_1 and K_2 are the reaction rate constants and m is the order of the reaction. This empirical reaction kinetic model is unsuitable for modeling the kinetic behavior as obtained from FTIR, which yields α rather than $d\alpha/dt$; so a modified form of the equation of the form is widely used:

$$d\alpha/dt = (K\alpha^m)(\alpha_{\max} - \alpha)^{2-m}. \quad (15)$$

This approximation is justified since K_1 values as obtained from DSC data (Table 2) are usually negligible as compared to the K_2 values. This expression can be integrated to yield α :

$$\alpha = \{\alpha_{\max}[K\alpha_{\max}(1 - m)]^{1/(1-m)}\} / \{1 + [K\alpha_{\max}(1 - m)]^{1/(1-m)}\}. \quad (16)$$

The autocatalytic parameters obtained from FTIR data for 411-C-50 [4] and 441-400 are presented in Tables 4 and 5.

3.6 Section Summary

The cure kinetics of Derakane 411-C-50 and Derakane 441-400 were studied using FTIR. Derakane 441-400 was used for the effect of styrene concentration studies as Derakane 411-C-50 already contains approximately 48 weight-percent

Table 4. Kinetic parameters corresponding to VE 411-C-50 FTIR data.

Temperature (°C)	30	40	50
VE Monomer			
K	0.00079071	0.0018584	0.0012285
m	0.63813	0.66051	0.55319
$\alpha_{\max}(\%)$	58.981	59.163	60.808
Styrene Monomer			
K	0.00055487	0.0010582	0.0015359
m	0.69773	0.68739	0.67882
$\alpha_{\max}(\%)$	66.149	71.794	69.308

Table 5. Autocatalytic parameters for FTIR data of VE 441-400 cured at 40 °C.

Styrene Concentration	28 weight-percent	37 weight-percent	47 weight-percent	57 weight-percent
VE Monomer				
K (min ⁻¹)	0.238	0.116	0.0652	0.052
m.	0.689	0.659	0.622	0.604
α_{\max}	0.562	0.650	0.699	0.684
Styrene Monomer				
K (min ⁻¹)	0.147	0.087	0.055	0.031
m.	0.653	0.660	0.688	0.656
α_{\max}	0.669	0.676	0.708	0.704

styrene. This section discusses the effect of styrene concentration on the network development during cure. Styrene-concentration effect, therefore, manifests itself as difference in the T_g development between different resin mixtures. The initial concentration of styrene also determines the degree of homopolymerisation during cure.

The temperature effects result in accelerating the cure kinetics of the resin mixture at higher cure temperature. Also, the T_g development with cure is different for different cure temperatures [11]. Since the modeling approach relies on either the volumetric contribution of the microgels (percolation approach), or on T_g development with cure (free-volume approach), the cure kinetics-related experiments provide valuable information towards the development and verification of the continuum model.

Generally, the rate of fractional conversion of the VE monomers is higher than that of the styrene monomers due to their higher reactivity. The final conversion of styrene was, however, always higher than that of the VE double bonds due to the fact that the diffusional limitations affect the mobility of VE monomers more than the styrene monomers based on the difference in the size and molecular weights of the monomers. As the temperature was increased, the final conversions of both the monomers increased owing to higher monomer mobility. In the section 4, DC conductivity is measured and correlated with the kinetic data generated herein.

4. Cure Monitoring of VE Resin

4.1 Introduction

In this section, emphasis is placed on analyzing the cure signals obtained using SW and the dielectrometer. The signal is correlated to the FTIR data, viscometer data, and DMA data to establish the molecular events occurring during cure. A detailed description of the SW system and dielectric monitoring has been presented in section 1 and elsewhere [4].

Section 4.2 deals with the SW behavior. This section investigates the effect of styrene concentration in 441-400 and the effect of cure temperature on the SW behavior of 411-C-50. Section 4.3 deals with dielectric cure monitoring of 441-400 diluted to different concentrations of styrene content. This section also deals with effect-of-cure temperature on the dielectric response of 411-C-50. Section 4.3 compares and contrasts the dielectric behavior with SW behavior. Section 4.4 summarizes the results from this section.

4.2 SW Cure Data

This section discusses the DC cure monitoring results and their correlation to cure-related events discussed under section 3. Section 4.2.1 discusses the effects of styrene concentration, while section 4.2.2 deals with temperature effects.

4.2.1 Effect of Styrene

Figure 25 deals with the SW behavior exhibited by Derakane 441-400 diluted by (99% pure) styrene supplied by Aldrich Chemicals to a weight-percent of 28%, 37%, 47%, and 57% of styrene. Figure 25 reveals that the effect of styrene addition on the initial voltage is twofold. Firstly, the initial voltage of the system increases upon increasing the styrene content from 28 weight-percent to

37 weight-percent. However, upon further addition of styrene, the initial voltage of the resin system starts to decrease.

This seemingly contradictory behavior is explained by the fact that the styrene component of the resin system doesn't supply any of the conducting ions responsible for the observed conductivity behavior as shown in Figure 26. Therefore, an addition of styrene to the system is equivalent to diluting the concentration of the conducting ions supplied by the VE component of the resin system. This explains why an addition of styrene to the system results in a lower initial voltage. However, this doesn't explain the initial increase in the voltage from 28 weight-percent to 37 weight-percent styrene system. Figure 27 reveals that the viscosity of the resulting resin system after the styrene addition decreases with increasing styrene concentration. This reduction in viscosity can be interpreted as higher molecular mobility of the monomers and the conducting ions, resulting in higher initial voltages, consistent with the model of England [4] described in section 1.

The overall initial conductivity is therefore the result of these two competing effects and in case of 28 weight-percent to 37 weight-percent styrene system, the increase in mobility dominates the dilution effect due to the additional styrene, resulting in higher initial conductivity. On further addition of styrene to the system, the dilution effect governs over higher molecular mobility resulting in the reduced initial voltage observed in the experiments. Increasing ion concentration through doping has been investigated by England [4] by introducing 0.1 weight-percent of TA. Preliminary investigations conducted as a part of this research work involved the use of tetrabutyl ammonium iodide (TI), a cheaper alternative to TA, as dopants. A comparison of the TI based results with England's work has been presented under Appendix D.

From Figure 25, it is observed that the gelation of resin mixtures containing different concentrations of styrene gets shifted further along the time axis with increasing styrene content. The gelation in Figure 25 is given by the point of inflection in the SW profile as discussed in section 1.3 (Figure 5). The same trend is observed with SW cutoff. The viscosity data shown in Figure 28 confirms the fact that the gelation happens earlier in case of lower styrene systems. This is due to the fact that an increase in VE concentration results in an increased reaction rate as shown in the FTIR data (Figures 21 and 22) and shorter time to reach the gel point.

In order to understand the difference in the SW cutoff point (i.e., the point at which the SW signal drops to zero), a plot between degree of conversion and the styrene concentration at the instant when the SW signal becomes zero was constructed and is shown in Figure 29. From the graph, it can be concluded that the degree of conversion of both the VE and styrene monomers decrease initially followed by an increase with increase in the styrene content. This can be

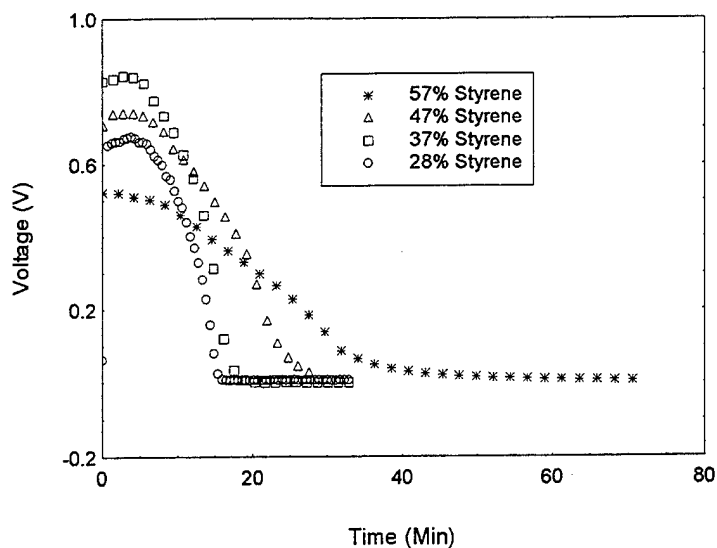


Figure 25. SW behavior of Derakane 441-440 cured at 40 °C.

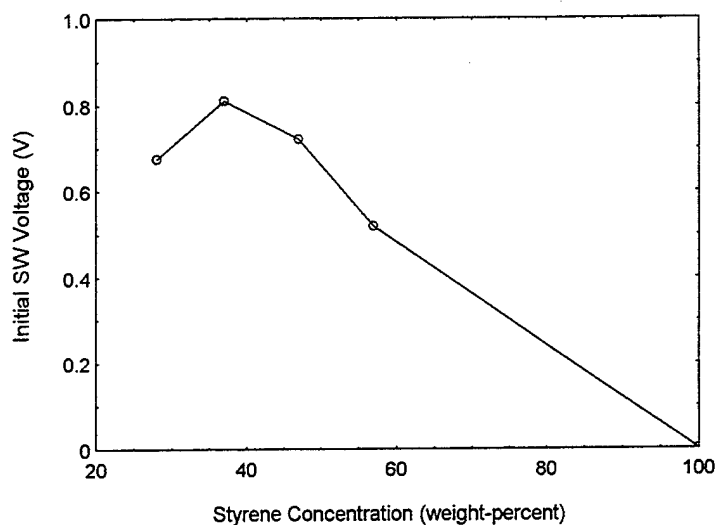


Figure 26. Initial DC signal vs. styrene concentration in Derakane 441-400.

explained: in the case of resin systems with 37 and 47 weight-percent of styrene, the cross-linking density is higher thereby cutting off the mobility of the conducting ions at a much lower conversion value. In case of 57 weight-percent styrene system, the presence of excess styrene results in the formation of a much looser network with long linear chains of styrene between the cross-links, thereby facilitating an increased mobility of the conducting ions.

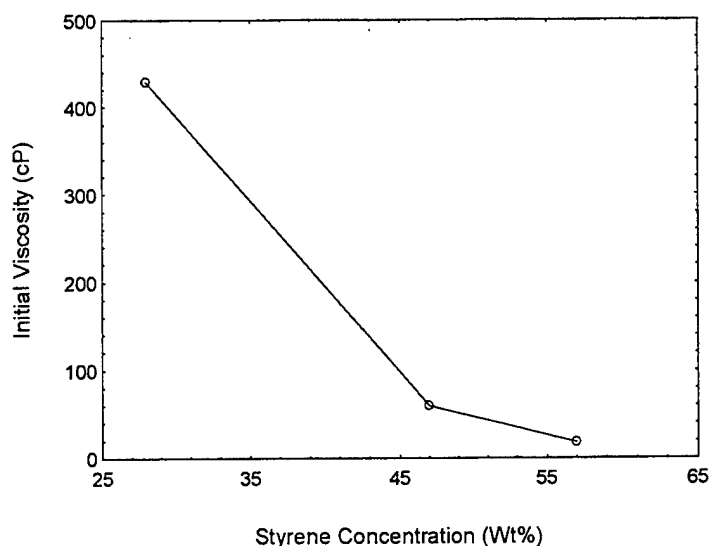


Figure 27. Initial viscosity vs. styrene concentration in Derakane 441-400.

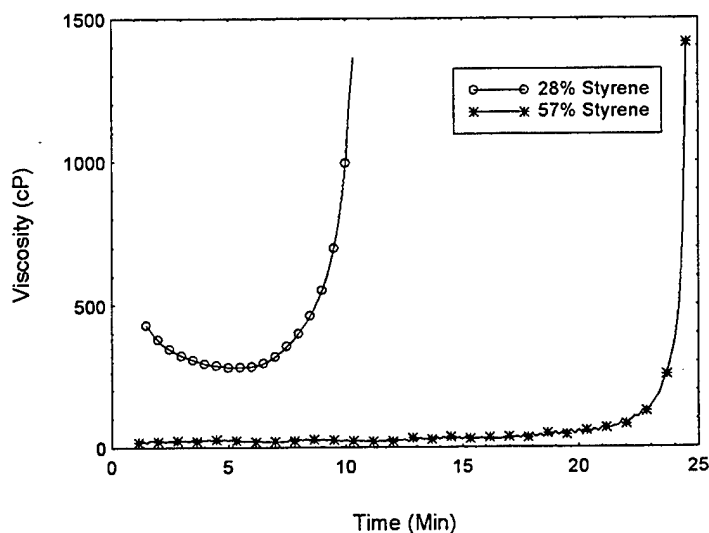


Figure 28. Viscosity development in Derakane 441-400 cured at 40 °C.

A confirmation of the previous hypothesis comes from analyzing the DMA data (T_g) of the corresponding systems. T_g is a measure of the cross-link density of the resulting network. It is clear from the T_g data of Derakane 441-400 presented in Figure 30, that indeed the cross-link density in the cases of 37 and 47 weight-percent styrene is higher than that of 28 and 57 weight-percent styrene, since T_g is an estimation of the cross-link density of the resulting network. Hence, it can be concluded that the addition of styrene, even though it is electrically inert, plays a very significant role in determining the SW behavior by way of being an inherent part of the polymer network and directly affecting the cure kinetics.

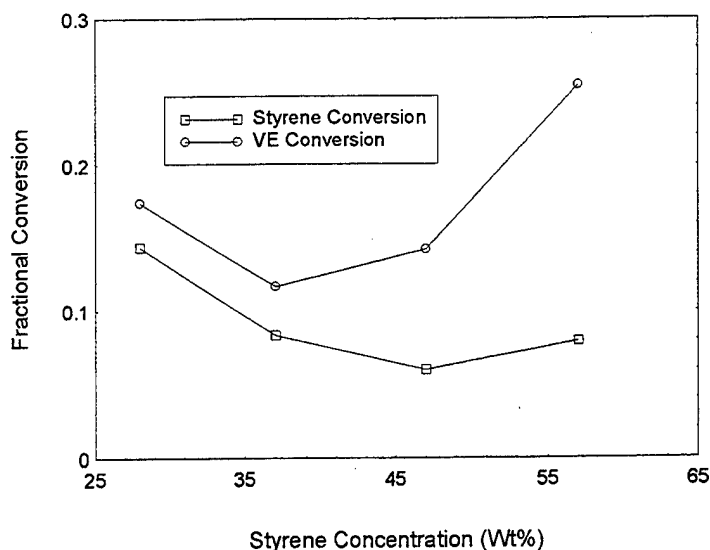


Figure 29. Fractional double-bond conversion vs. styrene concentration in Derakane 441-400 at DC signal cutoff.

4.2.2 Effect of Temperature

Figure 31 shows the effect of temperature on the SW signal for Derakane 411-C-50. A common feature observed in all of these figures is that the initial SW voltage increases with an increase in the temperature. This is due to the fact that the increase in temperature results in a decrease in the resin viscosity, which, as explained in section 4.2.1, results in an increased initial voltage.

Figure 31 shows that the resin systems cured at higher temperatures reaches the gel point sooner than the system cured at a lower temperature. However, the SW cutoff point occurs at a much longer time period for higher temperature systems. Figure 32 shows the viscometer data, which confirms that the gelation occurs sooner for higher temperature systems. A close inspection of Figures 23 and 24 shows that the reaction rates in the case of the higher temperature systems were indeed higher thereby resulting in gelation, much quicker than the system cured at lower temperature.

Table 6 shows the T_g data obtained by using DMA for all three cure temperatures. From Table 6, it becomes apparent that the cross-link density increases with the cure temperature that exerts a negative effect on the molecular mobility. However, the additional thermal energy imparted to the molecular mobility at higher temperatures, enables the ionic species to negotiate through the network for a longer time resulting in the SW signal being observed for longer times in high-temperature systems. So the dominating factor that determines the SW cutoff is the thermal energy, which results in increased mobility and decreased local viscosity.

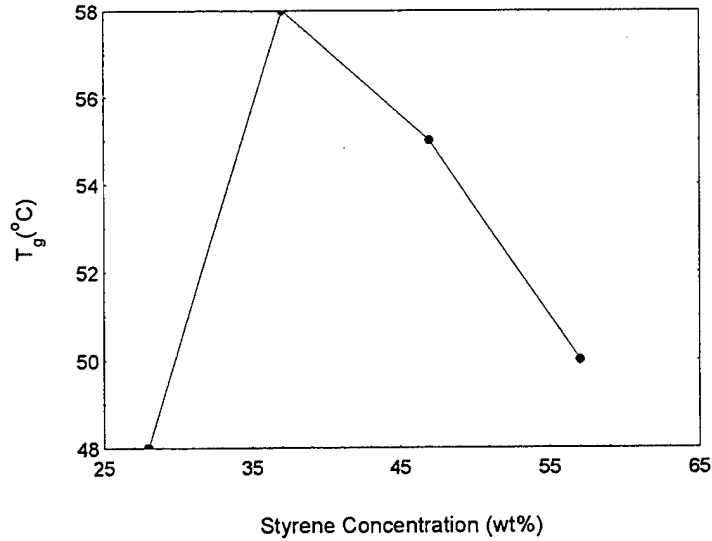


Figure 30. Glass transition temperature vs. styrene concentration for Derakane 441-400 resin.

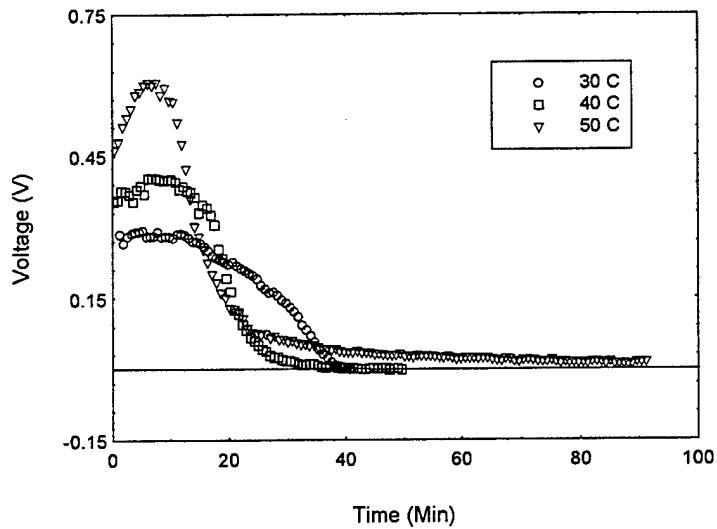


Figure 31. SW signal vs. time for Derakane 411-C-50 at different isothermal cure temperatures.

4.3 Dielectric Cure Monitoring

This research makes use of dielectric cure sensing in order to benchmark the performance of DC sensing for cure monitoring purposes. This section discusses the advantages and disadvantages of each system, delineating ways in which one technique can complement the other to obtain a better insight into cure related processes.

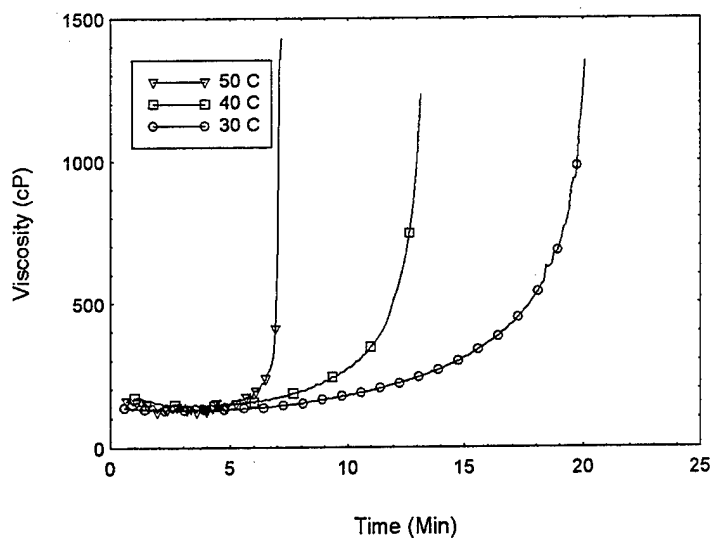


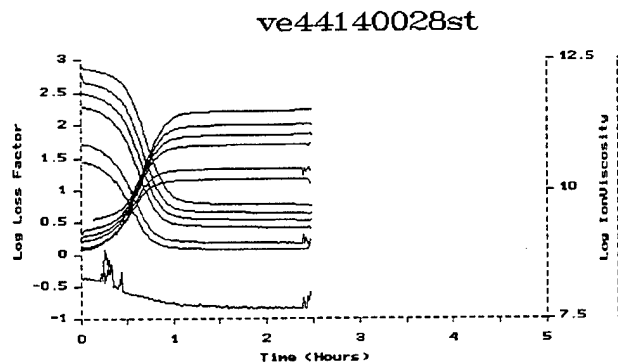
Figure 32. Viscosity development in Derakane 411-C-50 at different isothermal cure temperatures.

Table 6. DMA results for Derakane 411-C-50.

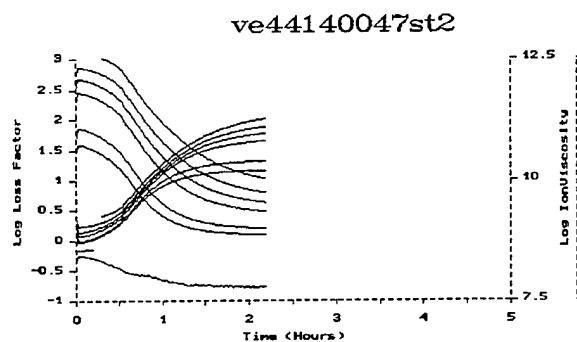
Cure Temperature (°C)	T _g (°C)
30	58
40	66
50	76

4.3.1 Effect of Styrene

Figure 33 illustrates the effect of styrene concentration on the dielectric cure behavior of Derakane 441-400 at an isothermal cure temperature of 40 °C. As a general observation, the time period at which the loss factor and the ion viscosity levels off gets shifted further along the time axis with increased styrene concentration. This observed behavior qualitatively follows similar observations in the case of DC behavior. However, a quantitative comparison of the time scale at which the log-loss factor levels off to that at which SW signal ceases indicates that the SW signal ceases much earlier than the former. This is due to the fact that the DC signal is a measure of long-range motion of ions towards one of the electrodes. However, dielectric behavior is a measure of the possibility of short-range molecular motion (i.e., dipolar rotation). Therefore, during cure,



(a)



(b)

Figure 33. Effect of styrene on Derakane 441-400 cured at 40 °C using dielectric cure monitoring at (a) 28 weight-percent styrene, and (b) 47 weight-percent styrene concentration.

the formation of a 3-D network impedes and, possibly prevents, long-range transport of ions. However, dipolar rotation continues for a longer time scale. A comparison between the dielectric signal with the fractional conversion of monomers obtained from FTIR reveals that the dielectric signal levels off much earlier than the FTIR signal. This is due to the fact that long after dipolar rotation ceases to be possible, reactions between the contiguous monomers continue to occur.

Therefore, one can compartmentalize molecular mobility into three regions. The first region is characterized by the possibility of long-range motion. The second region extends until short-range dipolar rotations cease. The third region is characterized by the possibility of further reaction between contiguous monomers leading to an increase in fractional double-bond conversion.

SW is an effective online monitoring tool owing to its sensitivity to long-range molecular motion. As discussed in section 1.3, the SW signal dies soon after

vitrification for the reasons previously discussed. This is a significant feature of SW for cure monitoring of processes, since the onset of vitrification is an important processing parameter related to part removal and cycle times.

4.3.2 Effect of Temperature

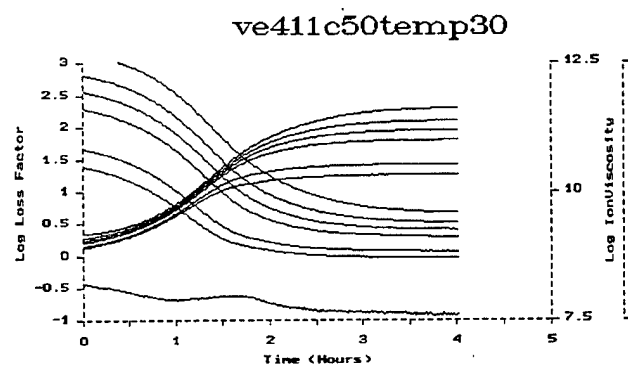
Figure 34 presents the dielectric response of Derakane 411-C-50 cured at different isothermal cure temperatures. The qualitative responses follow similar behavior as observed in the case of a DC signal with loss factor and ionic viscosity leveling off earlier for low-temperature cures. The quantitative comparison follows the argument discussed in section 4.3.1.

Figure 35 presents the ionic conductivity obtained from dielectric measurements for the case study at 30 °C. It is seen that the drop in ionic conductivity very much follows time-scale trends previously discussed. However, the time at which ionic conduction ceases differs widely from that of the SW signal. A clearer comparison between the sensitivity of SW and the dielectrometer to molecular level events can be obtained from Figure 36 that shows the conductivity observed by SW alongside that derived from dielectric measurement at 2.5 Hz for Derakane 411-C-50 cured at an isothermal temperature of 30 °C. It is seen that SW data undergoes much larger changes in conductivity corresponding to gelation and vitrification as compared to the dielectrometer measured ionic conductivity, which remains roughly a straight-incline line. This comparison illustrates one of the advantages of DC signal over AC measurements, where greater sensitivity to cure behavior is demonstrated early in the cure. The greater sensitivity of SW makes it ideal for integration into control systems.

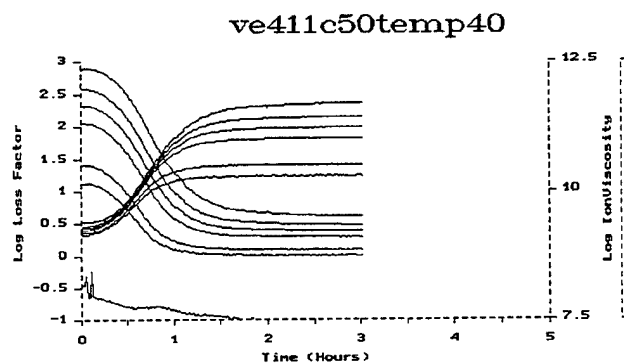
Tables 7 and 8 compare the maximum degree of conversions respective to when the DC and AC signals cease to yield further information. From Tables 7 and 8, it can be seen that the AC technique remains sensitive to the degree of conversion for a larger range of α , whereas the DC signal ceases early in the cure. It can be inferred that the dielectric related ionic conductivity gives information on the degree of conversion for a longer range of α as compared to DC-based ionic conductivity. So dielectric cure monitoring holds promise as an effective point sensor for cure monitoring in the later stages of cure.

4.4 Section Summary

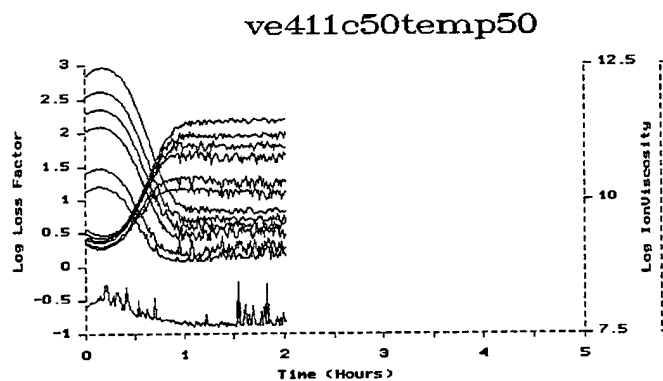
A study of the effect of styrene concentration on the SW behavior of 441-400 revealed that the slower rate of reaction with increased styrene content gets manifested as delayed gelation (inflection in the SW data) and delayed SW cutoff. Comparison of viscosity data confirms that the gelation time scales are consistent with the DC inflection point. Glass-transition temperature, T_g , data



(a)



(b)



(c)

Figure 34. Dielectric cure monitoring of Derakane 411-C-50 at isothermal temperatures of (a) 30°, (b) 40°, and (c) 50 °C.

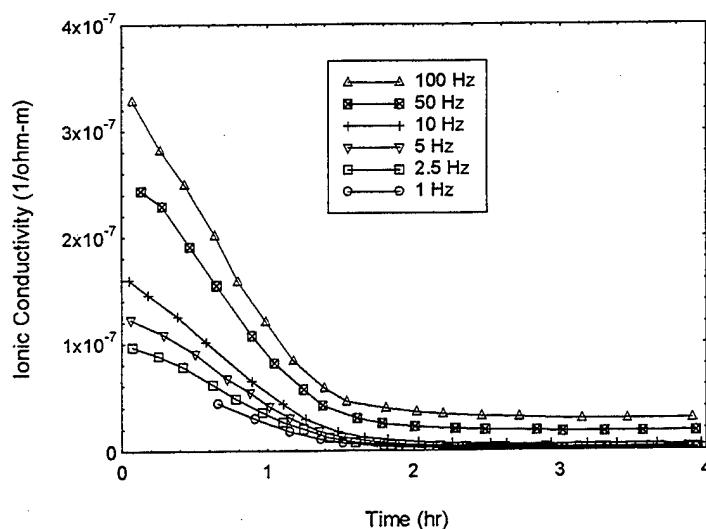


Figure 35. Ionic conductivity from dielectric measurements on Derakane 411-C-50 at 30°C isothermal cure temperature.

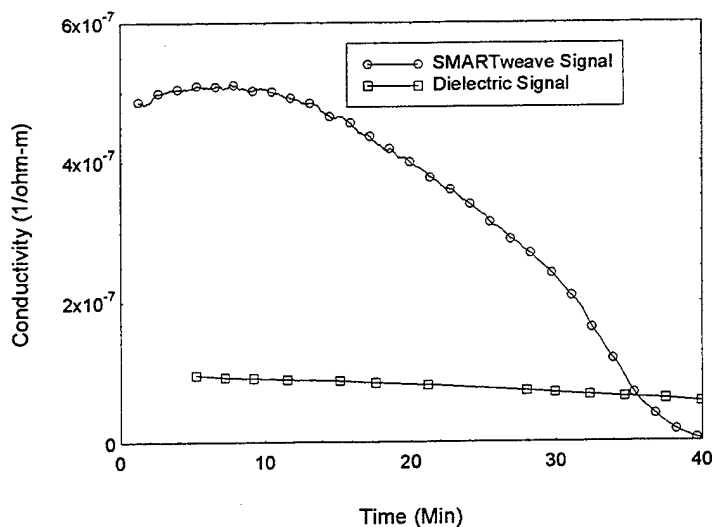


Figure 36. Comparison of SW behavior of ionic conductivity with dielectric behavior of Derakane 411-C-50 at 30 °C cure temperature.

for different styrene concentrations revealed differences in the cross-linking density between the resin compositions conforming to the observed differences in the SW cutoff point. This illustrates the fact that styrene, despite being electrically inert, significantly affects the SW behavior by being an inherent part of the network formation.

Table 7. Maximum conversion of 411-C-50 from DC and AC cure monitoring.

Cure Temperature (°C)	α_{\max} DC Monitoring	α_{\max} AC Monitoring
30	0.129	0.637
40	0.275	0.63

Table 8. Maximum conversion of 441-400 from DC and AC cure monitoring.

Styrene Concentration (weight-percent)	α_{\max} DC Monitoring	α_{\max} AC Monitoring
28	0.152	0.524
47	0.069	0.610

Temperature effects on 411-C-50 reveals faster reaction rates leading to faster gelation times with increased cure temperature as confirmed by the viscometer data. However the SW cutoff happens at a later time for higher temperatures. A comparison of the T_g revealed an increase in the cross-linking density with cure temperature. Hence one can conclude that the differences in the SW cutoff is due to the increased mobility induced by higher thermal energy, which overcomes the negative effect of cross-linking on the molecular mobility.

Dielectric behavior of both 441-400 and 411-C-50 followed the SW behavior qualitatively. However, owing to differences in the parameter being measured, quantitative differences were observed. SW, due to its better sensitivity to cure events like gelation and vitrification, is an effective tool for cure monitoring in the early stages of the cure. However, the dielectric signal far outlasts the DC signal, enabling its use for cure monitoring in the later stages of cure. A combination of SW, dielectric and FTIR techniques could be used to follow the different scale of possible motions with the proceeding of cure.

The experimental results discussed in this section, along with cure kinetics measurements provided in section 3 are used as the basis for developing a free-volume continuum model as shown schematically in Figure 7. In section 5, the role of microgels is investigated to understand their influence on the ionic conductivity. Cure kinetic data along with cure monitoring results are used to investigate the feasibility of a percolation-based continuum model.

5. Characterization of Microgels

5.1 Introduction

This section investigates the influence of microgels on the ionic conductivity of VE resins. Microgels are highly cyclized and cross-linked spherical entities, whose number increases with cure. As discussed in section 1.5, the increase in the number of microgels forces the conducting ions to travel increasingly tortuous paths around the microgels to reach the electrodes. This results in a decrease in the observed ionic conductivity with cure. The percolation-based continuum model investigated in this section takes into account the increasing volumetric contribution of the microgels with cure, as illustrated in Figure 7.

The Flory-Stockmayer theory [13] has been in use for over 50 years to predict and understand the gelation mechanisms. Using combinatorial arguments, Batch and Macosko [24] were successful in predicting both the gel point and the weight-average molecular weight of the branched aggregates at gel point. Flory coined the term "infinite network" to describe the resulting network formation at gel point. The network reaches a macroscopic dimension by occupying the entire volume of the reacting sample itself. Since, on the molecular level, the network is unbounded, it is referred to as an infinite network.

Experiences with styrene-unsaturated polyester resins and vinyl-divinyl systems, however, seems contradictory to the previously mentioned gel point predictions [32, 26, 27]. The measured gel point conversion for these systems was far greater than Flory-Stockmayer predictions. Dusek and Spevacek [26] and Dusek et al. [27] have shown that predominant cyclization is observed in the beginning stages of the reaction involving free radical polymerization systems. Dusek and colleagues described such cyclized structures with high cyclization and cross-linking density as "microgels." Owing to heavy cyclization, the reactive end groups of the polymer chains are physically tucked away, disabling further participation of these end groups in the reaction process. The molecular shielding plays an important role in the free-radical polymerization reaction and is a possible cause for the final conversion of the reacting monomers to fall short of 100%. Dusek and colleagues found that the deviation from the Flory-Stockmayer theory increased with the increase in the concentration of multifunctional monomers. They showed that in a copolymerization reaction involving monovinyl and divinyl components, the deviation from the Flory-Stockmayer predictions increased with the increase in concentration of the divinyl component. Three factors are held responsible for the previously mentioned deviation: (1) cyclization, (2) reduced reactivity of the pendant vinyl reactive groups, and (3) microgel formation. In the case of heavily cyclized

structures, these three causes occur simultaneously in that cyclization leads to the formation of microgels which are then responsible for molecular shielding of the pendant double bonds leading to an apparent reduction in the reactivity of the pendant vinyl groups.

5.2 Background

At the beginning of a copolymerization reaction involving styrene and unsaturated polyester resins, the system contains styrene monomers, unsaturated polyester molecules, and inhibitors. When the reaction starts, the initiators decompose and form free radicals to trigger polymerization. At the very beginning of the reaction, most of the free radicals formed from the initiators are immediately consumed by the inhibitors. Very little polymerization occurs due to the inhibition effect at this stage, which is called the induction stage.

After this stage, the initiators continuously decompose creating free radicals which link adjacent unsaturated polyesters and form primary polymer chains through connecting styrene monomers by both inter- and intra-molecular reactions. These long chain molecules tend to form spherical structures due to the intra-molecular cross-linking among the pendant C=C double bonds of the polyester molecule leading to the formation of the microgels. Because of the high cross-link within the microgel, the free radicals on the polymer ends are likely to be buried in the microgels. This means that termination among the polymer radicals may not be an important factor and can be neglected.

As the polymerization proceeds, the concentration of the microgels increases continuously. This leads to macrogelation in the system. This mechanism is illustrated by several key steps in Figure 37. Since gel conversion is very low for radical chain-growth polymerization reactions, it is difficult to relate gelation to the resin conversion or molecular weight. For the case of chain copolymerization involving Derakane 411-C-50 and styrene monomers, the conversion predicted by the Flory-Stockmayer theory [13] has been calculated by Dua [10] to be 0.2 volume-percent. However, the volume conversions at gelation, based on viscosity measurements, normally fall in the range of 10 volume-percent. This large discrepancy in the conversion values suggests the occurrence of similar cyclization phenomenon. Also, an observation of the T_g - α relationship of curing VE 411-C-50 obtained by Stone [11] suggests that during cure, for a large range of α , the T_g remains nearly the same. This is contrary to epoxy systems where the T_g increases linearly with cure α , since microgel formation does not appreciably increase the T_g of the curing system.

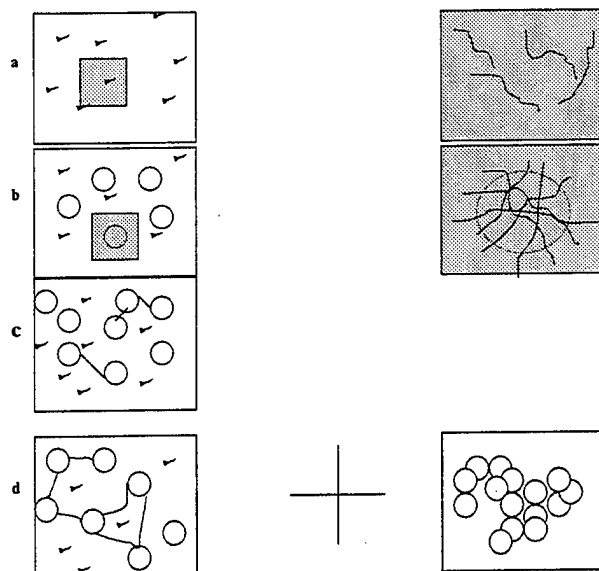


Figure 37. Illustration of cross-linking polymerization (a) at beginning, (b) initiation, (c) reaction in progress, and (d) possible gelation schemes.

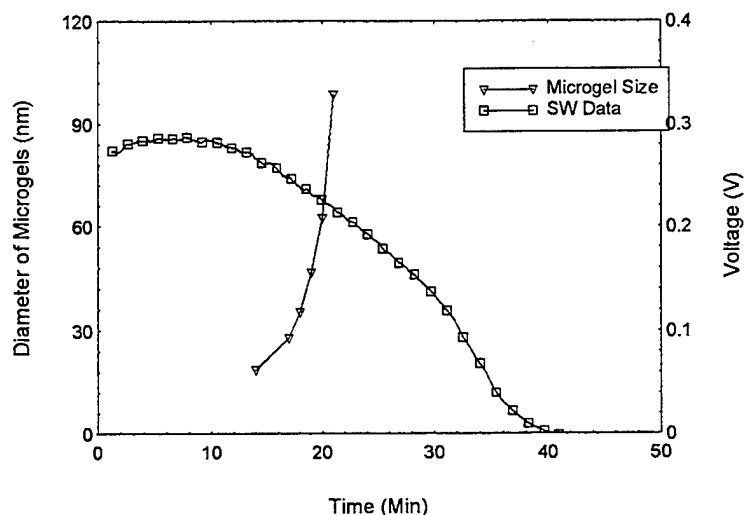
The abnormal behavior of 411-C-50, therefore, indicates a minimal increase in the cross-linking density and an increase in the volume fraction of microgels. This study attempts to characterize these microgels for possible influence on ionic conductivity.

5.3 Results

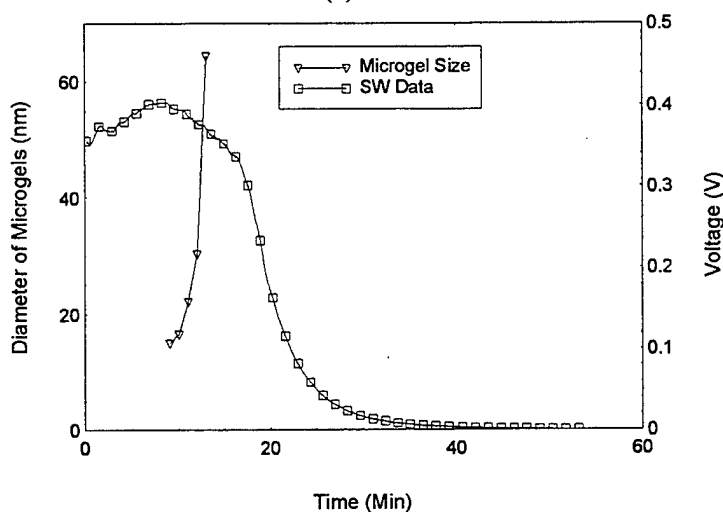
Section 5.3.1 investigates the role of microgels on the ionic conductivity. A comparison of the growth of microgels with a decrease in the DC signal indicates a coupling between the two events. Section 5.3.2 presents the preliminary results on the chemical characterization of microgels. A thorough understanding of the chemical composition of microgels would enable identification of the chemical composition of the unreacted resin and the network development surrounding the microgels. Section 5.3.3 deals with the AFM analysis of microgels to obtain an insight into the size and number density of the microgels. The microgel size is used as input for the percolation-based model presented in section 5.4.

5.3.1 Comparison of Microgel Growth Kinetics with SW Data

Figures 38 and 39 show the change in size of microgels as observed using dynamic light scattering (DLS) experiment [10] as compared to the simultaneous change in the DC signal observed by the SW setup. A detailed discussion on



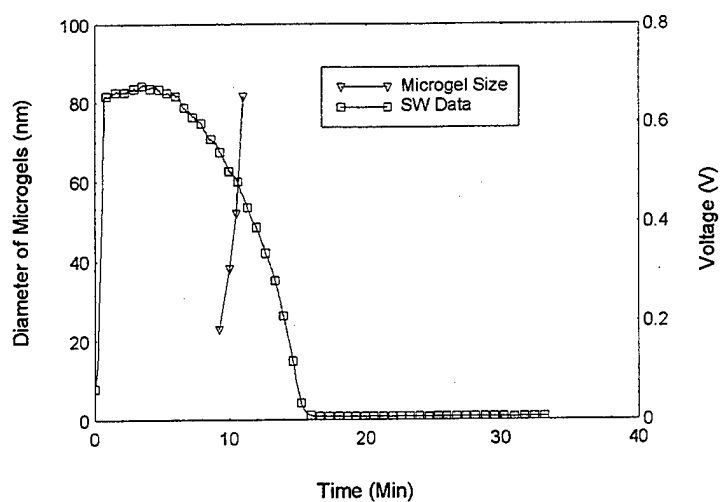
(a)



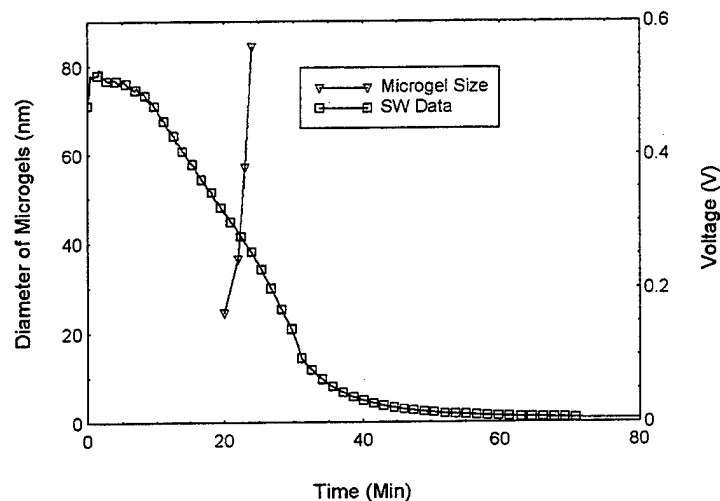
(b)

Figure 38. Influence of microgels on SW behavior of 411-C-50 for (a) 30° and (b) 40 °C, respectively.

DLS and sample preparation are found elsewhere [22]. An interesting observation is that these microgels rapidly increase in size at the same time when one observes a drastic drop in the SW voltage. This time range coincides with the occurrence of macrogelation as observed from the viscometer data (Figures 28 and 32). This essentially indicates the importance of microgel in the development of macroviscosity and hence SW signal. As discussed in section 1, ionic conductivity is significant beyond gelation. The role of microgels on ionic conductivity is investigated in section 6.



(a)



(b)

Figure 39. DLS data showing influence of microgels on SW response of 441-400 at (a) 28% and (b) 57% styrene.

5.3.2 Separation of Microgels

Figures 40–42 show the HPLC responses for pure styrene, pure VE and fractionated sample of microgels, respectively. The VE peak and styrene peak occur around 875 s and 1,100 s, respectively, along the time axis. After multiple cycles of dissolving followed by precipitation of microgels in order to remove the unreacted monomers, the fractionated high molecular weight microgel and the effective removal of the VE and styrene monomers can be observed in Figure 42.

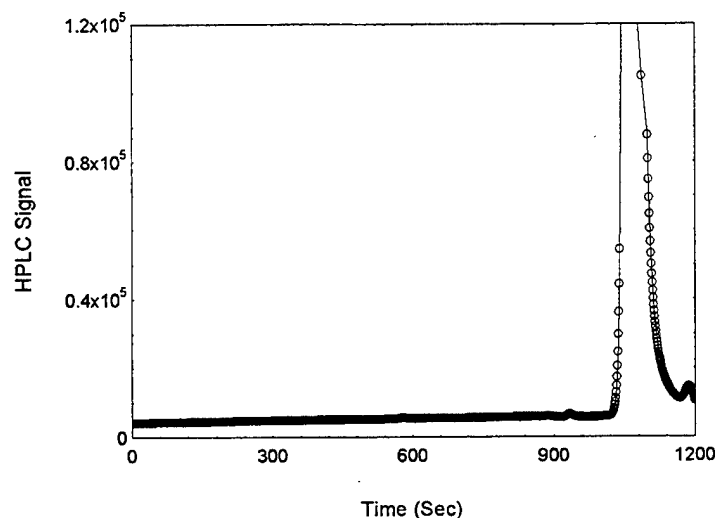


Figure 40. HPLC response (in μV) of pure styrene.

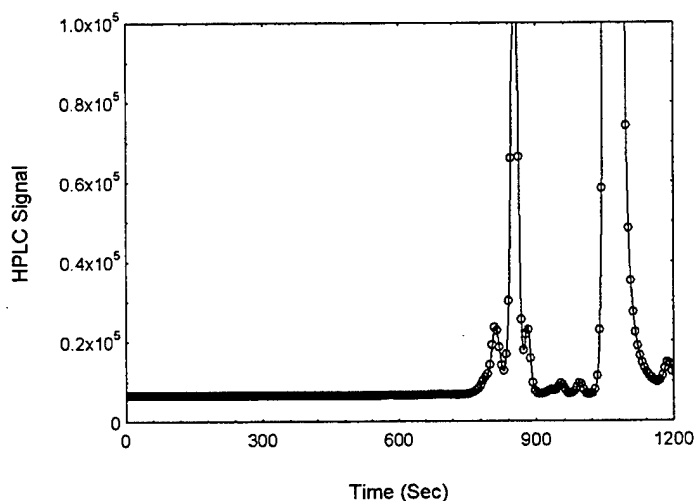


Figure 41. HPLC response (in μV) of pure unreacted VE825 with 28 weight-percent styrene.

Figure 43 shows the FTIR spectra of curing VE825 [33] at an isothermal temperature of $40\text{ }^{\circ}\text{C}$. When it is compared with Figure 44 showing the FTIR spectra of the fractionated microgel, one observes an anomalous decrease in the peak height at 700 cm^{-1} as compared to the one at 910 cm^{-1} , which remains a topic for future work. The peak at 910 cm^{-1} appears slightly shifted and is observed to occur at 900 cm^{-1} . A comparison of the reference peaks of VE at 830 cm^{-1} and styrene at 700 cm^{-1} indicates a predominance of VE in the fractionated microgel as compared to the reacting mixture. This confirms the

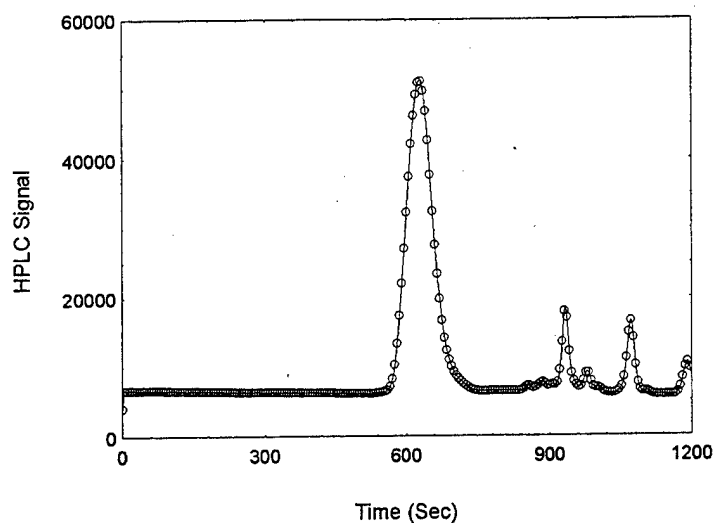


Figure 42. HPLC response (in μV) of fractionated microgels.

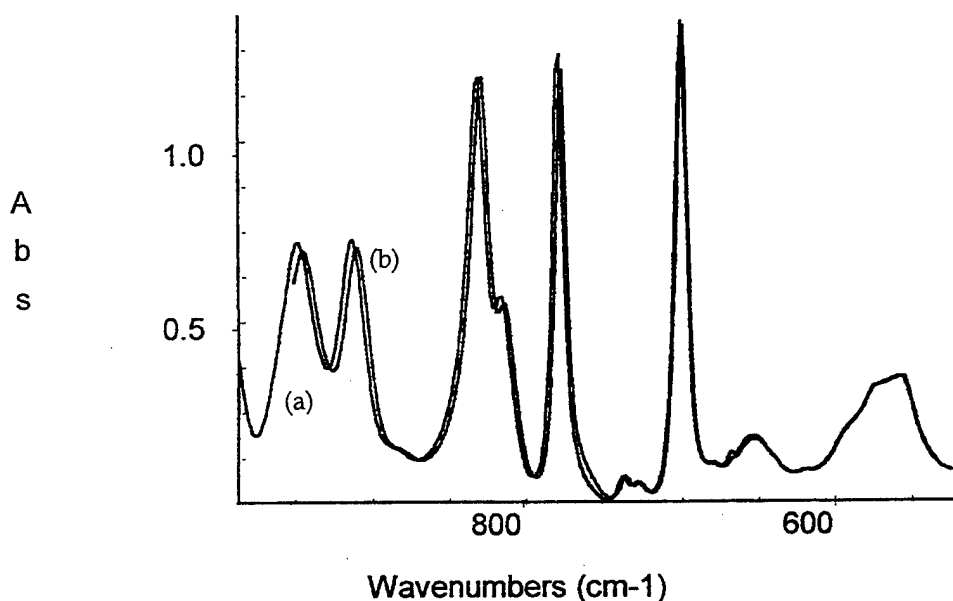


Figure 43. FTIR spectra of VE825 (a) at the beginning of cure and (b) at 9 min at 40°C cure temperature.

hypothesis that microgels are highly cyclized and densely cross-linked structures, since only VE monomers can act as cross-linkages. The separation of the microgels and the FTIR spectra of these fractionated microgels were not a reliably repeatable phenomenon. Of the multiple successful attempts at microgel separation, the FTIR spectra qualitatively agrees with the above mentioned sample results. However, quantitatively, they showed a high degree of

Table 3. Tapping mode specifications.

Drive Frequency Range	10 kHz–1MHz
Drive Voltage Range	0–20 V
Drive Amplitude and Frequency Adjustment	Software Controlled
Detector	RMS to DC Amplitude Detector
Cantilevers	Etched Silicon Cantilevers 60–400 kHz Resonant Frequencies
Tip-Sample Approach	Motorized Sample Approach

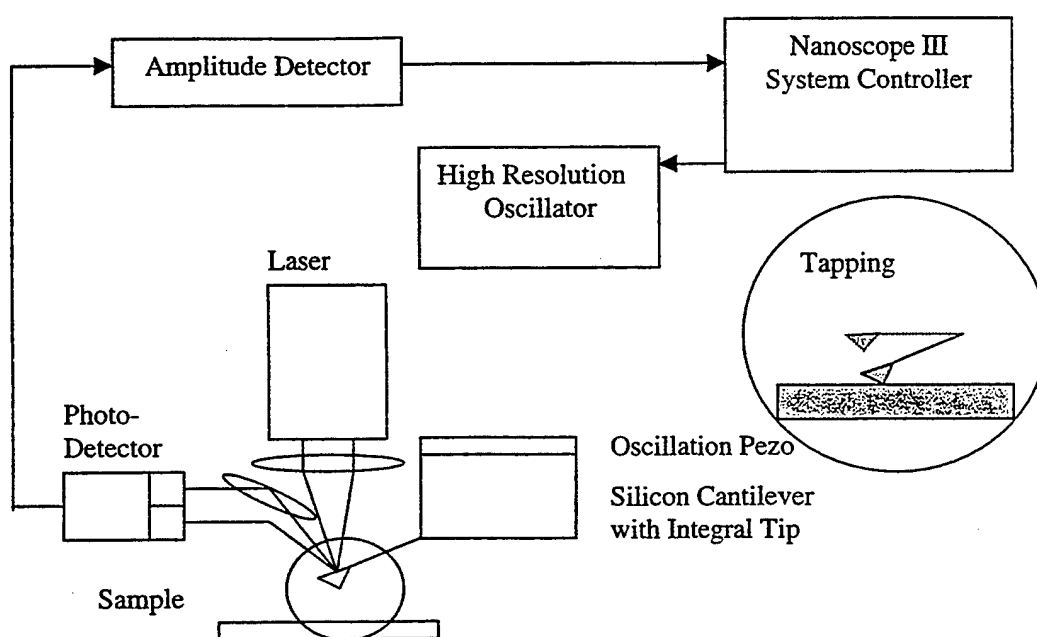


Figure 19. Block diagram for tapping mode operation.

3. Cure Kinetics of VE Resins

3.1 Introduction

A thorough understanding of the SW signal or that of any other cure monitoring technique, requires a comprehensive understanding of the molecular events associated with curing. This section analyzes some of the parameters that must be considered to develop the continuum model for ionic conductivity. As presented in Figure 7, cure kinetic studies are the first step in the development of the model. Using the experimental techniques described in section 2, it becomes possible to understand the effects of initial concentration of styrene and cure temperature on the cure processes and their relationship to ionic conductivity.

Thermal analysis using DSC has been used extensively by other researchers in both isothermal and nonisothermal mode to study the cure kinetics of the resin. However, DSC suffers from a disadvantage of not being able to yield any information regarding the degree of conversion of the individual components (i.e., VE and styrene) in the reacting mixture. Since the objective of this research work was to obtain as much information as possible regarding the individual components, FTIR was employed to obtain the degree of conversions of VE and styrene individually.

In this work, emphasis has been placed on understanding the effects of styrene concentration, temperature and molecular weight on cure kinetics. A thorough understanding of the previously mentioned factors is an important prerequisite in developing the conductivity model described in Figure 7.

3.2 Cure Kinetics Using FTIR

Figure 20 shows typical FTIR data of the degree of conversion of VE double bonds and styrene double bonds with time. The degree of conversion is expressed here as the percentage ratio between the number of double bonds consumed and the initial number of double bonds. Therefore, care should be taken in comparing the conversion data between different species and for different FTIR runs. As mentioned before, VE has two reactive double bonds whereas styrene has just one. When a double bond reacts, it could be the first double bond of a new VE monomer or it could be the second double bond of an already reacted and, hence, bound to the network VE monomer. In short, the double bond conversion of the VE monomer is not the same as the double conversion obtained from FTIR. Figure 20 shows three distinct regions.

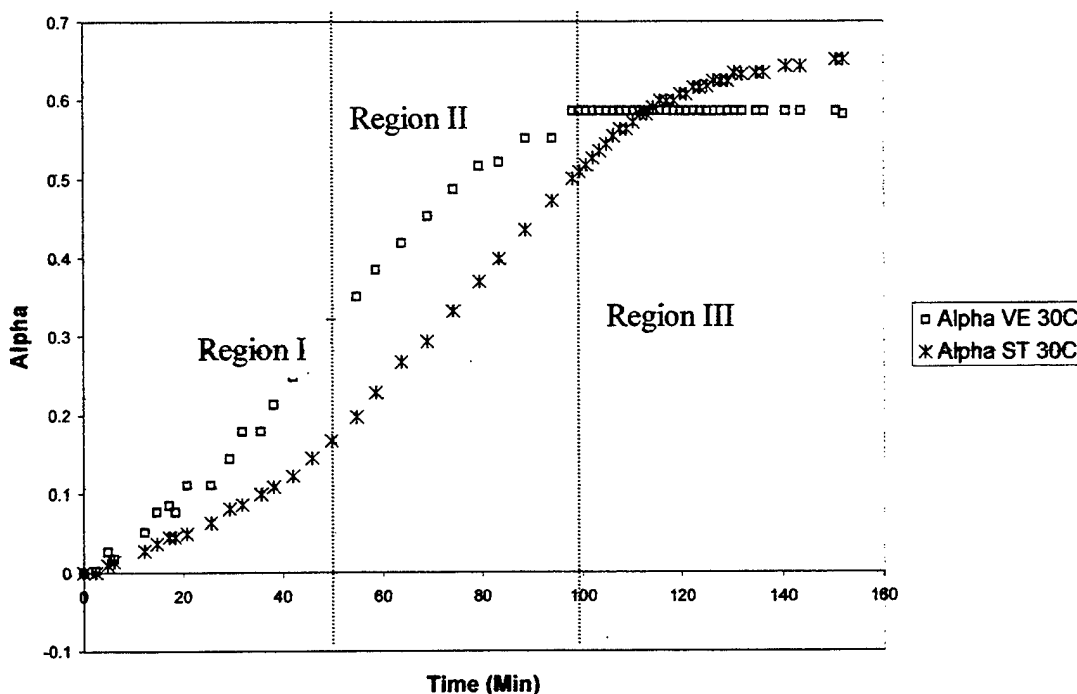


Figure 20. Typical profiles of VE and styrene double-bond conversion.

It should be noted however that the boundaries of these three regions are not definitive and they are likely to be quite diffuse. In Regions I and II, the conversion of the VE double bonds is greater than the conversion of the styrene double bonds. In Region III, VE plateaus can be seen, while styrene conversion continues and eventually exceeds the final VE conversion. In Region I, the reaction kinetics are determined by the reactivity ratios of VE and styrene. The higher conversion of VE suggests that the VE double bonds have a higher affinity to react with the free radicals as compared to the styrene double bonds [10, 15]. In Region II, due to gelation, the bimolecular termination rate is lowered due to the decrease in mobility of the growing radical species. The hindered bimolecular termination results in an increase in the concentration of the free radicals and accelerates the reaction. This effect is termed the Trommsdorf effect [24, 25]. In Region III, the diffusional limitations play a significant role. With the onset of vitrification, the serious restrictions placed on the molecular mobility is said to be the reason for the final conversion not being able to reach 100% [24, 25]. The higher final conversion of the styrene double bond suggests that since styrene is a smaller molecule compared to the VE monomer, it would be better able to diffuse to reactive sites.

An important feature of many free-radical, chain-growth, cross-linking copolymerization systems is the formation of localized, highly cross-linked, submicron size regions called microgels [26, 27]. These microgels are in the range of 100–150 nm in diameter and come into existence in the sea of VE resin,

almost instantaneously (as compared to the time scale of the curing process) [28]. With the proceeding of cure, the number of microgels in the reacting mixture increases with time, as opposed to the classical nucleation theory, where nucleation occurs simultaneously and the nucleated sites grow in size with time. Consequently, microgel formation is highly heterogeneous in nature. Another important factor that is believed to strongly affect the cure behavior of VE resins is the phase separation of the macromolecules from the unreacted monomers. Based on theoretical thermodynamic calculations, Palmese [28] and Ziaee [29] suggested that there is a high probability of phase separation in VE resins due to enthalpic contributions.

3.3 Effect of Styrene Concentration

Figures 21 and 22 show the effect of styrene concentration on the fractional conversions of VE and styrene double bonds for Derakane 441-400. The reactions were performed at 28%, 37%, 47% and 57% by weight of styrene. Owing to better temperature control available at 40 °C, all the reactions were conducted isothermally at 40 °C with 1.0 weight-percent Trigonox and 0.2 weight-percent CoNap. From the observation of Figures 21 and 22, it is clear that the initial conversion of VE double bonds decreases with an increase in the styrene concentration as is the case of styrene double-bond conversion. The same effect was observed by researchers working with DSC on similar systems [24]. The initial decrease in the VE conversion can be explained based on the fact that with increasing concentration of styrene, the VE concentration decreases leaving fewer VE double bonds to participate in the cure reaction. Dua [10] argues that the seemingly strange decrease in the reaction rate with an increase in the styrene content is due to the fact that the reactivity ratio of the VE monomers is higher than that of the styrene monomer. Therefore, the VE monomers react faster with the primary free radicals to give VE chain radicals which, in turn, react with the styrene monomers. This phenomenon explains why an increase in the styrene conversion with increasing VE concentration is observed, or conversely, why the styrene conversion decreases with increasing styrene content in the reacting mixture.

Lee and Lee [30] and Dua [10] have observed the formation of polystyrene during the latter stages of the cure and at higher styrene concentrations (47% and 57%). They attribute the formation of this homopolymer to the phenomenon of phase separation. Two phases are said to form during the course of copolymerization. The first phase essentially is the copolymer network swelled by the unreacted VE monomer and, perhaps, residual styrene monomers. The second phase essentially is made of unreacted styrene. It is hypothesized that even though copolymerization stops in the first phase due to vitrification of that phase, the homopolymerization continues in the styrene-rich second phase.

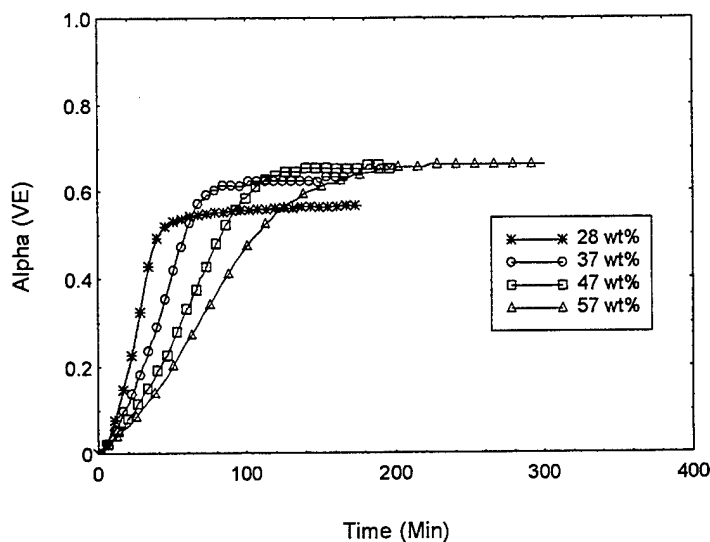


Figure 21. Fractional conversion of VE double bonds in Derakane 441-400 cured at 40 °C.

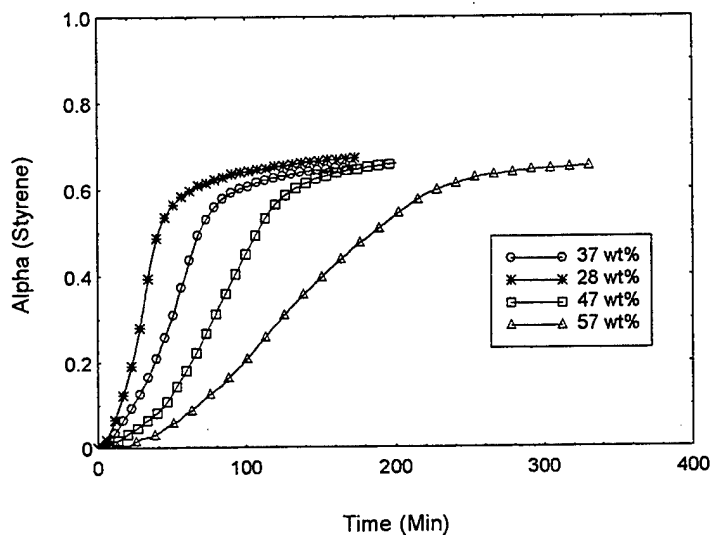


Figure 22. Fractional conversion of styrene double bond in Derakane 441-400 cured at 40 °C.

Dua [10] hypothesized that the copolymerization reaction could result in the formation of the microgels which are responsible for trapping a large number of the pendant VE double bonds due to the compactness of the microgel structure. The microgels are rich in VE and are surrounded by the styrene-rich region.

From Figures 21 and 22, it becomes apparent that the final conversion of the VE double bonds increases with the increase in styrene concentration, whereas in the case of styrene double-bond conversion, there seems to be no significant change in the final fractional conversion with styrene concentration. Similar results have been reported by Dua [10] and Brill and Palmese [21] for the same resin system. They argue that with an increase in the concentration of styrene, more styrene gets incorporated in the network leading to loosely networked structure. In other words, it leads to a structure with lower cross-linking density. This basically facilitates better mobility of the VE monomers enabling them to reach the reactive sites, hence, a higher final fractional conversion is achieved. The seemingly contradictory constant final fractional conversion of styrene is explained by the fact that the methacrylate groups of VE reacts faster and reach their maximum conversion much earlier than styrene (see Figures 21 and 22). This results in the onset of vitrification. The vitrified system may not allow the free diffusion of the styrene monomer to reactive sites thereby sealing them off, leading to almost the same final conversion for styrene monomers. It is argued that the phenomenon of phase separation becomes a significant factor in case of styrene concentrations beyond 47 weight-percent leading to the formation of VE rich and styrene rich phases. Due to the phase separation, the effect of increased styrene concentration is not really felt by the VE monomers that are copolymerizing in the other phase thereby resulting in the same final fractional conversion of VE monomers irrespective of styrene concentration beyond 47 weight-percent. The previously mentioned hypotheses are verified for accuracy using DC cure monitoring and DMA in section 4.2. The experimental results show that for 37- and 47-weight-percent styrene systems, the cross-link density is higher than for 28- and 57-weight-percent styrene systems. This indicates that an increase in the initial concentration of styrene in the reacting mixture does not necessarily result in a loose network, suggesting various degrees of homopolymerization between the resin mixtures under consideration.

3.4 Effect of Temperature

Figures 23 and 24 show the effect of temperature on the cure kinetics of Derakane 411-C-50. CoNap at 0.2 weight-percent was used along with 2-weight-percent Trigonox to initiate the reaction. From Figures 23 and 24, it is apparent that the reaction rates and the final conversion for both VE and styrene monomers increases with an increase in the reaction temperature. This can be explained by the fact that the additional thermal energy enables higher diffusion of these monomers so that more monomers are able to reach the reactive sites at higher temperatures. Another observation is that the final conversion of styrene is higher than that of the corresponding VE monomer. As described in section 3.2, styrene monomers are better able to overcome the diffusional limitations

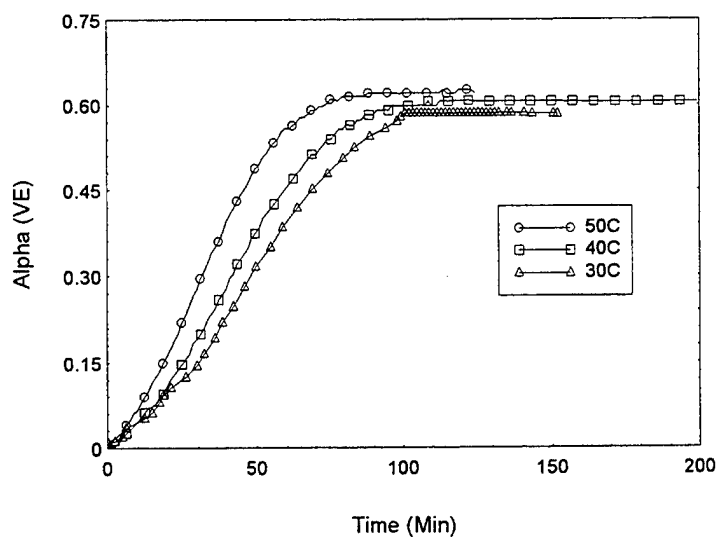


Figure 23. Fractional conversion of VE double bonds in Derakane 411-C-50 cured at isothermal temperatures of 30°, 40°, and 50 °C.

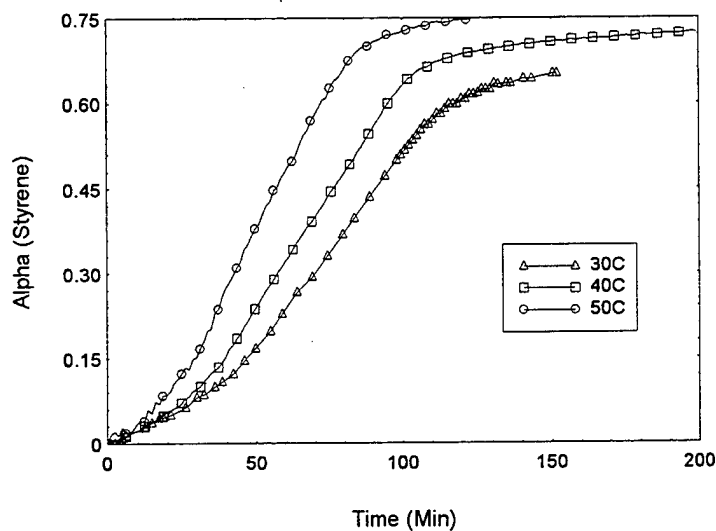


Figure 24. Fractional conversion of styrene double bonds in Derakane 411-C-50 cured at isothermal temperatures of 30°, 40°, and 50 °C.

imposed by network formation due to their relatively smaller size; the styrene monomers also exhibit higher final conversion. This, combined with the fact that one observes change in styrene fractional conversion long after the VE fractional conversion levels off, suggests polystyrene formation and hence a possibility of phase separation. Section 4 deals with the effect of temperature on the DC signal and how different aspects of the cure kinetics of Derakane 411-C-50 such as

development of cross-link density, formation of homopolymerised microgels and molecular mobility contribute towards the development of the continuum model presented in sections 5 and 6.

On comparison of the final fractional conversion of monomer double bonds of Derakane 441-400 (diluted to 47% styrene) maintained at 40 °C to that of Derakane 411-C-50 at 40 °C, one observes a higher VE fractional conversion in the case of 441-400 as compared to 411-C-50. As discussed previously, the VE monomers in 441-400 are of lower molecular weight as compared to those in 411-C-50 and hence exhibit higher mobility. However, the final fractional conversion of the styrene monomer in both cases is roughly the same owing to the fact that the styrene monomers are much smaller entities and the network structure does not restrict their mobility in both the cases. As will be discussed in section 4, the T_g value for 411-C-50 is much lower than that of 441-400, partly due to the higher fractional conversion of VE monomers.

3.5 Autocatalytic Kinetics Model Parameters

Autocatalytic kinetic models are widely used for fitting the experimental cure kinetic data for a number of VE and unsaturated polyester resins. For low temperature isothermal cure kinetics, the following relationship is widely used [30, 31]:

$$d\alpha/dt = (K_1 + K_2\alpha^m)(\alpha_{\max} - \alpha)^{2-m}, \quad (14)$$

where α is the fractional conversion at time t , α_{\max} is the maximum degree of conversion at that isothermal cure temperature, K_1 and K_2 are the reaction rate constants and m is the order of the reaction. This empirical reaction kinetic model is unsuitable for modeling the kinetic behavior as obtained from FTIR, which yields α rather than $d\alpha/dt$; so a modified form of the equation of the form is widely used:

$$d\alpha/dt = (K\alpha^m)(\alpha_{\max} - \alpha)^{2-m}. \quad (15)$$

This approximation is justified since K_1 values as obtained from DSC data (Table 2) are usually negligible as compared to the K_2 values. This expression can be integrated to yield α :

$$\alpha = \{\alpha_{\max}[Kt\alpha_{\max}(1 - m)]^{1/(1-m)}\} / \{1 + [Kt\alpha_{\max}(1 - m)]^{1/(1-m)}\}. \quad (16)$$

The autocatalytic parameters obtained from FTIR data for 411-C-50 [4] and 441-400 are presented in Tables 4 and 5.

3.6 Section Summary

The cure kinetics of Derakane 411-C-50 and Derakane 441-400 were studied using FTIR. Derakane 441-400 was used for the effect of styrene concentration studies as Derakane 411-C-50 already contains approximately 48 weight-percent

Table 4. Kinetic parameters corresponding to VE 411-C-50 FTIR data.

Temperature (°C)	30	40	50
VE Monomer			
K	0.00079071	0.0018584	0.0012285
m	0.63813	0.66051	0.55319
$\alpha_{\max}(\%)$	58.981	59.163	60.808
Styrene Monomer			
K	0.00055487	0.0010582	0.0015359
m	0.69773	0.68739	0.67882
$\alpha_{\max}(\%)$	66.149	71.794	69.308

Table 5. Autocatalytic parameters for FTIR data of VE 441-400 cured at 40 °C.

Styrene Concentration	28 weight-percent	37 weight-percent	47 weight-percent	57 weight-percent
VE Monomer				
K (min ⁻¹)	0.238	0.116	0.0652	0.052
m.	0.689	0.659	0.622	0.604
α_{\max}	0.562	0.650	0.699	0.684
Styrene Monomer				
K (min ⁻¹)	0.147	0.087	0.055	0.031
m.	0.653	0.660	0.688	0.656
α_{\max}	0.669	0.676	0.708	0.704

styrene. This section discusses the effect of styrene concentration on the network development during cure. Styrene-concentration effect, therefore, manifests itself as difference in the T_g development between different resin mixtures. The initial concentration of styrene also determines the degree of homopolymerisation during cure.

The temperature effects result in accelerating the cure kinetics of the resin mixture at higher cure temperature. Also, the T_g development with cure is different for different cure temperatures [11]. Since the modeling approach relies on either the volumetric contribution of the microgels (percolation approach), or on T_g development with cure (free-volume approach), the cure kinetics-related experiments provide valuable information towards the development and verification of the continuum model.

Generally, the rate of fractional conversion of the VE monomers is higher than that of the styrene monomers due to their higher reactivity. The final conversion of styrene was, however, always higher than that of the VE double bonds due to the fact that the diffusional limitations affect the mobility of VE monomers more than the styrene monomers based on the difference in the size and molecular weights of the monomers. As the temperature was increased, the final conversions of both the monomers increased owing to higher monomer mobility.

In the section 4, DC conductivity is measured and correlated with the kinetic data generated herein.

4. Cure Monitoring of VE Resin

4.1 Introduction

In this section, emphasis is placed on analyzing the cure signals obtained using SW and the dielectrometer. The signal is correlated to the FTIR data, viscometer data, and DMA data to establish the molecular events occurring during cure. A detailed description of the SW system and dielectric monitoring has been presented in section 1 and elsewhere [4].

Section 4.2 deals with the SW behavior. This section investigates the effect of styrene concentration in 441-400 and the effect of cure temperature on the SW behavior of 411-C-50. Section 4.3 deals with dielectric cure monitoring of 441-400 diluted to different concentrations of styrene content. This section also deals with effect-of-cure temperature on the dielectric response of 411-C-50. Section 4.3 compares and contrasts the dielectric behavior with SW behavior. Section 4.4 summarizes the results from this section.

4.2 SW Cure Data

This section discusses the DC cure monitoring results and their correlation to cure-related events discussed under section 3. Section 4.2.1 discusses the effects of styrene concentration, while section 4.2.2 deals with temperature effects.

4.2.1 Effect of Styrene

Figure 25 deals with the SW behavior exhibited by Derakane 441-400 diluted by (99% pure) styrene supplied by Aldrich Chemicals to a weight-percent of 28%, 37%, 47%, and 57% of styrene. Figure 25 reveals that the effect of styrene addition on the initial voltage is twofold. Firstly, the initial voltage of the system increases upon increasing the styrene content from 28 weight-percent to

37 weight-percent. However, upon further addition of styrene, the initial voltage of the resin system starts to decrease.

This seemingly contradictory behavior is explained by the fact that the styrene component of the resin system doesn't supply any of the conducting ions responsible for the observed conductivity behavior as shown in Figure 26. Therefore, an addition of styrene to the system is equivalent to diluting the concentration of the conducting ions supplied by the VE component of the resin system. This explains why an addition of styrene to the system results in a lower initial voltage. However, this doesn't explain the initial increase in the voltage from 28 weight-percent to 37 weight-percent styrene system. Figure 27 reveals that the viscosity of the resulting resin system after the styrene addition decreases with increasing styrene concentration. This reduction in viscosity can be interpreted as higher molecular mobility of the monomers and the conducting ions, resulting in higher initial voltages, consistent with the model of England [4] described in section 1.

The overall initial conductivity is therefore the result of these two competing effects and in case of 28 weight-percent to 37 weight-percent styrene system, the increase in mobility dominates the dilution effect due to the additional styrene, resulting in higher initial conductivity. On further addition of styrene to the system, the dilution effect governs over higher molecular mobility resulting in the reduced initial voltage observed in the experiments. Increasing ion concentration through doping has been investigated by England [4] by introducing 0.1 weight-percent of TA. Preliminary investigations conducted as a part of this research work involved the use of tetrabutyl ammonium iodide (TI), a cheaper alternative to TA, as dopants. A comparison of the TI based results with England's work has been presented under Appendix D.

From Figure 25, it is observed that the gelation of resin mixtures containing different concentrations of styrene gets shifted further along the time axis with increasing styrene content. The gelation in Figure 25 is given by the point of inflection in the SW profile as discussed in section 1.3 (Figure 5). The same trend is observed with SW cutoff. The viscosity data shown in Figure 28 confirms the fact that the gelation happens earlier in case of lower styrene systems. This is due to the fact that an increase in VE concentration results in an increased reaction rate as shown in the FTIR data (Figures 21 and 22) and shorter time to reach the gel point.

In order to understand the difference in the SW cutoff point (i.e., the point at which the SW signal drops to zero), a plot between degree of conversion and the styrene concentration at the instant when the SW signal becomes zero was constructed and is shown in Figure 29. From the graph, it can be concluded that the degree of conversion of both the VE and styrene monomers decrease initially followed by an increase with increase in the styrene content. This can be

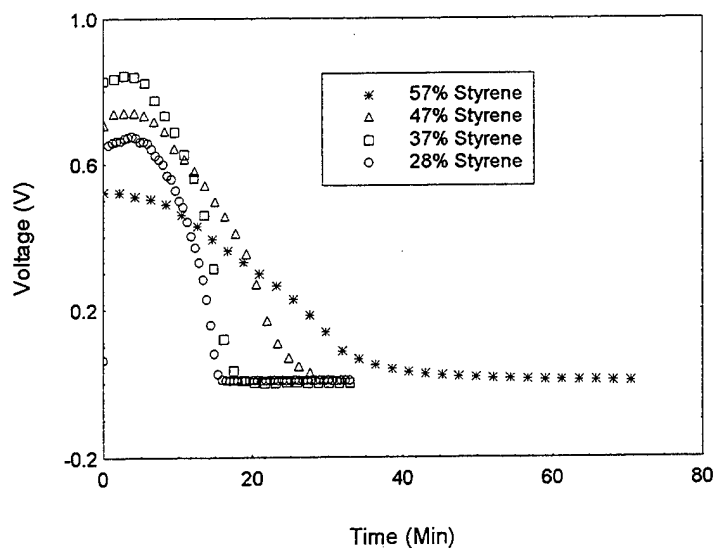


Figure 25. SW behavior of Derakane 441-440 cured at 40 °C.

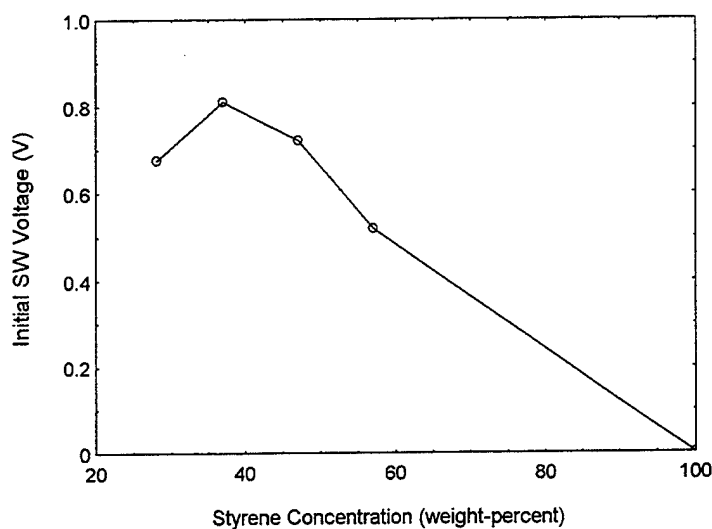


Figure 26. Initial DC signal vs. styrene concentration in Derakane 441-400.

explained: in the case of resin systems with 37 and 47 weight-percent of styrene, the cross-linking density is higher thereby cutting off the mobility of the conducting ions at a much lower conversion value. In case of 57 weight-percent styrene system, the presence of excess styrene results in the formation of a much looser network with long linear chains of styrene between the cross-links, thereby facilitating an increased mobility of the conducting ions.

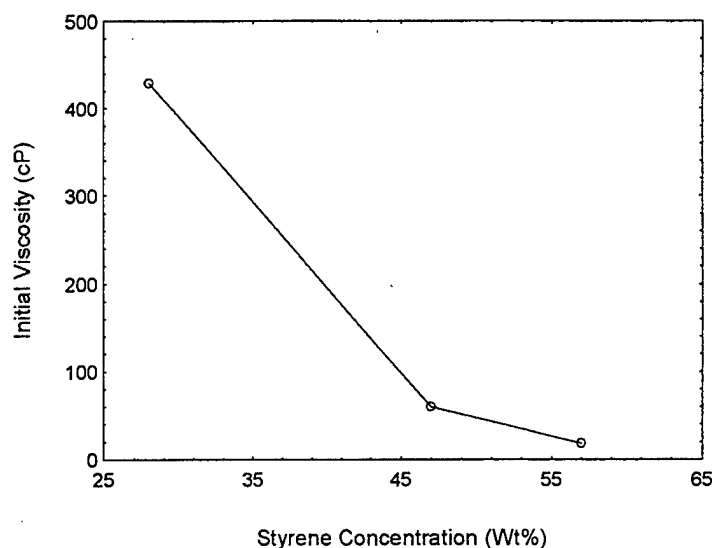


Figure 27. Initial viscosity vs. styrene concentration in Derakane 441-400.

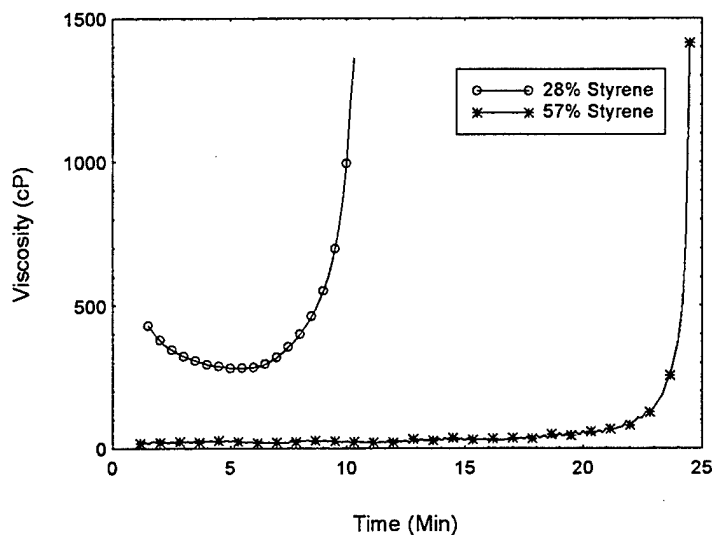


Figure 28. Viscosity development in Derakane 441-400 cured at 40 °C.

A confirmation of the previous hypothesis comes from analyzing the DMA data (T_g) of the corresponding systems. T_g is a measure of the cross-link density of the resulting network. It is clear from the T_g data of Derakane 441-400 presented in Figure 30, that indeed the cross-link density in the cases of 37 and 47 weight-percent styrene is higher than that of 28 and 57 weight-percent styrene, since T_g is an estimation of the cross-link density of the resulting network. Hence, it can be concluded that the addition of styrene, even though it is electrically inert, plays a very significant role in determining the SW behavior by way of being an inherent part of the polymer network and directly affecting the cure kinetics.

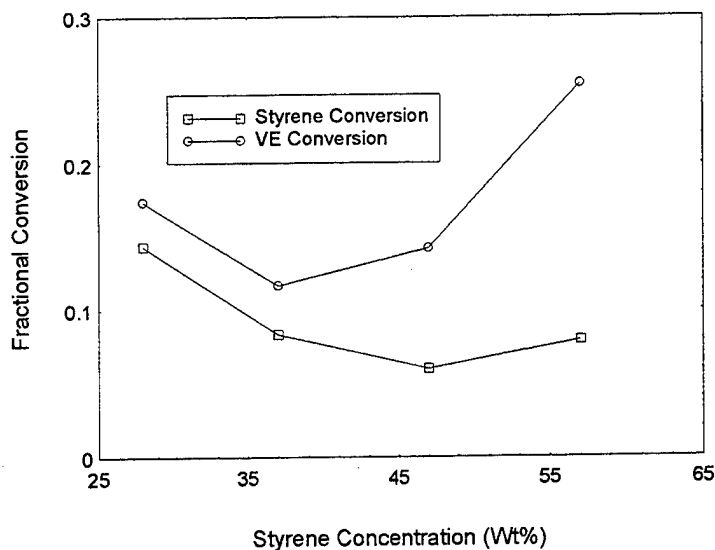


Figure 29. Fractional double-bond conversion vs. styrene concentration in Derakane 441-400 at DC signal cutoff.

4.2.2 Effect of Temperature

Figure 31 shows the effect of temperature on the SW signal for Derakane 411-C-50. A common feature observed in all of these figures is that the initial SW voltage increases with an increase in the temperature. This is due to the fact that the increase in temperature results in a decrease in the resin viscosity, which, as explained in section 4.2.1, results in an increased initial voltage.

Figure 31 shows that the resin systems cured at higher temperatures reaches the gel point sooner than the system cured at a lower temperature. However, the SW cutoff point occurs at a much longer time period for higher temperature systems. Figure 32 shows the viscometer data, which confirms that the gelation occurs sooner for higher temperature systems. A close inspection of Figures 23 and 24 shows that the reaction rates in the case of the higher temperature systems were indeed higher thereby resulting in gelation, much quicker than the system cured at lower temperature.

Table 6 shows the T_g data obtained by using DMA for all three cure temperatures. From Table 6, it becomes apparent that the cross-link density increases with the cure temperature that exerts a negative effect on the molecular mobility. However, the additional thermal energy imparted to the molecular mobility at higher temperatures, enables the ionic species to negotiate through the network for a longer time resulting in the SW signal being observed for longer times in high-temperature systems. So the dominating factor that determines the SW cutoff is the thermal energy, which results in increased mobility and decreased local viscosity.

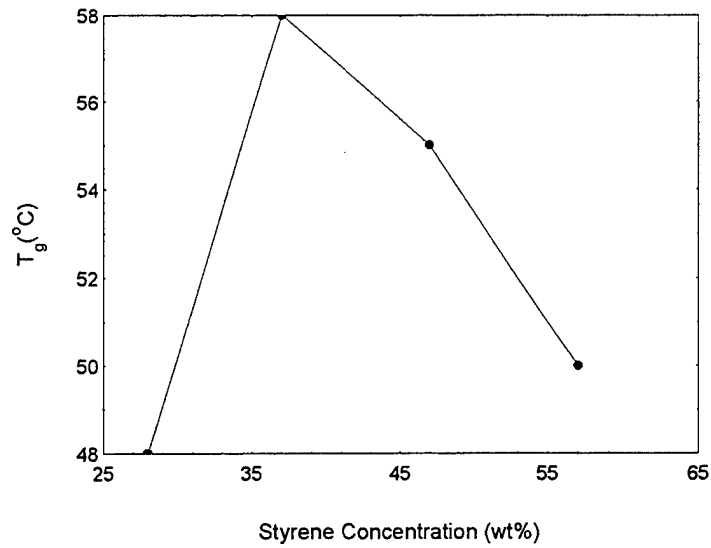


Figure 30. Glass transition temperature vs. styrene concentration for Derakane 441-400 resin.

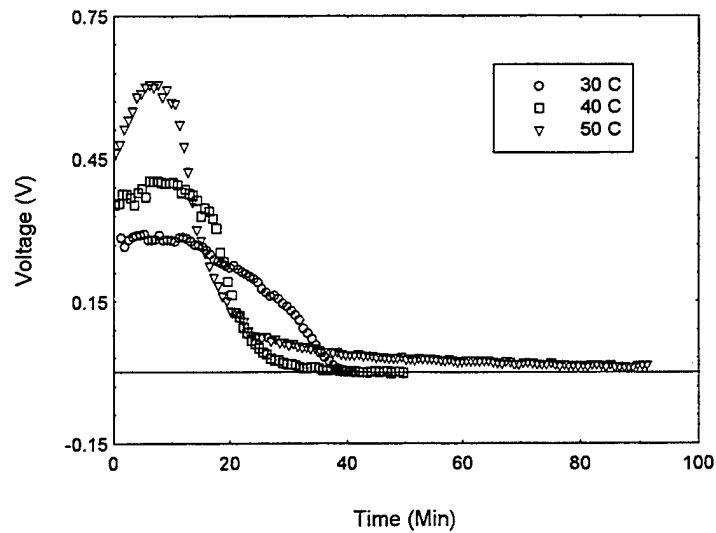


Figure 31. SW signal vs. time for Derakane 411-C-50 at different isothermal cure temperatures.

4.3 Dielectric Cure Monitoring

This research makes use of dielectric cure sensing in order to benchmark the performance of DC sensing for cure monitoring purposes. This section discusses the advantages and disadvantages of each system, delineating ways in which one technique can complement the other to obtain a better insight into cure related processes.

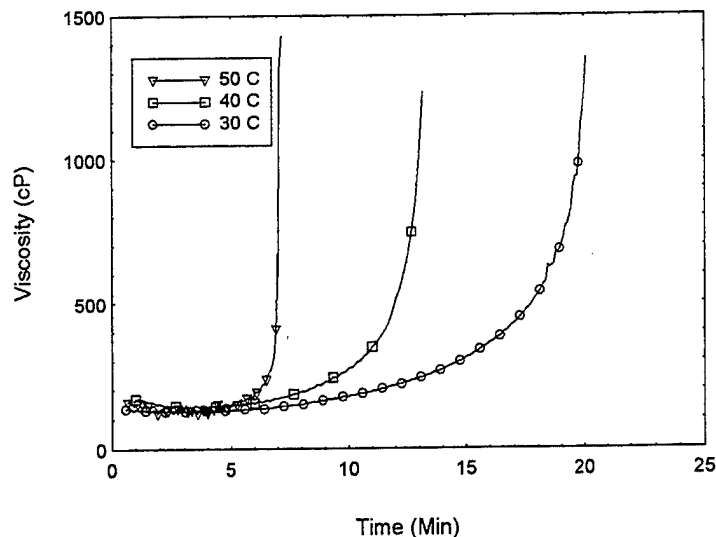


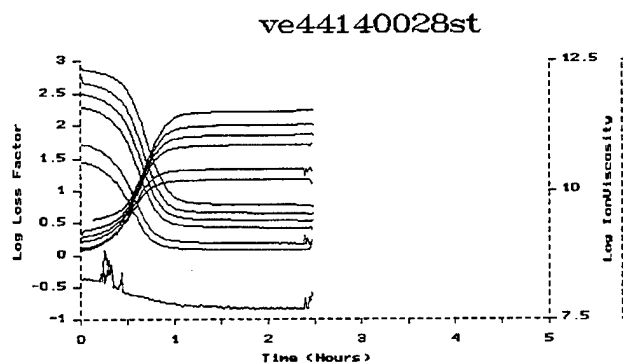
Figure 32. Viscosity development in Derakane 411-C-50 at different isothermal cure temperatures.

Table 6. DMA results for Derakane 411-C-50.

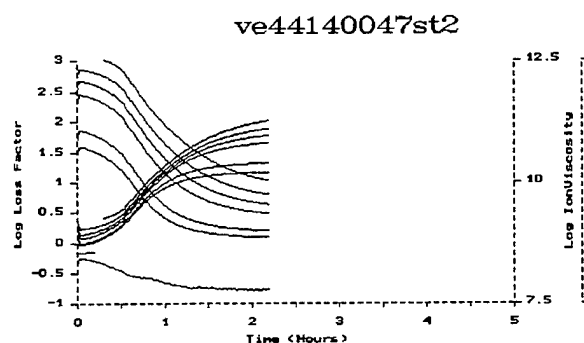
Cure Temperature (°C)	T _g (°C)
30	58
40	66
50	76

4.3.1 Effect of Styrene

Figure 33 illustrates the effect of styrene concentration on the dielectric cure behavior of Derakane 441-400 at an isothermal cure temperature of 40 °C. As a general observation, the time period at which the loss factor and the ion viscosity levels off gets shifted further along the time axis with increased styrene concentration. This observed behavior qualitatively follows similar observations in the case of DC behavior. However, a quantitative comparison of the time scale at which the log-loss factor levels off to that at which SW signal ceases indicates that the SW signal ceases much earlier than the former. This is due to the fact that the DC signal is a measure of long-range motion of ions towards one of the electrodes. However, dielectric behavior is a measure of the possibility of short-range molecular motion (i.e., dipolar rotation). Therefore, during cure,



(a)



(b)

Figure 33. Effect of styrene on Derakane 441-400 cured at 40 °C using dielectric cure monitoring at (a) 28 weight-percent styrene, and (b) 47 weight-percent styrene concentration.

the formation of a 3-D network impedes and, possibly prevents, long-range transport of ions. However, dipolar rotation continues for a longer time scale. A comparison between the dielectric signal with the fractional conversion of monomers obtained from FTIR reveals that the dielectric signal levels off much earlier than the FTIR signal. This is due to the fact that long after dipolar rotation ceases to be possible, reactions between the contiguous monomers continue to occur.

Therefore, one can compartmentalize molecular mobility into three regions. The first region is characterized by the possibility of long-range motion. The second region extends until short-range dipolar rotations cease. The third region is characterized by the possibility of further reaction between contiguous monomers leading to an increase in fractional double-bond conversion.

SW is an effective online monitoring tool owing to its sensitivity to long-range molecular motion. As discussed in section 1.3, the SW signal dies soon after

vitrification for the reasons previously discussed. This is a significant feature of SW for cure monitoring of processes, since the onset of vitrification is an important processing parameter related to part removal and cycle times.

4.3.2 Effect of Temperature

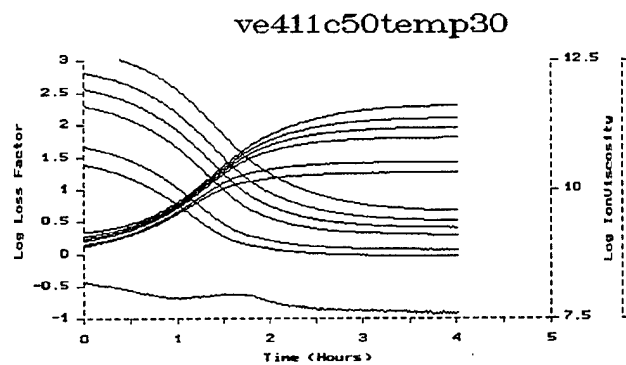
Figure 34 presents the dielectric response of Derakane 411-C-50 cured at different isothermal cure temperatures. The qualitative responses follow similar behavior as observed in the case of a DC signal with loss factor and ionic viscosity leveling off earlier for low-temperature cures. The quantitative comparison follows the argument discussed in section 4.3.1.

Figure 35 presents the ionic conductivity obtained from dielectric measurements for the case study at 30 °C. It is seen that the drop in ionic conductivity very much follows time-scale trends previously discussed. However, the time at which ionic conduction ceases differs widely from that of the SW signal. A clearer comparison between the sensitivity of SW and the dielectrometer to molecular level events can be obtained from Figure 36 that shows the conductivity observed by SW alongside that derived from dielectric measurement at 2.5 Hz for Derakane 411-C-50 cured at an isothermal temperature of 30 °C. It is seen that SW data undergoes much larger changes in conductivity corresponding to gelation and vitrification as compared to the dielectrometer measured ionic conductivity, which remains roughly a straight-incline line. This comparison illustrates one of the advantages of DC signal over AC measurements, where greater sensitivity to cure behavior is demonstrated early in the cure. The greater sensitivity of SW makes it ideal for integration into control systems.

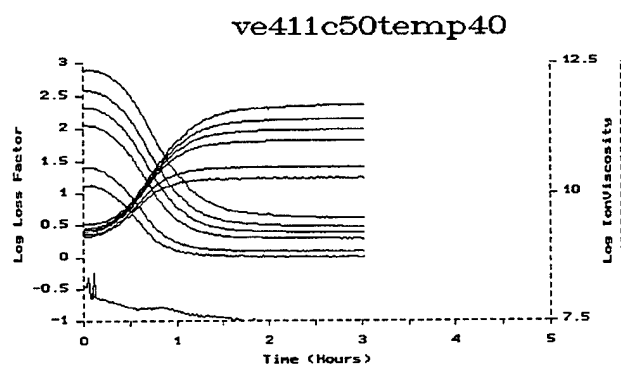
Tables 7 and 8 compare the maximum degree of conversions respective to when the DC and AC signals cease to yield further information. From Tables 7 and 8, it can be seen that the AC technique remains sensitive to the degree of conversion for a larger range of α , whereas the DC signal ceases early in the cure. It can be inferred that the dielectric related ionic conductivity gives information on the degree of conversion for a longer range of α as compared to DC-based ionic conductivity. So dielectric cure monitoring holds promise as an effective point sensor for cure monitoring in the later stages of cure.

4.4 Section Summary

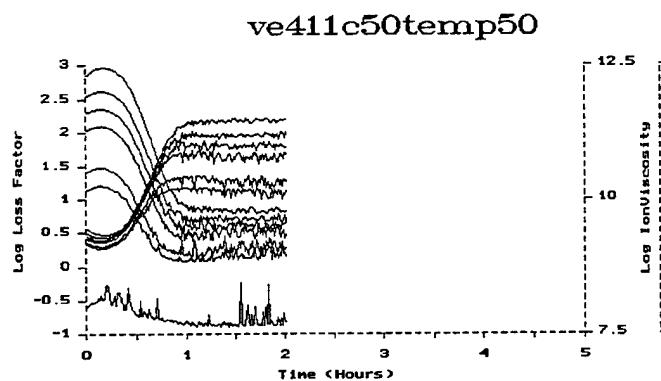
A study of the effect of styrene concentration on the SW behavior of 441-400 revealed that the slower rate of reaction with increased styrene content gets manifested as delayed gelation (inflection in the SW data) and delayed SW cutoff. Comparison of viscosity data confirms that the gelation time scales are consistent with the DC inflection point. Glass-transition temperature, T_g , data



(a)



(b)



(c)

Figure 34. Dielectric cure monitoring of Derakane 411-C-50 at isothermal temperatures of (a) 30°, (b) 40°, and (c) 50 °C.

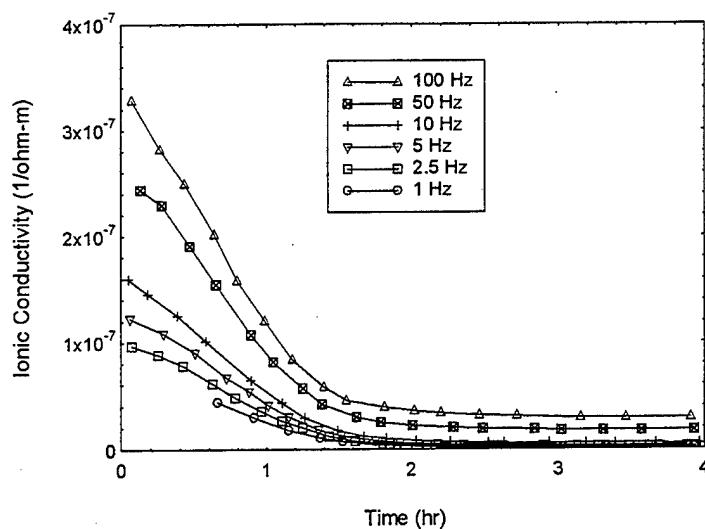


Figure 35. Ionic conductivity from dielectric measurements on Derakane 411-C-50 at 30°C isothermal cure temperature.

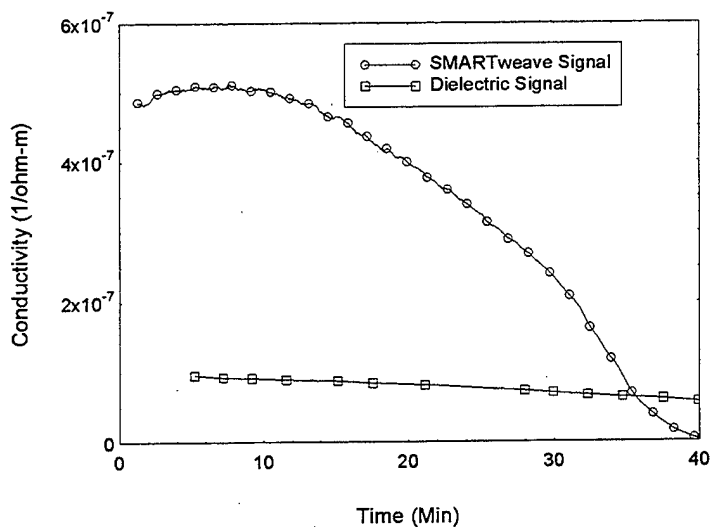


Figure 36. Comparison of SW behavior of ionic conductivity with dielectric behavior of Derakane 411-C-50 at 30 °C cure temperature.

for different styrene concentrations revealed differences in the cross-linking density between the resin compositions conforming to the observed differences in the SW cutoff point. This illustrates the fact that styrene, despite being electrically inert, significantly affects the SW behavior by being an inherent part of the network formation.

Table 7. Maximum conversion of 411-C-50 from DC and AC cure monitoring.

Cure Temperature (°C)	α_{\max} DC Monitoring	α_{\max} AC Monitoring
30	0.129	0.637
40	0.275	0.63

Table 8. Maximum conversion of 441-400 from DC and AC cure monitoring.

Styrene Concentration (weight-percent)	α_{\max} DC Monitoring	α_{\max} AC Monitoring
28	0.152	0.524
47	0.069	0.610

Temperature effects on 411-C-50 reveals faster reaction rates leading to faster gelation times with increased cure temperature as confirmed by the viscometer data. However the SW cutoff happens at a later time for higher temperatures. A comparison of the T_g revealed an increase in the cross-linking density with cure temperature. Hence one can conclude that the differences in the SW cutoff is due to the increased mobility induced by higher thermal energy, which overcomes the negative effect of cross-linking on the molecular mobility.

Dielectric behavior of both 441-400 and 411-C-50 followed the SW behavior qualitatively. However, owing to differences in the parameter being measured, quantitative differences were observed. SW, due to its better sensitivity to cure events like gelation and vitrification, is an effective tool for cure monitoring in the early stages of the cure. However, the dielectric signal far outlasts the DC signal, enabling its use for cure monitoring in the later stages of cure. A combination of SW, dielectric and FTIR techniques could be used to follow the different scale of possible motions with the proceeding of cure.

The experimental results discussed in this section, along with cure kinetics measurements provided in section 3 are used as the basis for developing a free-volume continuum model as shown schematically in Figure 7. In section 5, the role of microgels is investigated to understand their influence on the ionic conductivity. Cure kinetic data along with cure monitoring results are used to investigate the feasibility of a percolation-based continuum model.

5. Characterization of Microgels

5.1 Introduction

This section investigates the influence of microgels on the ionic conductivity of VE resins. Microgels are highly cyclized and cross-linked spherical entities, whose number increases with cure. As discussed in section 1.5, the increase in the number of microgels forces the conducting ions to travel increasingly tortuous paths around the microgels to reach the electrodes. This results in a decrease in the observed ionic conductivity with cure. The percolation-based continuum model investigated in this section takes into account the increasing volumetric contribution of the microgels with cure, as illustrated in Figure 7.

The Flory-Stockmayer theory [13] has been in use for over 50 years to predict and understand the gelation mechanisms. Using combinatorial arguments, Batch and Macosko [24] were successful in predicting both the gel point and the weight-average molecular weight of the branched aggregates at gel point. Flory coined the term "infinite network" to describe the resulting network formation at gel point. The network reaches a macroscopic dimension by occupying the entire volume of the reacting sample itself. Since, on the molecular level, the network is unbounded, it is referred to as an infinite network.

Experiences with styrene-unsaturated polyester resins and vinyl-divinyl systems, however, seems contradictory to the previously mentioned gel point predictions [32, 26, 27]. The measured gel point conversion for these systems was far greater than Flory-Stockmayer predictions. Dusek and Spevacek [26] and Dusek et al. [27] have shown that predominant cyclization is observed in the beginning stages of the reaction involving free radical polymerization systems. Dusek and colleagues described such cyclized structures with high cyclization and cross-linking density as "microgels." Owing to heavy cyclization, the reactive end groups of the polymer chains are physically tucked away, disabling further participation of these end groups in the reaction process. The molecular shielding plays an important role in the free-radical polymerization reaction and is a possible cause for the final conversion of the reacting monomers to fall short of 100%. Dusek and colleagues found that the deviation from the Flory-Stockmayer theory increased with the increase in the concentration of multifunctional monomers. They showed that in a copolymerization reaction involving monovinyl and divinyl components, the deviation from the Flory-Stockmayer predictions increased with the increase in concentration of the divinyl component. Three factors are held responsible for the previously mentioned deviation: (1) cyclization, (2) reduced reactivity of the pendant vinyl reactive groups, and (3) microgel formation. In the case of heavily cyclized

structures, these three causes occur simultaneously in that cyclization leads to the formation of microgels which are then responsible for molecular shielding of the pendant double bonds leading to an apparent reduction in the reactivity of the pendant vinyl groups.

5.2 Background

At the beginning of a copolymerization reaction involving styrene and unsaturated polyester resins, the system contains styrene monomers, unsaturated polyester molecules, and inhibitors. When the reaction starts, the initiators decompose and form free radicals to trigger polymerization. At the very beginning of the reaction, most of the free radicals formed from the initiators are immediately consumed by the inhibitors. Very little polymerization occurs due to the inhibition effect at this stage, which is called the induction stage.

After this stage, the initiators continuously decompose creating free radicals which link adjacent unsaturated polyesters and form primary polymer chains through connecting styrene monomers by both inter- and intra-molecular reactions. These long chain molecules tend to form spherical structures due to the intra-molecular cross-linking among the pendant C=C double bonds of the polyester molecule leading to the formation of the microgels. Because of the high cross-link within the microgel, the free radicals on the polymer ends are likely to be buried in the microgels. This means that termination among the polymer radicals may not be an important factor and can be neglected.

As the polymerization proceeds, the concentration of the microgels increases continuously. This leads to macrogelation in the system. This mechanism is illustrated by several key steps in Figure 37. Since gel conversion is very low for radical chain-growth polymerization reactions, it is difficult to relate gelation to the resin conversion or molecular weight. For the case of chain copolymerization involving Derakane 411-C-50 and styrene monomers, the conversion predicted by the Flory-Stockmayer theory [13] has been calculated by Dua [10] to be 0.2 volume-percent. However, the volume conversions at gelation, based on viscosity measurements, normally fall in the range of 10 volume-percent. This large discrepancy in the conversion values suggests the occurrence of similar cyclization phenomenon. Also, an observation of the T_g - α relationship of curing VE 411-C-50 obtained by Stone [11] suggests that during cure, for a large range of α , the T_g remains nearly the same. This is contrary to epoxy systems where the T_g increases linearly with cure α , since microgel formation does not appreciably increase the T_g of the curing system.

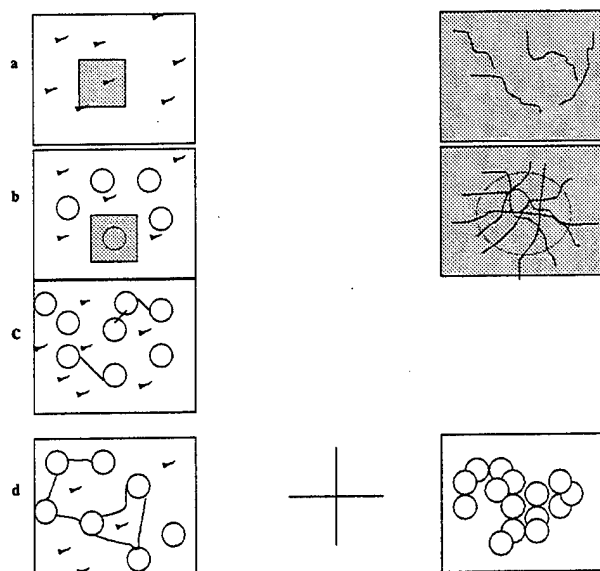


Figure 37. Illustration of cross-linking polymerization (a) at beginning, (b) initiation, (c) reaction in progress, and (d) possible gelation schemes.

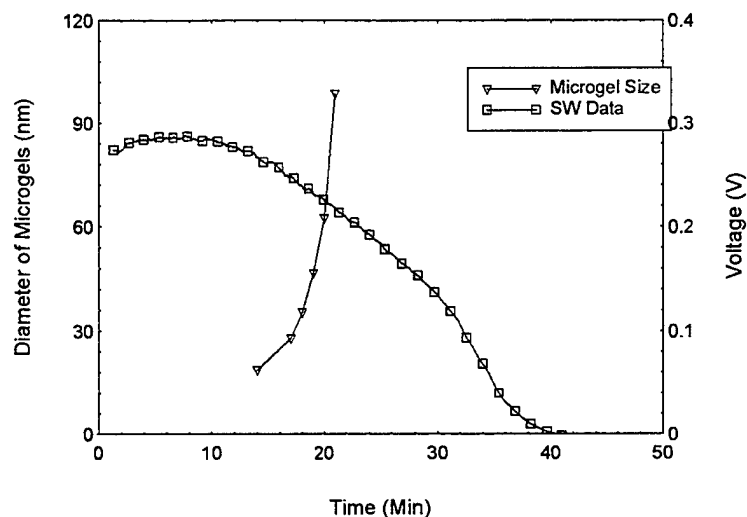
The abnormal behavior of 411-C-50, therefore, indicates a minimal increase in the cross-linking density and an increase in the volume fraction of microgels. This study attempts to characterize these microgels for possible influence on ionic conductivity.

5.3 Results

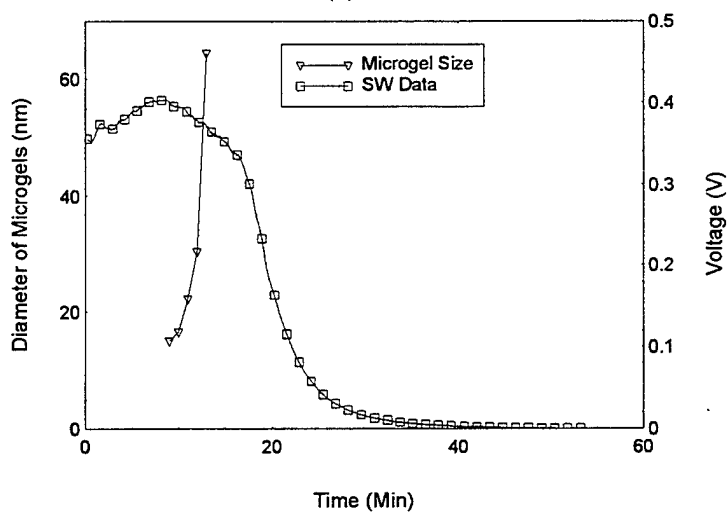
Section 5.3.1 investigates the role of microgels on the ionic conductivity. A comparison of the growth of microgels with a decrease in the DC signal indicates a coupling between the two events. Section 5.3.2 presents the preliminary results on the chemical characterization of microgels. A thorough understanding of the chemical composition of microgels would enable identification of the chemical composition of the unreacted resin and the network development surrounding the microgels. Section 5.3.3 deals with the AFM analysis of microgels to obtain an insight into the size and number density of the microgels. The microgel size is used as input for the percolation-based model presented in section 5.4.

5.3.1 Comparison of Microgel Growth Kinetics with SW Data

Figures 38 and 39 show the change in size of microgels as observed using dynamic light scattering (DLS) experiment [10] as compared to the simultaneous change in the DC signal observed by the SW setup. A detailed discussion on



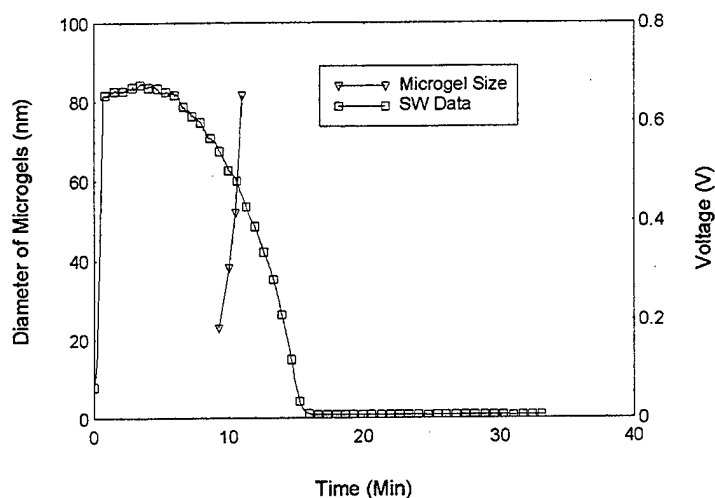
(a)



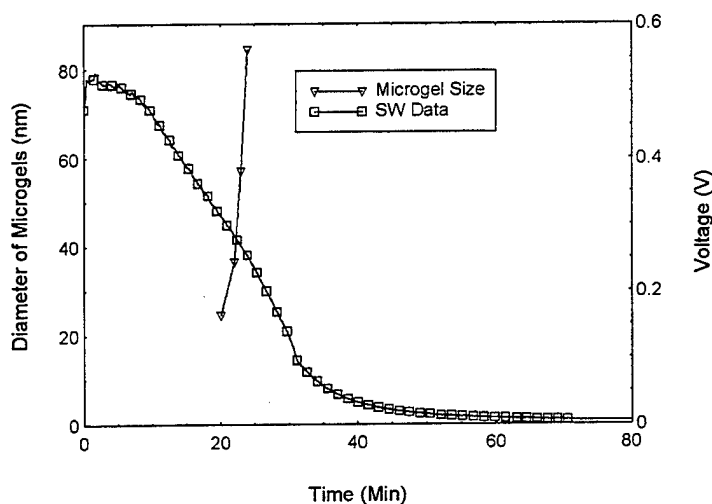
(b)

Figure 38. Influence of microgels on SW behavior of 411-C-50 for (a) 30° and (b) 40 °C, respectively.

DLS and sample preparation are found elsewhere [22]. An interesting observation is that these microgels rapidly increase in size at the same time when one observes a drastic drop in the SW voltage. This time range coincides with the occurrence of macrogelation as observed from the viscometer data (Figures 28 and 32). This essentially indicates the importance of microgel in the development of macroviscosity and hence SW signal. As discussed in section 1, ionic conductivity is significant beyond gelation. The role of microgels on ionic conductivity is investigated in section 6.



(a)



(b)

Figure 39. DLS data showing influence of microgels on SW response of 441-400 at (a) 28% and (b) 57% styrene.

5.3.2 Separation of Microgels

Figures 40-42 show the HPLC responses for pure styrene, pure VE and fractionated sample of microgels, respectively. The VE peak and styrene peak occur around 875 s and 1,100 s, respectively, along the time axis. After multiple cycles of dissolving followed by precipitation of microgels in order to remove the unreacted monomers, the fractionated high molecular weight microgel and the effective removal of the VE and styrene monomers can be observed in Figure 42.

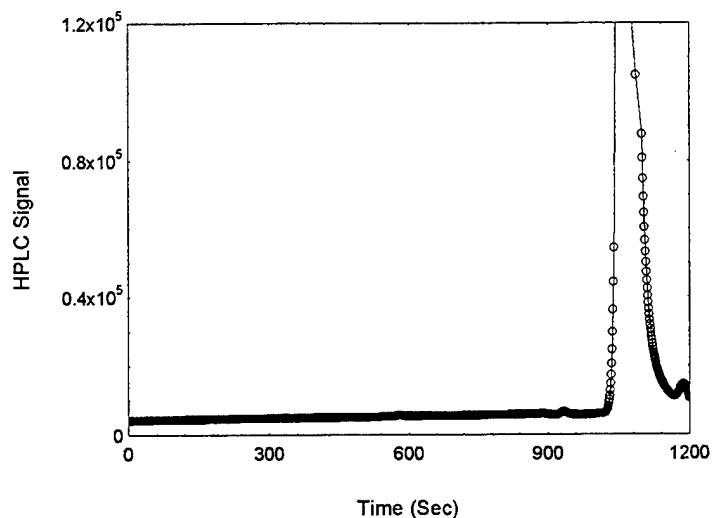


Figure 40. HPLC response (in μV) of pure styrene.

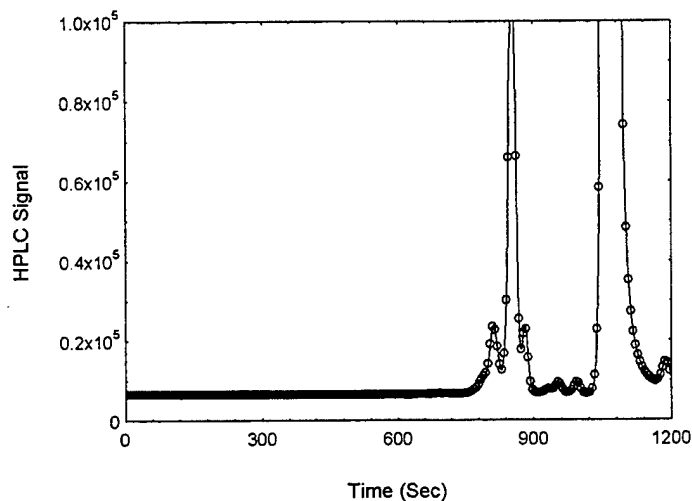


Figure 41. HPLC response (in μV) of pure unreacted VE825 with 28 weight-percent styrene.

Figure 43 shows the FTIR spectra of curing VE825 [33] at an isothermal temperature of 40°C . When it is compared with Figure 44 showing the FTIR spectra of the fractionated microgel, one observes an anomalous decrease in the peak height at 700 cm^{-1} as compared to the one at 910 cm^{-1} , which remains a topic for future work. The peak at 910 cm^{-1} appears slightly shifted and is observed to occur at 900 cm^{-1} . A comparison of the reference peaks of VE at 830 cm^{-1} and styrene at 700 cm^{-1} indicates a predominance of VE in the fractionated microgel as compared to the reacting mixture. This confirms the

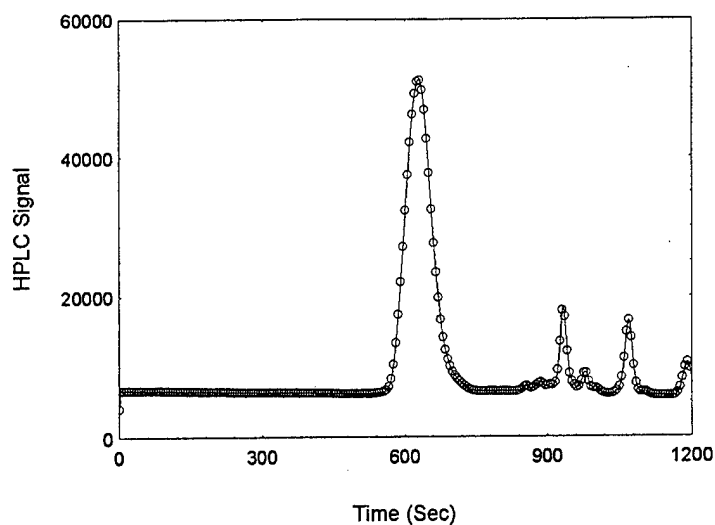


Figure 42. HPLC response (in μV) of fractionated microgels.

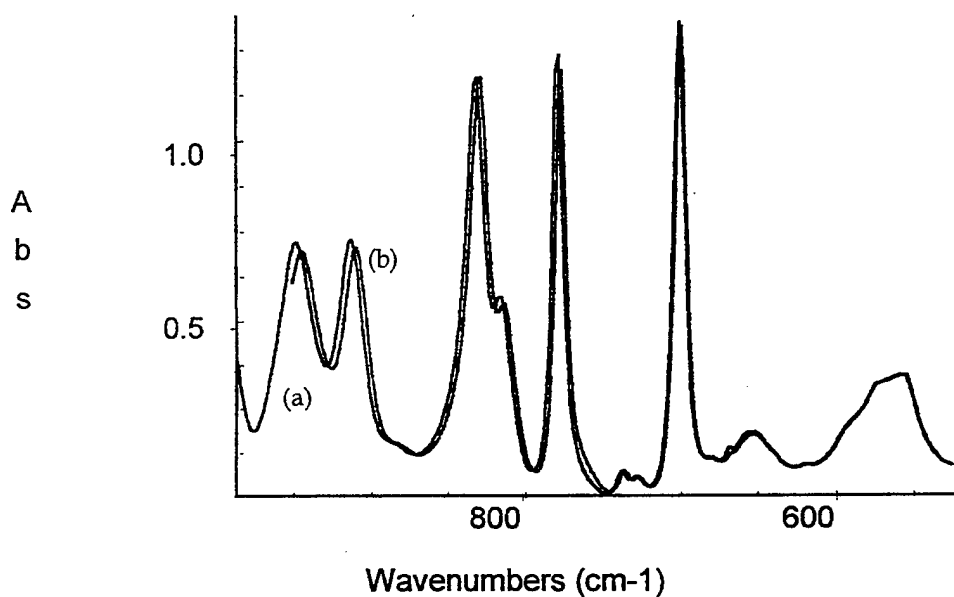


Figure 43. FTIR spectra of VE825 (a) at the beginning of cure and (b) at 9 min at $40\text{ }^{\circ}\text{C}$ cure temperature.

hypothesis that microgels are highly cyclized and densely cross-linked structures, since only VE monomers can act as cross-linkages. The separation of the microgels and the FTIR spectra of these fractionated microgels were not a reliably repeatable phenomenon. Of the multiple successful attempts at microgel separation, the FTIR spectra qualitatively agrees with the above mentioned sample results. However, quantitatively, they showed a high degree of

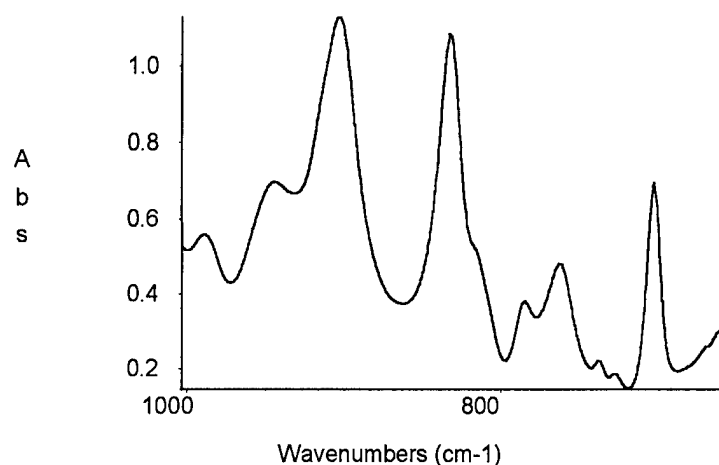


Figure 44. FTIR spectra of fractionated microgels formed in the first 9 min of isothermal cure of VE825 at 40 °C.

variation. One can conclude from these results that the microgels do not contribute directly to ionic conduction but represents dead zones that increase tortuosity for ionic transport.

5.3.3 AFM Analysis of Microgels

To investigate the potential contribution of the microgels to tortuosity, information on microgel size is essential. This is achieved using AFM. Figures 45 and 46 show AFM pictures of microgels as observed on the fractured surfaces of cured Derakane 411-C-50 (isothermal cure temperatures of 40° and 50 °C, respectively). A comparison of the AFM pictures suggest an increase in the number density and size of the microgels with cure temperature. Effort needs to be directed towards the observation of such a trend. It should be borne in mind that similar to the case mentioned in section 5.3.2, from Figures 45 and 46, it is seen that the average size of microgels vary between 150 nm (at 40 °C) and 200 nm (at 50 °C) in diameter. Similar AFM pictures of microgels corresponding to a cure temperature of 70 °C have been obtained by Brill and Palmese [21]. These AFM pictures show microgels of roughly 150 nm in diameter. The microgel size as observed by DLS show an exponential increase from 20 nm to 90 nm at gelation. This most likely indicates that the microgels grow rapidly to their equilibrium size of around 150 nm. This postulation is in keeping with the nature of free-radical chain-growth copolymerization [20].

5.4 Percolation Model

Based on the experimental work previously described, it can be surmised that microgels, due to their nonconductive nature, are considered as dead zones and conduction through microgels need not be modeled explicitly. The formation of

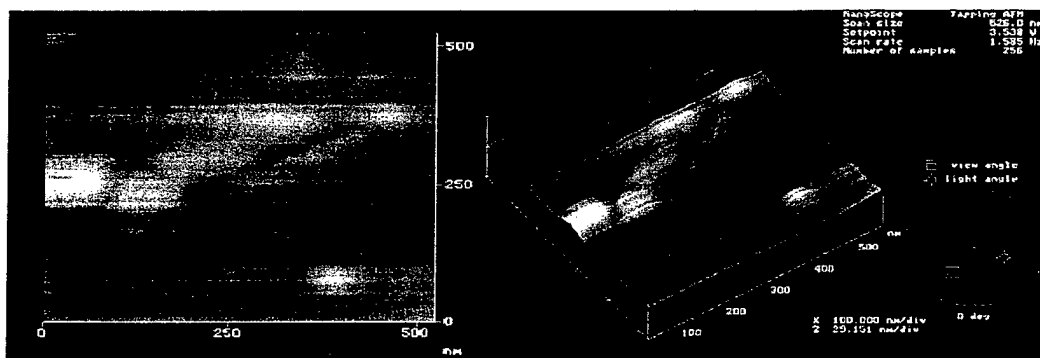


Figure 45. AFM pictures of microgels as observed on a fractured surface of 411-C-50 sample cured at an isothermal temperature of 40 °C.

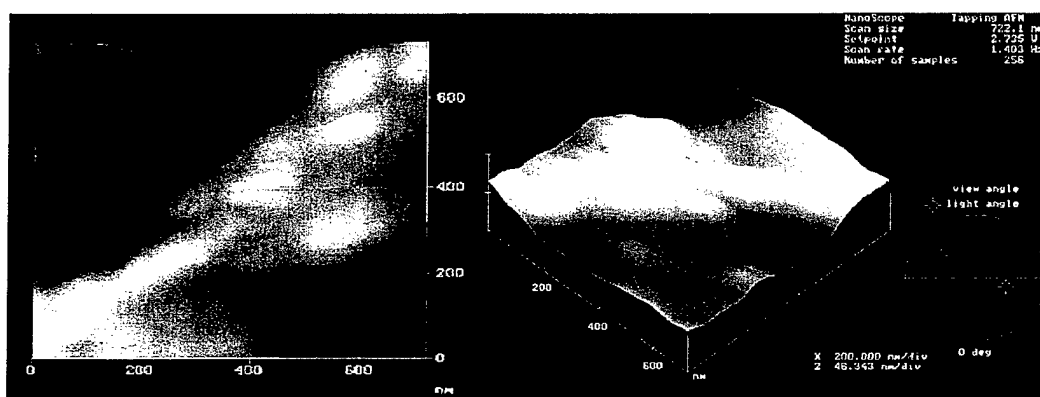


Figure 46. AFM pictures of microgels as observed on a fractured surface of 411-C-50 sample cured at an isothermal temperature of 50 °C.

microgels does not influence the concentration of the conducting ions in the surrounding unreacted resin, i.e., the conductivity of the unreacted resin remains unchanged. The increasing volumetric contribution of the microgels, however, increases the tortuosity of the curing system resulting in a decreased DC signal. In this section, an effort is made to describe the ionic conductivity and viscosity development based solely on the microgel formation. For purposes of simplicity it is assumed that all reaction goes into the formation of microgels; i.e., the α_{VE} and α_{St} , as observed using FTIR, go only into the formation of microgels which is surrounded by unreacted resin. In reality, however, curing results in the formation of both microgels and network formation outside the microgels. Theoretical calculations to determine the volume fraction required for the infinite network formation have been reported by Dua [10] and fall in the range of 0.2% for 411-C-50. However, in reality a reacted volume fraction of 10% is observed by gelation. This suggests a large fraction of the reacted resin (as large as the remaining 98%) goes into the formation of microgels lending support to the aforementioned assumption.

This section investigates the effectiveness of such an assumption in describing the ionic conductivity and the viscosity development during cure. A review of the percolation theory is presented in Appendix E.

5.4.1 Modeling Approach

Traditionally, the conductivity behavior using the percolation theory has been modeled based on assuming a network of resistances [34-40]. In one experimental work, Last and Thouless [41] peppered a conducting sheet of colloidal graphite paper of a finite resistance with holes (the resistance of holes is infinity, analogous to our microgels), according to coordinates obtained using a random number generator. A graphical illustration of the observed conductivity behavior as a fraction of the concentration of holes is shown in Figure 47. It is seen that the observed conductivity tapers off to zero when the fractional concentration of holes reaches 0.4. This experiment was modeled by Yuge and Onizuka [40] using a two-dimensional (2-D) resistor network consisting of two kinds of special unit resistor with different conductances, K1 and K2. The resistors are placed at random as shown in Figure 48. Yuge and Onizuka [40] designed and studied such a 200×200 site random-resistor network. A simulation of Last and Thouless' experiment [41] by making K1 as unity (as in graphite) and K2 as zero (as in holes) yielded the critical fraction of K1 to be 0.591, and K2 to be 0.409. The value of 0.409 obtained compared to a critical fraction of 0.4 obtained by Last and Thouless illustrates the success of resistor network simulations in describing conductivity through continuous medium. The success of resistor network simulations, has since been applied to 3-D systems [34-36]. Figure 49 shows a 3-D network simulation by Kirkpatrick [35]. For K2 of very low conductivity, a critical volume fraction of conducting material near 0.3 was obtained. Figure 50 illustrates how the microgel formation during cure can be related to a 3-D resistor network similar to the work of Last and Thouless. At time $t=0$, the resin system is unreacted and therefore equivalent to a resistor network of only say K1 with a conductivity value of unity. At time $t=t_1$ into the cure, the reacting system is a mixture of reacted microgels and unreacted resin surrounding the microgels (similar to holes in graphite sheet in 2-D). These microgels are added at random to the reacting system. At this stage, the resin system can be simulated using a 3-D resistor network containing, K1 and K2 at random, with increasing fraction of K2 (corresponding to microgels) in the network. Since microgels are assumed to be of negligible conductivity, the resistor K2 is assigned negligible conductivity. With time, the volumetric contribution of the microgels in the reacting system increases which is simulated by progressively increasing the fraction of K2 at random in the resistor network. At a critical volume fraction, the conductivity of the reacting resin system reaches zero (SW cutoff). This theoretical critical volume fraction is given by Figure 49 to be 0.31 of K1 (corresponding to the volume fraction of unreacted resin) or 0.69 of K2 (corresponding to the volume fraction of reacted microgels).

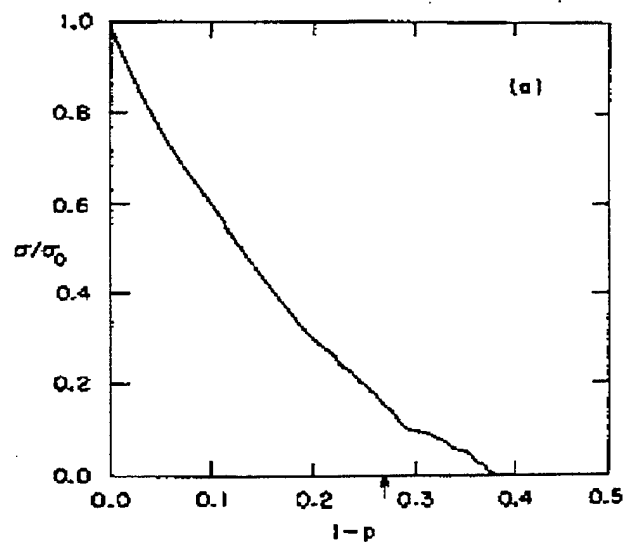


Figure 47. 2-D percolation behavior of a continuous conducting medium [41].

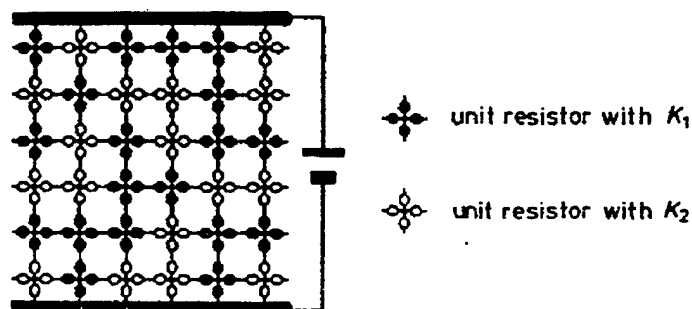


Figure 48. 2-D percolation behavior modeling using resistor network [40].

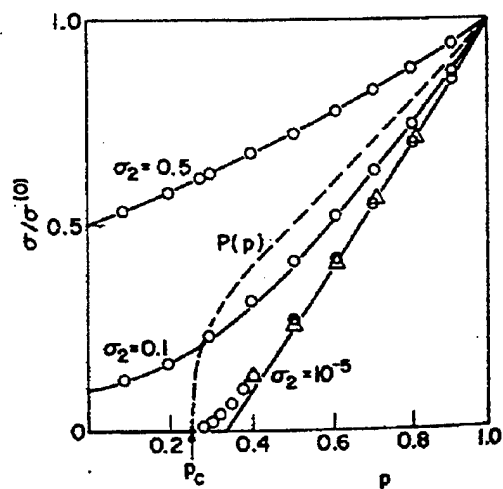


Figure 49. 3-D percolation modeling using non-zero resistor values [35].

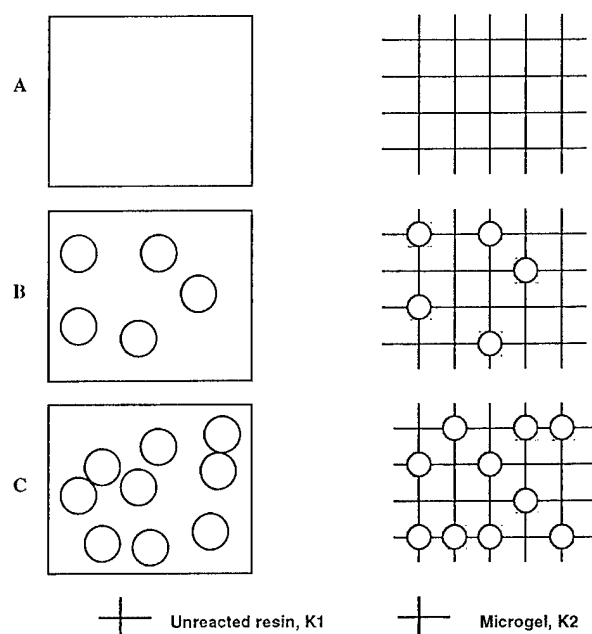


Figure 50. Development of resistor network model for curing VE resin at (a) time $t=0$, (b) time $t=t_1$, and (c) time $t=SW$ cutoff. The left side illustrates different stages of cure and the right side illustrates equivalent resistor network.

5.4.2 Percolation-Based Continuum Model

5.4.2.1 Conductivity Model

The volume fraction of microgels were calculated using the degree of conversion results from FTIR. Calculations and assumptions regarding the volume fraction estimation are given in Appendix B. Figures 51 and 52 show the corresponding results for 411-C-50 and 441-400, respectively.

Figures 51 and 52 indicate that even for widely varying composition and cure conditions, the volume fraction corresponding to the abrupt decrease in the SW signal falls within the same range of the microgel volume fraction (20%). This significant grouping of the signal suggests that the development of phenomena that are responsible for controlling the DC signal all develop the same way in systems under consideration and are determined predominantly by the volume fraction of microgels as suggested by the percolation theory. Another similarity between the SW response and the percolation model is the tail formation at the end of the response signal, as opposed to an abrupt drop to zero. This phenomenon is explained by Last and Thouless [41], based on the fact that with decreasing volume fraction of the conducting material, the ions will have to travel more and more tortuous paths, ultimately making the path length

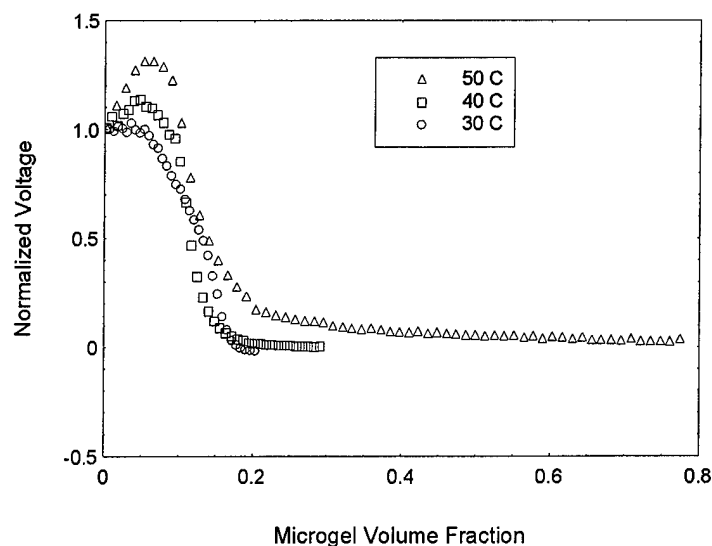


Figure 51. Normalized DC signal vs. microgel volume fraction of Derakane 411-D-50 at different isothermal cure temperatures.

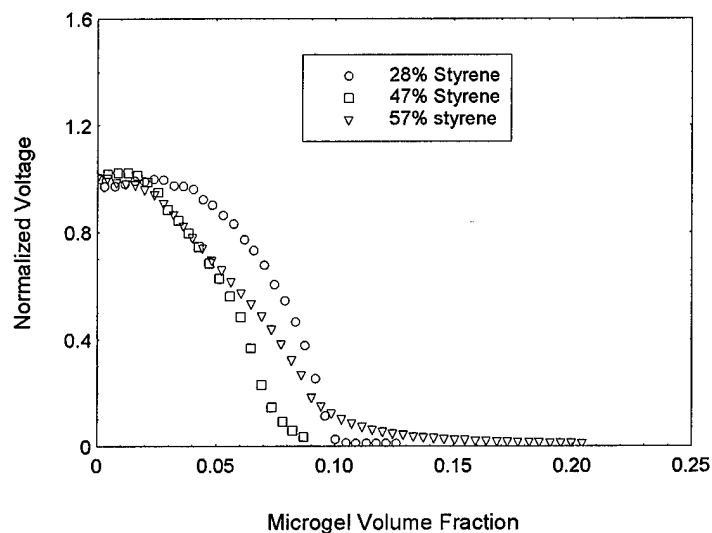


Figure 52. Normalized DC signal vs. microgel volume fraction of Derakane 441-400 at different styrene concentrations.

prohibitively long. This is seen as the drop in ionic conductivity with increase in microgel concentration.

A comparison between Figures 51 and 52 with 53 indicates a quantitative discrepancy even though qualitatively the response signals are similar. The SW conductivity drops to zero near a volume fraction of 0.20 of microgels in the case of 411-C-50 and at around 0.10 for 441-400. This is very different from an

expected value of 0.69 from the 3-D resistor simulation presented in Figure 49. This discrepancy between the actual behavior and the percolation model implies that the assumption of curing resin systems to be composed only of randomly distributed microgels surrounded by unreacted resin is an incomplete description of reality. The formation of cross-links outside the microgels, though negligible in volume fraction due to their highly distributed nature, introduces higher tortuosities in the ionic path length. As explained by Last and Thouless [41], the cessation of ionic conductivity happens due to the fact that the path length that an ion has to traverse to reach the corresponding electrode reaches prohibitively large values. The presence of these infinite networks in VE induces a similar effect on the ionic path length resulting in the cessation of conductivity long before the expected volume fraction of 0.69.

Another complication one faces in modeling the resin behavior is the exothermic nature of the cure itself. The exotherm influences the ionic mobility and local viscosity, thereby making the identification of the isothermal cure effects a difficult exercise. The region of volume percent over which one observes the conductivity, increases with temperature even though the initial drastic reduction in the conductivity occurs around the same volume percent for all three temperatures. This observation, as explained in previous discussions, is due to the higher mobility induced by way of increased cure temperatures.

5.4.2.2 Viscosity Model

In keeping with the above assumption of a curing VE system to be composed of only microgels (reacted component) and sea of VE resin (unreacted component), an attempt was made to explain the development of macroscopic viscosity with cure. It was originally intended to relate the three relevant material properties like viscosity, ionic conductivity and degree of cure to one another using the volumetric contribution of the microgels as illustrated in Figure 7. Section 5.4.2.1 highlighted the discrepancy between the model assumption and reality. However, it is desirable to investigate the efficiency of such a model in describing the viscosity development.

Literature presents a number of models to describe the development of viscosity for a wide range of volume fractions [42, 43]. A modified Einstein equation was used in this study:

$$\phi_r = 1 - KC, \quad (17)$$

where K is a constant in the range of 2.35 and 2.60, and C is the volume concentration of spherical particles (microgels). The apparent relative fluidity, ϕ_r , is given by:

$$\phi_r = \mu_f / \mu_s, \quad (18)$$

where the subscript f represents the pure suspending fluid (unreacted resin) and the subscript s represents the suspension (suspension of microgels in unreacted resin).

Oliver and Ward [44] have shown that at concentrations below 30%, a large range of particulate suspensions are well represented by this correlation. Since our systems rarely exhibit a volume percentage higher than 30%, the aforementioned relation would be a sufficient description. Figure 53 shows the development of fluidity with cure as estimated by the model alongside actual viscometer data. As explained in section 5.4.2.1, the discrepancy between the model and experimental data is due to the assumption that cure reaction results only in microgel formation. In reality, however, curing leads to both microgel and infinite network formation. It is the presence of this infinite network that forces the macroscopic viscosity to asymptotically increase to infinity much earlier than dictated by the modified Einstein's relationship. Results are consistent with percolation. Both these results imply that the network formation outside microgels play a important role in determining ionic conductivity of the reacting resin system.

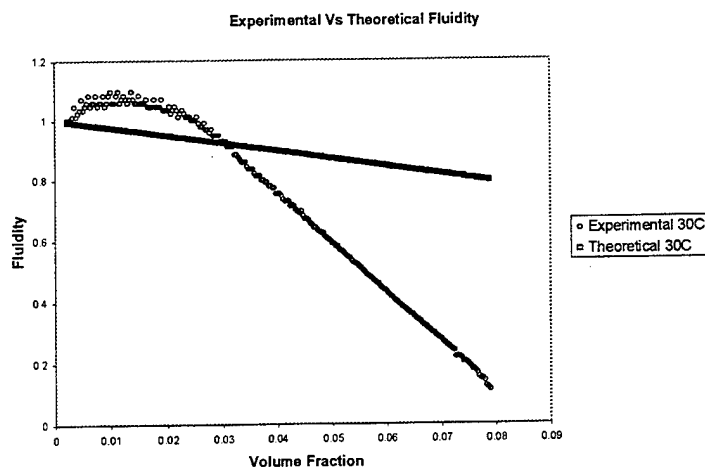


Figure 53. Experimental vs. theoretical fluidity of Derakane 411-C-50 at isothermal cure temperature of 30 °C.

5.5 Summary

Based on DLS data [10], FTIR analysis and AFM imaging, a valuable insight into the growth kinetics, chemical makeup and equilibrium size estimation were made possible. A comparison of the DLS data with SW behavior revealed that an increase in the volumetric contribution of microgels forces the conducting ions to travel increasingly tortuous paths. This results in the observed decrease in DC signal with cure. A possible extension of the influence of microgels to modeling the ionic conductivity behavior requires a thorough understanding of

the role of microgels in the formation of network structure. This is, however, an issue of contention. From percolation theory, Dua [10] argued that linking of microgels alone to form gelation would require a higher volume fraction of conversion of nearly 20% and above whereas the actual conversion falls in the range of 10%. An infinite network formation based on the Flory-Stockmayer model [13] suggests too low a fractional conversion at gel point. Therefore a hybrid model including both of the previously mentioned phenomena is proposed by Dua [10]. Dua argues that the final gelation scheme could be a combination of network structures as illustrated in Figure 37, whereby the microgels have a reasonable statistical chance of being incorporated into the overall network, if they possess at least 18 surface-reactive double bonds.

Section 5.4 explored the possibility of modeling ionic conductivity and viscosity development during cure based solely on the influence of microgels. A large discrepancy between the model prediction and the experimental data implied the significant role of network formation on the ionic conductivity behavior and viscosity development. Section 6 presents a free volume-based continuum model which takes into account the role of network formation during cure. The free volume model utilizes the development of T_g with cure to describe the resulting network structure. Since microgel formation does not result in an appreciable increase in the T_g , the T_g - α profile of the curing resin system is a representation of the influence of both the infinite network and the microgels.

6. Mathematical Model of the Ionic Conductivity Behavior

6.1 Introduction

A brief outline of different efforts directed towards modeling ionic conductivity to yield predictive capabilities with respect to the processing parameters such as viscosity and degree of cure can be found in section 1.4. Schwab et al. [9] modeled the observed resistance of the resin as a function of the macroviscosity to yield the relation:

$$R_j(t) = 6\pi\eta L / A \sum_i (C_i Q_i^2 / r_i) , \quad (18)$$

where $R_j(t)$ is the resistance of the resin at time t ; L and A are the conduction path length and the area of the effective electric field, respectively; and η , C_i , Q_i and R_i are the viscosity, concentration of ions, charge of ions and radius of ions, respectively.

This relation is derived based on balance between the electromotive force and the viscous drag force as dictated by the Stoke's-Einstein relationship. A detailed derivation can be found elsewhere [4] with an analysis of diffusion relation for pregel and postgel stages presented in Appendix F.

Equation 18 enjoys success in modeling the macroscopic viscosity until gelation. However, the construction of the model around the macroscopic viscosity limits its use beyond gelation. As evident from the SW signal response, one still observes DC conductivity beyond gelation and it is desirable to model this phenomenon making use of a "continuum" model, with predictive capabilities through gelation to vitrification. Equation 18 also yields no information regarding the development of the degree of cure even though DC conductivity, viscosity and degree of conversion are related to each other. This work attempts to fill this gap. The biggest drawback of equation 18 as used for modeling the VE behavior is the implied relation of the resistivity being directly proportional to viscosity. This relation holds good only in systems exhibiting time correlation between viscosity minimum and ionic conductivity maximum [45]. However, in some systems such as Epon 828, Epon 834, VE 411-C-50, etc., there is an offset between the time when the viscosity reaches minimum and when the ionic conductivity reaches a maximum as evident from comparison of SW data with the viscosity data. Usually, the minimum in viscosity precedes the maximum in ionic conductivity. This unusual behavior of 411-C-50 renders itself unsuitable for modeling using the previous approach. Section 6.2 details a free volume-based approach that successfully models ionic conductivity and viscosity development during cure.

6.2 Free Volume Model

This section details the adaptation of classical free volume theory for describing ionic conductivity and viscosity development during cure. Sections 6.2.1 and 6.2.2 present the relevant background and theory regarding the free volume theory. Section 6.2.3 deals with the conductivity modeling of VE 411-C-50; section 6.2.4 deals with viscosity modeling.

6.2.1 Background

In polymer systems, viscosity and ion conductivity are macroscopic properties that characterize chain segment mobility and ion mobility, respectively. While viscosity is a measure of the response of polymer chain segments to an applied stress field, ionic conductivity is the response of ions subjected to an electric field. Although an inverse relationship has been shown to exist between viscosity and ionic conductivity prior to gelation these have not been extended beyond gelation to model the ionic conductivity.

A fundamental understanding of the relationship between rheological, structural and DC conductivity properties throughout the entire polymerization of a thermoset would be extremely valuable for online cure monitoring and control. In general, it is difficult to characterize in-situ rheological and structural properties during cure. However with the development of SW, one can observe the changes in the ionic conductivity of the resin system in real time both in the pregel and postgel regions. This suggests that it would be beneficial if rheological or structural information including the degree of cure information could be interpreted from these DC signals.

Free volume models have been widely used for characterizing and correlating the viscosity and the ionic conductivity for pregelled systems [46, 47]. The basic principle behind these models is that sufficient free volume must be available for the diffusion of a molecular unit through a polymer matrix. This polymer unit may be a solvent, an ion, or a small chain segment of the polymer itself. The current study attempts to develop a continuum model specific for the VE resins system under consideration to describe viscosity and degree of cure using DC signal for both pregel and postgel regions of the thermoset polymerization.

6.2.2 Theory

Free volume theory proposes that the controlling mechanism for molecular transport in polymeric systems (for $T < T_g + 100\text{ }^{\circ}\text{C}$) is the availability of sufficient free volume for the mobility of the given molecular species [46]. When there is a relatively large amount of free volume, the chains may move unhindered. However, as the cure proceeds, the free volume decreases and the chain becomes crowded by the neighbors, leaving very little room for the chains to move without colliding with its neighboring chains. This limits the ability of the polymer to rapidly respond to a perturbation by moving to a new equilibrium state.

A commonly used definition of the free volume is the volume due to thermal expansion, $V_f = V - V_0$ where V_f is the free volume, V is the total volume and V_0 is the volume at 0 K. Another commonly used definition comes from the argument that the volume of the polymer is the sum of the volume occupied by the chains of the polymer itself and the volume between the polymer chains, i.e., the interstitial volume.

The fractional free volume f defined as V_f/V is given by the expression

$$f = f_g + \alpha_f(T - T_g), \quad (19)$$

where f_g is the fractional free volume at the glass transition temperature, α_f is the thermal expansion coefficient of free volume, and T_g is the glass transition temperature, defined as the temperature at which the material changes from the glassy state to a rubbery state.

The first free volume theory application to polymer near the glass transition temperature is attributed to Flory [13] while studying the viscosity and specific volume of polystyrene over a range of temperatures. He noted that the traditional Arrhenius theory wasn't sufficient to explain the viscosity behavior thereby leading to the conclusion that the temperature dependence of the viscosity was governed largely by the available free volume in contrast to the activation energy approach.

The most widely used free volume relationship was proposed by Williams, Landel, and Ferry (WLF) as an empirical equation to describe the relaxation time during dielectric studies at a given temperature relative to the glass transition temperature and is given as [48]:

$$\text{Log } a_T = \text{Log}(\tau_T/\tau_{T_g}) = C_1(T - T_g)/(C_2 + (T - T_g)), \quad (20)$$

where a_T is the shift factor, τ_T is the relaxation time at the isothermal cure temperature T K, τ_{T_g} is the relaxation time at the glass transition temperature, and C_1 and C_2 are empirically determined parameters.

The WLF relationship has been widely used for modeling the temperature dependent viscosity behavior of various polymers and polymer blends near the T_g [49, 50]. The WLF relationship also enjoys success in the modeling of dielectric responses and ionic conductivity of various epoxy amine systems [46, 47].

Although the WLF equation was proposed as an empirical expression, theoretical support for equation 20 has been derived by Cohen and Turnbull [51], Bueche [52] and Adam and Gibbs [53]. These approaches were based on molecular events, statistical mechanical and molecular kinetic theories, yielding relationships equivalent to the WLF model. Senturia and Sheppard [54] has proposed with theoretical support, an extension to the WLF relationship:

$$\text{Log } a_T = \text{Log}(\tau_T/\tau_{T_g}) = C_1(T - T_g)/((C_2 + C_3T_g) + (T - T_g)). \quad (21)$$

The shift factor a_T is the ratio of the material property like conductivity, viscosity or dielectric relaxation time at cure temperature to that at the glass-transition temperature. All temperature values are in K. In this work, the shift factor is taken to be the ratio of conductivities (for conductivity modeling) or viscosities (for viscosity modeling).

6.2.3 Conductivity Model

The use of WLF relationship to model the polymer behavior comprises of three steps that are three modeling efforts in themselves. First, one must develop a cure kinetic relationship relating degree of cure with time and the isothermal cure temperature. For 411-C-50 system, the relationship between the degree of conversion as estimated by FTIR is different from as estimated using DSC (equations 13 and 16). In this section, only the degree of conversion obtained

from FTIR is used for modeling. Modeling details based on a DSC-estimated degree of cure are presented in Appendix G. Equation 22 describes the degree-of-cure relationships for FTIR. The model parameters are given in Table 5.

$$\alpha = \{\alpha_{\max}[K\alpha_{\max}(1 - m)]^{1/(1-m)}\} / \{1 + [K\alpha_{\max}(1 - m)]^{1/(1-m)}\} \quad (22)$$

where α is the degree of conversion of either VE or styrene monomers.

The second step in the free volume modeling is the development of the T_g vs. degree-of-cure relationship. Linear relationships of the form $T_g = T_{g0} + K\alpha$ have usually been used in the literature for the T_g - α model. However, in this study, the T_g - α model developed by Stone [11] is used. For many thermosetting systems, such as epoxy and polyimide systems, the T_g - α curve for various isothermal temperatures have all been found to collapse on to one curve [55–58], showing a one-to-one relationship between T_g and α . However, in the case of 411-C-50, a one-to-one relationship wasn't obtained. This is because the VE resin system exhibits competing reactions and the influence of these competing reactions also vary with temperature [11]. Thus, a single model cannot be used to describe the T_g as a function of conversion; however, the estimated T_g - α parameters for fitting the Venditti's relationship (equation 23) to the experimental data for different isothermal cure temperatures were used:

$$\ln(T_g) = ((1-\alpha)\ln(T_g) + (C_{pr}) \alpha \ln(T_g^\infty)) / ((1 - \alpha) + (C_{pr}) \alpha) . \quad (23)$$

Stone [11] had proposed a set of T_g - α parameters applicable for the isothermal cure temperatures of 30° and 40 °C (Table 9). These parameters, however, were obtained for relating T_g to α determined using DSC. Since this experimental work aims to utilize FTIR for cure kinetics, a different set of parameters specific to FTIR-based α were estimated. Equation 16, in conjunction with the kinetic parameters for styrene presented in Table 5, is used to calculate conversion as a function of time. The new set of T_g - α parameters are presented in Table 10. The total degree of cure α was obtained from α_{VE} and α_{St} using the relationship [4]:

$$\alpha_{\text{Total}} = 0.2\alpha_{VE} + 0.8\alpha_{St} . \quad (24)$$

Table 9. T_g - α model parameters for 411-C-50 corresponding to DSC.

Temperature (K)	$0 < \alpha < \alpha_{vit}$			$\alpha_{vit} < \alpha < 1$		
	$(C_{pr})_1$	$(T_{go})_1$	$(T_g^\infty)_1$	$(C_{pr})_2$	$(T_{go})_2$	$(T_g^\infty)_2$
293	150	248.15	294.15	0.15	289.15	398.15
303	100	248.15	308.15	0.15	303.15	398.15
313	35	248.15	330.15	0.15	319.15	398.15

Table 10. T_g - α parameters for Venditti's relationship for 411-C-50 corresponding to FTIR.

Temperature (K)	$0 < \alpha < \alpha_{vit}$		
	$(C_{pr})_1$	$(T_{go})_1$	$(T_g^\infty)_1$
303	39.314	248.15	309.95
313	53.103	248.15	331.09

The third step is the estimation of "constants" in the WLF equation for ionic conductivity and viscosity. These constants, though, usually are invariant from one cure temperature to the other [53]. Similar to the case of T_g , the coefficients are slightly different from each other for the cure temperatures under study. The WLF equation used for the modeling of ionic conductivity is given by relation 25 and the estimated WLF constants are given in Table 11.

$$\log(\text{Cond}_T / \text{Cond}_{T_g}) = C_1(T - T_g) / ((C_2 + C_3 T_g) + (T - T_g)),$$

and

$$\log(\text{Cond}_{T_g}) = C_4. \quad (25)$$

The ionic conductivity data in equation 25, were obtained using SW, while the T_g data were generated using equation 24 with α as the model input. The ionic conductivity and the T_g data were time correlated to yield conductivity vs. T_g . A commercial curve-fitting software was used to fit equation 25 to the previously mentioned data, from which the WLF constants were estimated. The WLF parameters determined previously are presented in Table 11 for ionic conductivity at 303 and 313 K.

Table 11. WLF Parameters for conductivity model.

Temperature (K)	C_1	C_2	C_3	C_4
303	0.98553	6.3703	-0.012869	-7.2115
313	0.27303	4.7636	-0.0085545	-6.4166

Figures 54 and 55 illustrate the free volume model fit to the experimental data. Excellent agreement is achieved for 30 °C, while some deviation is noted for 40 °C. This is due to the slight temperature increase due to the exotherm which increases the conductivity. Shutoff is predicted accurately for both temperatures.

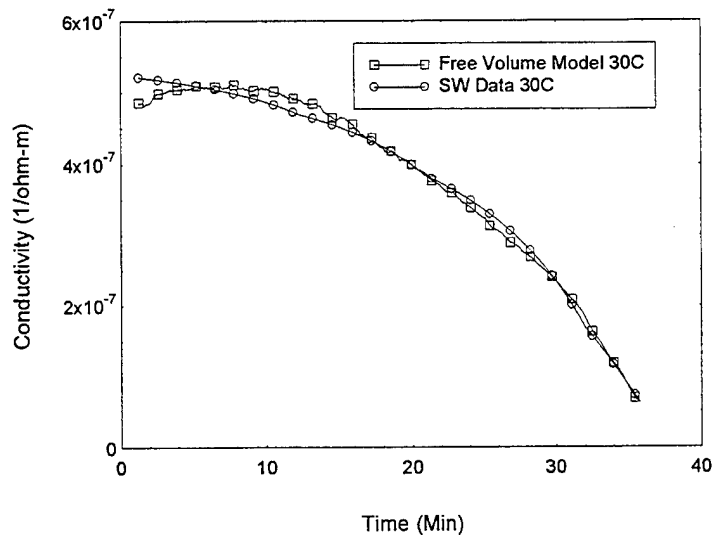


Figure 54. SW behavior prediction using free volume theory at 30 °C. (Degree of conversion obtained using FTIR.)

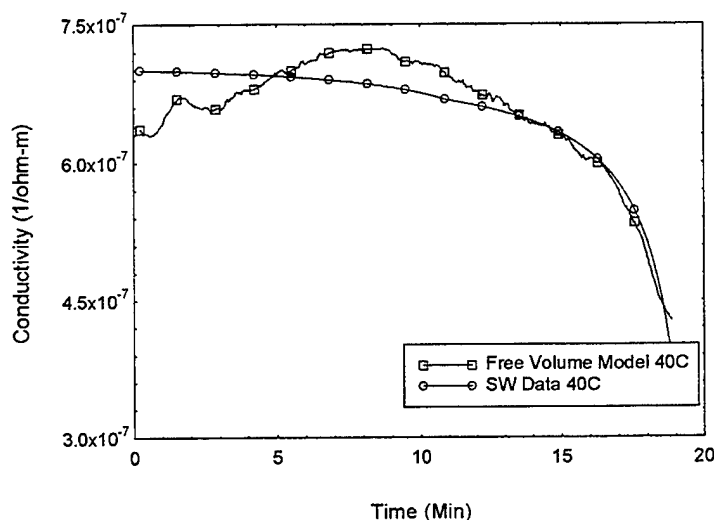


Figure 55. SW behavior prediction using free volume theory at 40 °C. (Degree of conversion obtained using FTIR.)

6.2.4 Viscosity Model

Equation 26 gives the WLF relationship used for describing the viscosity behavior. A similar procedure explained in section 6.2.3 was adopted for obtaining the WLF constants. Table 12 gives the estimated values of the WLF constants. A value of 15 was chosen for the $\log(\eta_{T_g})$ value [59].

$$\log(\eta_T/\eta_{T_g}) = C_1(T - T_g)/((C_2 + C_3T_g) + (T - T_g)), \quad (26)$$

and

$$\log(\eta_{T_g}) = C_4 = 15.$$

Table 12. WLF parameters for viscosity modeling.

Temperature (°C)	C ₁	C ₂	C ₃	C ₄
30	-13.507	7.2620	-0.020030	15
40	-13.372	7.3472	-0.020304	15

Figures 56 and 57 illustrate the comparison of the free volume model to the experimental data. Excellent agreement is achieved at both temperatures.

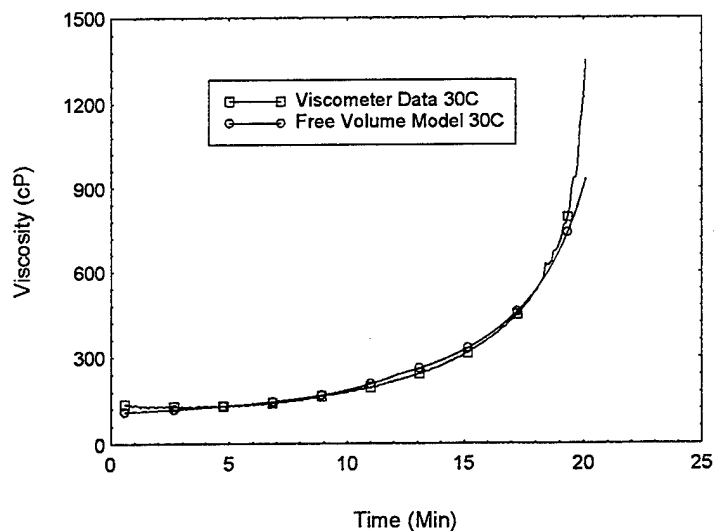


Figure 56. Viscosity prediction using free volume theory at 30 °C. (Degree of conversion obtained using FTIR.)

The estimation of the WLF constants for both ionic conductivity and viscosity models, presents an elegant way of "sensing" viscosity and degree of cure using the SW signal as the model input. Figure 58 illustrates the model input and model predictions, i.e., viscosity and degree of cure. From Figure 58, it is seen that the model input (SW signal) is used to generate the corresponding T_g data. This, in turn, is used to yield predictions of viscosity and degree of cure.

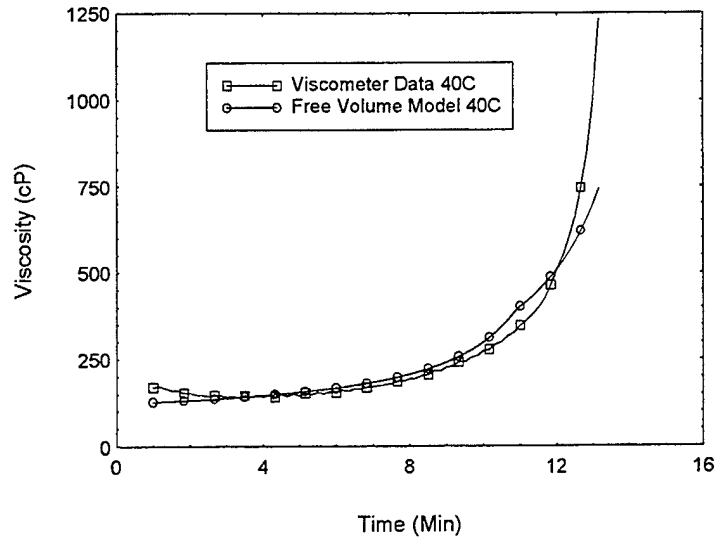


Figure 57. Viscosity prediction using free volume theory at 40 °C. (Degree of conversion obtained using FTIR.)

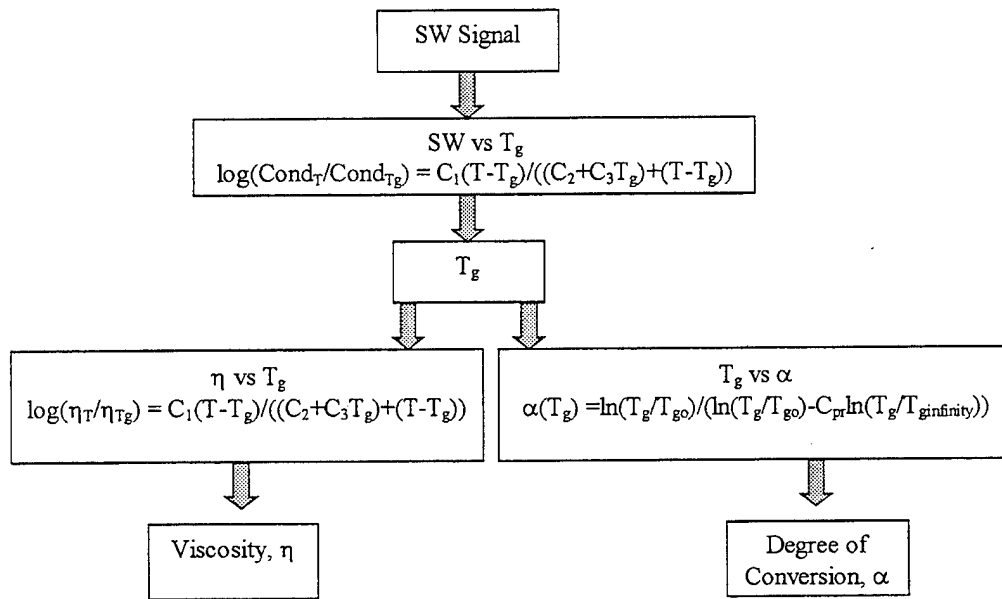


Figure 58. Schematic of viscosity and cure sensing using SMARTweave signal as the model input.

In essence, the glass transition temperature T_g is used as the common link to relate the three material parameters: (1) ionic conductivity, (2) viscosity, and (3) degree of cure. Figure 59 presents the development of T_g with cure time as predicted by the conductivity model using SW signal as the input.

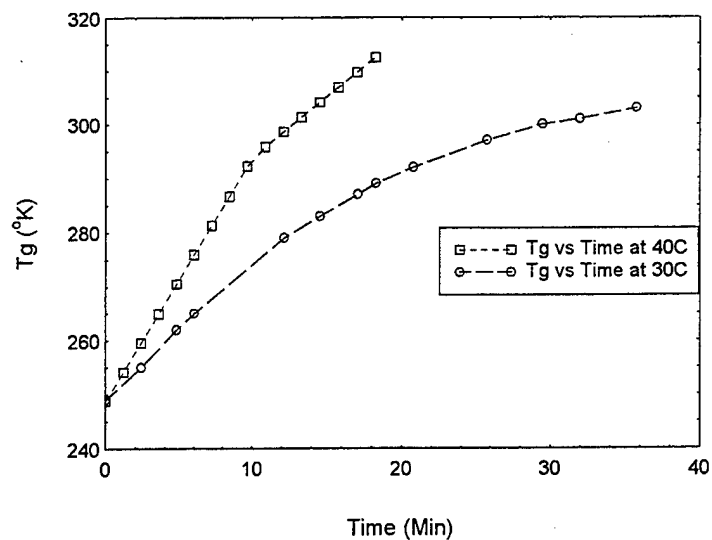


Figure 59. T_g (K) development with cure time as predicted by the free volume model.

As shown in Figure 58, this forms the intermediate step prior to the prediction of viscosity and degree of cure by using the WLF relationship and Venditti's relationship, respectively. While Figures 56 and 57 illustrated the predictive capability of the free volume model in estimating the macroscopic viscosity using the DC SW signal as the model input, Figures 60 and 61 present the degree of cure as predicted by the free volume model.

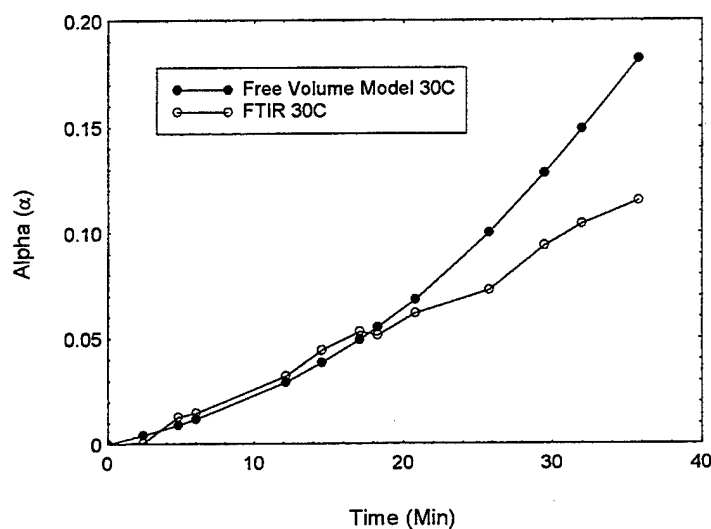


Figure 60. Degree of cure prediction from SW data at 30 °C using free volume theory.

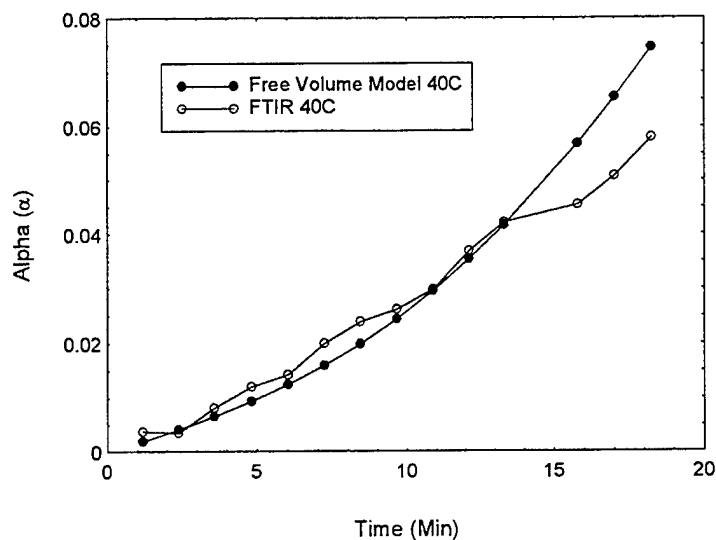


Figure 61. Degree of cure prediction from SW data at 40 °C using free volume theory.

Figures 62 and 63 present a parametric study performed using the previously described free volume model corresponding to an isothermal cure temperature of 40 °C. The parametric study was aimed at identifying the effect of experimental deviation of the ionic conductivity from the WLF model predicted by equation 25. A deviation of 1% and 5% were artificially introduced into the theoretical ionic conductivity predicted by the free volume model, and the subsequent effect on the model predictions of viscosity and the degree of cure was quantified. Figure 62 presents the variation in degree-of-cure prediction while Figure 63 presents the variation predicted for viscosity development during cure. From these figures, it is observed that the degree of cure and viscosity predictions deviate further from the actual values as bigger deviations are introduced to the model input, i.e., ionic conductivity. Figure 63 shows that the viscosity profiles corresponding to the variations in ionic conductivity, still show accurate predictions of gel time with in ± 2 min. Figure 62 shows large variations in degree-of-cure prediction in the early stages of cure. However, the degree of conversion values merge at vitrification. This is significant in resin infusion molding processes, where an accurate prediction of vitrification is key to demolding.

6.3 Predictive Capability of the Free Volume Model

Section 6.2 highlighted the ability of the free volume theory to predict the degree of cure, α , and viscosity, η , from the observed DC conductivity at 30° and 40 °C. However, these predictive capabilities depend on the specific model parameters obtained for the corresponding cure temperatures. In order to evaluate the predictive capability of this model, one set of universal parameters that

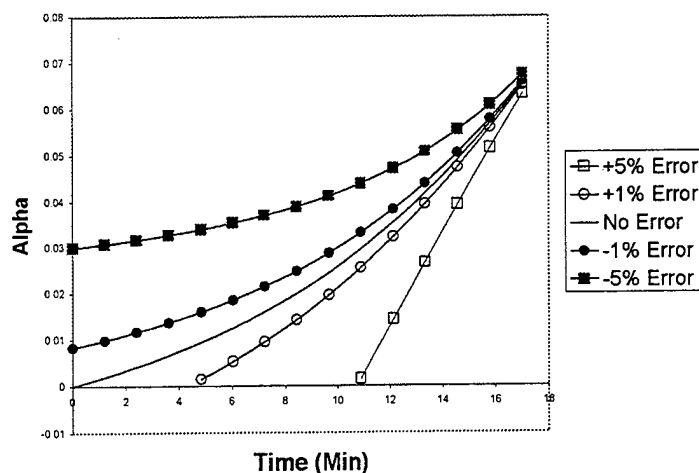


Figure 62. Effect of deviation of ionic conductivity on degree of cure prediction from the free volume model at 40 °C for 411-C-50.

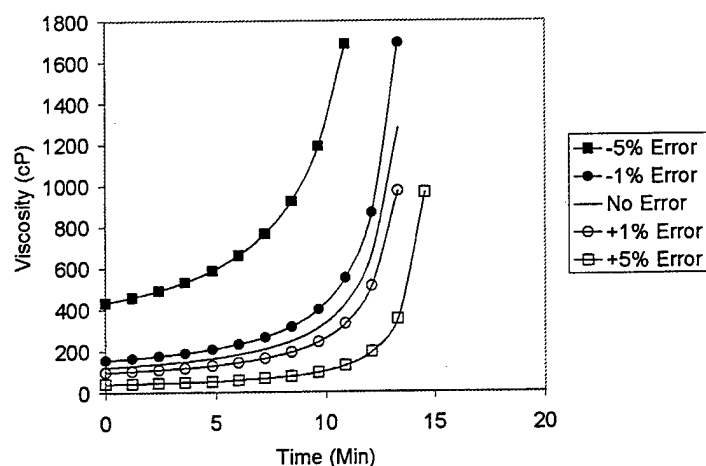


Figure 63. Effect of deviation of ionic conductivity on viscosity prediction from the free volume model at 40 °C for 411-C-50.

successfully describe the ionic conductivity and viscosity development within the temperature range of interest is used. These universal parameters were obtained as mathematical averages of the WLF constants corresponding to 30° and 40 °C in Tables 11 and 12. Section 6.3.1 discusses the effectiveness of these WLF parameters in describing the ionic conductivity behavior within the temperature range (30–40 °C) of interest. Section 6.3.2 presents the predictive capability of the WLF relationship in describing the viscosity development during cure.

6.3.1 Conductivity Model

As explained in section 6.2.3, the WLF relation given by equation 25 was used for ionic conductivity prediction:

$$\log(\text{Cond}_T / \text{Cond}_{T_g}) = C_1(T - T_g) / ((C_2 + C_3 T_g) + (T - T_g)) ,$$

and

$$\log(\text{Cond}_{T_g}) = C_4. \quad (25)$$

The WLF parameters C_1 - C_4 were obtained as the average of 30° and 40 °C given in Table 13. The averages are:

- $C_1 = 0.629$
- $C_2 = 5.567$
- $C_3 = -0.011$
- $C_4 = -6.814$

Figure 64 shows ionic conductivity behavior predicted at 30 °C and 40 °C by the free volume model. The predicted curves closely follow the time-related behavior of the experimental data. The theoretical ionic conductivity reflects the temperature effects on SW signal, by exhibiting slower rate of change at lower temperatures as discussed in section 4. An observation of Figure 64 is that the theoretical curves bound the experimental data on either side. For a lower temperature cure, the theoretical ionic conductivity is higher than the experimental data, while, in the case of 40 °C, the predicted values are lower than the experimental values. This suggests that, within the temperature range of 30° to 40 °C, the maximum deviation of the theoretical prediction from the experimental measurements will not exceed that shown in Figure 64. For temperatures between 30° and 40 °C, the theoretical predictions will be closer to the experimentally measured ionic conductivity. In all cases, the cutoff time for the SW signal is accurately predicted and serves as a good measure of vitrification.

6.3.2 Viscosity Model

Figure 65 shows the viscosity profile at 30° and 40 °C as predicted by the free volume model. The corresponding average WLF parameters are:

- $C_1 = -13.426$
- $C_2 = 7.3749$
- $C_3 = -0.020657$
- $C_4 = 15$

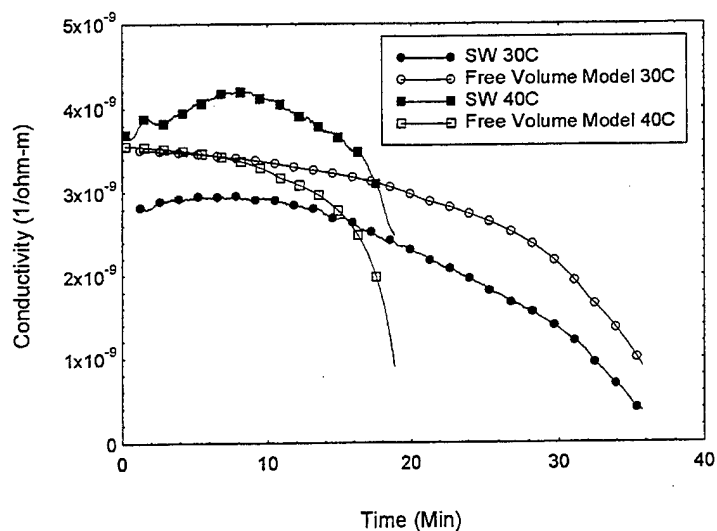


Figure 64. Free volume modeling of ionic conductivity using average WLF parameters.

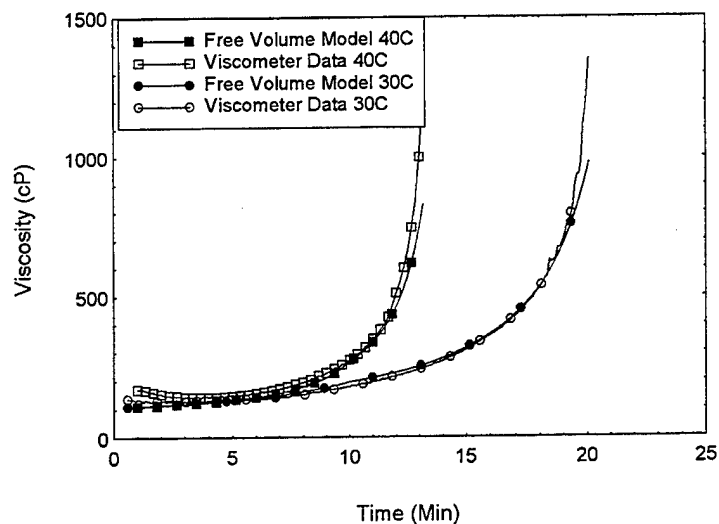


Figure 65. Free volume modeling of viscosity using average WLF parameters.

The predicted viscosity profiles closely follow the experimental values, highlighting the effectiveness of the average WLF constants in yielding accurate predictive capability to the free volume model. The predicted curves reflect differences in gel time and slower reaction rates at lower temperature as discussed in section 4.

6.4 Section Summary

This section discussed the applicability of free volume theory in modeling ionic conductivity and viscosity development during cure. The free volume modeling involved a three-step process, requiring cure kinetic model relating degree of cure and time, a T_g - α model relating the development of T_g during cure with the degree of conversion, and the use of WLF equation relating ionic conductivity and viscosity to the glass transition temperature, T_g . A modified form of the WLF equation was adopted for this research work. The conductivity model described in section 6.2.3 develops the free volume-based conductivity model at cure temperatures of 30° and 40 °C. WLF parameters specific to these processing temperatures were estimated. Section 6.2.4 develops the free volume modeling of viscosity. The free volume model serves as the continuum model, describing the material properties through gelation until vitrification. Figure 58 presents a schematic of the use of a free volume model in sensing the degree of cure and viscosity using the ionic conductivity observed by SW. This section also explored the feasibility of using a universal set of WLF constants for describing the ionic conductivity behavior and viscosity behavior within the temperature range (30–40 °C) of interest. The predicted ionic conductivity behavior and viscosity profiles closely followed experimental observations discussed in section 4.

The free volume model, similar to England's model, utilizes equations (27) and (28) for estimating ionic conductivity from the SW signal:

$$R_j(t) = (10/V_m(t))R_s - R_s, \quad (27)$$

$$\sigma = L/(R_j(t)A). \quad (28)$$

England [4] has shown the variation of the observed SW signal with changes in either the separation distance between the electrodes or the area of the electrodes. For relating the SW signal to the material properties like viscosity and the degree of cure, it is necessary to convert the observed SW signal to ionic conductivity, since ionic conductivity is an intrinsic material property and is independent of the way is measured. In this work, the observed SW voltage was converted to the resistance by equation 27. The resistance is related to the ionic conductivity by equation 28. An aspect ratio of 172.45 was estimated for the SNTC-3 single node test cells used in this research work. The conductivity hence obtained is related to the degree of conversion and viscosity through the WLF relationship.

The free volume model presented in this section satisfies the requirements of a continuum model. In short, the present model extends the capability of DC sensing as an effective cure monitoring tool, combining the ability to sense viscosity to gelation and degree of cure through gelation to vitrification.

7. Conclusions and Future Work

7.1 Introduction

SW is a flow front visualization and detection system that tracks the DC ionic conductivity of the polymer under consideration. This research is part of the ongoing effort to investigate how the DC signal could be utilized to measure in-situ the viscosity and degree of cure of the reacting resin. Previous work on conductivity modeling [4], though successful to gelation, failed to take advantage of the full capability of the SW system that reads the DC signal till vitrification. Above all, the current model attempts to correlate the intrinsic ionic conductivity changes to the resin's intrinsic parameters like viscosity and degree of conversion. The goals of this particular study which were successfully accomplished are:

- Develop a theoretical understanding of the ionic conductivity of the reacting resin system with an understanding of the relevant molecular events.
- Develop a continuum model describing SW data to vitrification with predictive capabilities with respect to degree of conversion and viscosity.
- Develop a methodology for characterizing other resin systems.

An attempt was made to extensively characterize the various molecular events possibly associated with the DC conductivity to develop the understanding of this phenomenon. The sensitivity of SW over the more widely used dielectric cure monitoring has been explored and possible reasons for the better capability of SW signal in representing the changes in resin properties were discussed. A free volume-based model was eventually adopted to describe the resin characteristics from the SW signal.

Section 7.2 provides a brief summary of sections 3-6, while section 7.3 outlines the free volume methodology for modeling any resin system based on DC sensing. Lastly, section 7.4 provides further insight into the possible research fronts one can adopt as a follow-on to this research effort.

7.2 Conclusions

Section 3 investigates the cure kinetics of two commercially used VE resins, namely 411-C-50 and 441-400, with emphasis on understanding the effect of temperature and styrene concentration. Autocatalytic modeling and the relevant kinetic parameters were obtained. FTIR measurements of the individual

conversions of VE and styrene were used for subsequent modeling in sections 5 and 6.

Section 4 dealt with the cure monitoring efforts on the previously mentioned resin systems using both SW and dielectrometer setups. The changes in the observed SW signal were linked with the molecular events such as macrogelation, network formation and cross-linking density. A comprehensive analysis of the dielectric behavior and the sensitivity of this cure monitoring technique to the previously mentioned molecular events have been explored. From the experimental results, it is seen that DC sensing is far more sensitive to cure-related changes in the early stages of cure, while AC sensing measures cure for a larger range of degree of cure.

Section 5 dealt with the analysis of heterogeneities in a VE resin system in the form of microgels. The relevance of microgels to the observed DC behavior was explored along with comprehensive efforts to separate the microgels from the reacting mixture for FTIR analysis. This section also presented visual evidence of the presence of these microgels in the form of AFM micrographs. Section 5 also explored the feasibility of a continuum model based solely on microgels. The discrepancy between the model predictions and the experimental results suggested a need for a better model, one that would take into account the development of network formation during cure.

Section 6 discussed the use of a classical free volume approach to model the conductivity behavior offering degree of cure and viscosity prediction capability based on the observed SW signal. This model takes into account the development of T_g with cure for relating ionic conductivity to degree of cure and viscosity. Since the development of T_g with cure reflects the extent of reaction going into network formation, the difficulty faced in section 5 is circumvented.

7.3 Summary of Free Volume Methodology

This research work presents a unique methodology of cure monitoring using DC sensors. The free volume model developed in section 6 presents a successful adaptation of the classical free volume theory to sense material properties till vitrification. The free volume-based continuum model, however, is even applicable to resin systems other than 411-C-50. A brief summary of the methodology that needs to be adopted for modeling other resin systems is presented.

The use of the WLF relationship to model the polymer behavior comprises three steps, which are three modeling efforts in themselves. First, one must develop a cure kinetic relationship relating degree of cure with time. Depending on the resin system, one can use either DSC or FTIR to obtain this information.

The second step comprises the development of T_g vs. the degree of cure relationship. This was accomplished using Venditti's equation (equation 23) in this research work. Typically linear or empirical relationships are utilized for the T_g - α model.

The third step is the adaptation of the modified WLF relationship (equations 25 and 26) for relating ionic conductivity and viscosity to the glass transition temperature T_g . The WLF parameters are obtained by fitting the corresponding WLF equations onto the experimental data. In systems such as epoxies, a set of temperature independent model parameters are known to exist. Figure 25 shows schematically how the continuum model already developed can be used for sensing the degree of conversion and viscosity during cure by making use of the measured SW signal as model input.

7.4 Recommendations for Further Research

7.4.1 Fundamental Understanding of T_g - α Relationship

The modeling effort presented in this research work highlighted the difference in the behavior of T_g vs. α at different cure temperatures. This necessitates the prediction of WLF parameters for discrete cure temperatures. However, a fundamental understanding of the T_g vs. α behavior in VE resins, would enable the development of a single T_g - α model. Such a development in the understanding of T_g behavior could be used for WLF modeling of ionic conductivity with a set of universal parameters, that would describe ionic conductivity behavior at any desirable cure temperature.

7.4.2 Positron Annihilation Studies

Effort should be directed to observe the actual development of the free volume through the use of positron annihilation studies [60]. A direct measurement of the free volume development with cure would eliminate the need for curve-fitting options to obtain the free volume parameters. Also this would eliminate the need to use the T_g - α relationship developed by Stone [11], which, as explained before, introduces variations in the observed WLF constants. Efforts should also be directed toward the use of radiotracers to identify the ionic pathways leading to the observed ionic conductivity.

8. References

1. Palmese, G. R. "Origin and Influence of Interphase Material Property Gradients in Thermosetting Composites," Ph.D. Dissertation, University of Delaware, Newark, DE, 1992.
2. Seemann III, W. H. "Plastic Transfer Molding Techniques for the Production of Fiber Reinforced Plastic Structures." U.S. Patent No. 4,902,215, February 20, 1990.
3. Walsh, S. M. "In-Situ Sensor Method and Device." U.S. Patent No. 5,210,499, May 11, 1993.
4. England, K. M. "Direct Current Sensing of Viscosity and Degree of Cure of Vinyl Ester Resins." Master's Thesis, University of Delaware, Newark, DE, 1997.
5. Fink, B. K., S. M. Walsh, D. C. DeSchepper, J. W. Gillespie, Jr., R. L. McCullough, R. C. Don, and B. J. Waibel. "Advances in Resin Transfer Molding Flow Monitoring Using SMARTweave Sensors." *Proceedings of the ASME Materials Division, MD-Vol. 69.2, 1995 International Mechanical Engineering Conference and Exposition*, pp. 999-1015, 1995.
6. Fink, B. K., S. M. Walsh, D. C. DeSchepper, J. Kleinmeyer, S. Bickerton, and R. C. Don. "Development of a Two-Sided Wiring Scheme for Resin Transfer Molding Flow Monitoring Using SMARTweave Sensor." CCM Report No. 95-08, University of Delaware-Center for Composite Materials, Newark, DE, 1995.
7. Walsh, S. M., and B. K. Fink. "Streamlining Material Acquisition Using Intelligent Processing and Prototyping." *Proceedings of the 20th Army Science Conference*, Norfolk, VA, 1996.
8. Kikuchi, A., E. Higuerey, and J. Coulter. "An Experimental Investigation of Resin Flow Sensing During Molding Processes," *Journal of Engineering Materials and Technology*, vol. 117, pp. 88-93, 1995.
9. Schwab, S. D., R. L. Levy, and G. G. Glover. "Sensor System for Monitoring Impregnation and Cure During Resin Transfer Molding." *Polymer Composites*, vol. 17, pp. 312-318, 1996.
10. Dua, S. "Network Formation in Styrene/Vinyl Ester Systems: Low Temperature Cure." CCM Report No. 98-02, University of Delaware-Center for Composite Materials, Newark, DE, 1998.

11. Stone, M. A. "Thermo-chemical and Thermo-mechanical Response of Reacting Polymers." CCM Report No. 97-13, University of Delaware-Center for Composite Materials, Newark, DE, 1997.
12. Stone, M. A., B. K. Fink, and J. W. Gillespie, Jr. "Thermo-Chemical Characterization of S2 Glass/Vinyl Ester Composites." Proceedings of the American Society for Composites Eleventh Technical Conference, Lancaster, PA: Technomic Publishing Company, Inc., 1996.
13. Flory, P. J. *Principles of Polymer Chemistry*. Ithaca, NY: Cornell University Press, 1953.
14. Stevens, M. P. *Polymer Chemistry, An Introduction*. Second ed., New York, NY: Oxford University Press, pp. 70-103, 1990.
15. Dua, S. Personal communication. University of Delaware, Newark, DE, 1998.
16. Brookfield Engineering Laboratories Inc. *Operating Instructions Manual for Brookfield Digital Viscometer Model DV-II+*. 1996.
17. England, K. M., B. K. Fink, and J. W. Gillespie, Jr. "In-Situ Sensing of Viscosity by Direct Current Measurements." *Processing and Manufacturing of Advanced Materials and Structures*, edited by T. J. Moon et al., ASME International Mechanical Engineering Congress and Exposition, 1996.
18. Bradley, J. E., B. K. Fink, and J. W. Gillespie, Jr. "On-line Process Monitoring and Analysis of Large Thick-Section Composite Parts Utilizing SMARTweave In-Situ Sensing Technology." Proceedings of the 43rd International SAMPE Symposium/Exhibition; Materials and Process Affordability-Keys to the Future, Covina, CA, 1998.
19. Heider, D., A. Graf, B. K. Fink, and J. W. Gillespie, Jr. "Feedback Control of the Vacuum-Assisted Resin Transfer Molding (VARTM) Process." *Proceedings of the SPIE International Symposium on NDE Techniques for Aging Infrastructure and Manufacturing: Process Control and Sensors for Manufacturing*, March 3-5, 1999, to be published.
20. Jadhav, N. C., U. K. Vaidya, M. V. Hosur, and J. W. Gillespie, Jr. "Flow and Cure Monitoring Using SMARTweave Sensing in Affordable Vacuum Assisted Resin Infusion Molding Process." *Proceedings of ASME symposium on Sensors and Controllers for Manufacturing, 1999 International Mechanical Engineering Congress and Exposition (IMECE)*, Nashville, TN, November 14-19, 1999, to be published.
21. Brill, R., and G. R. Palmese. Submitted to *Journal of Applied Polymer Science*.
22. Brill, R. P., R. L. McCullough, and G. R. Palmese. Proceedings of the 11th Technical Conference of ASC, 1996.

23. Bogetti, T. A., and J. W. Gillespie, Jr. "Process Induced Stress and Deformation in Thick Section Thermoset Laminates." *Journal of Composite Materials*, vol. 26, 1992.
24. Batch, G. L., and C. W. Macosko. "Kinetic Model for Crosslinking Free Radical Polymerization Including Diffusion Limitations." *Journal of Applied Polymer Science*, vol. 44, pp. 1711-1729, 1992.
25. Erns, J. B., and J. K. Gillham. "Time-Temperature-Transformation (TTT) Cure Diagram: Modeling the Cure Behavior of Thermosets." *Journal of Applied Polymer Science*, vol. 28, pp. 2567-2591, 1993.
26. Dusek, K., and J. Spevacek. "Cyclization in Vinyl-divinyl Copolymerization." *Polymer*, vol. 16, pp. 1043-1046, 1980.
27. Dusek, K., H. Galina, and J. Mikes. "Features of Network Formation in the Chain Crosslinking (Co)Polymerization." *Polymer Bulletin (Berlin)*, vol. 3, pp. 19-25, 1980.
28. Palmese, G. R. Personal communication. University of Delaware, Newark, DE, 1998.
29. Ziaee, S. Personal communication. University of Delaware, Newark, DE, 1998.
30. Lee, J. H., and J. W. Lee. "Kinetic Parameters Estimation for Cure Reaction of Epoxy Based Vinyl-ester Resin." *Polymer Engineering and Science*, vol. 34, no. 9, pp. 742-749, 1994.
31. Lam, P. W. K., T. Trans, and H. P. Plaumann. "An Improved Kinetic Model for the Autocatalytic Curing of Styrene Based Thermoset Resins." *Journal of Applied Polymer Science*, vol. 41, pp. 3043-3057, 1990.
32. Yang, Y. S., and L. J. Lee. "Rheokinetic Studies of Unsaturated Polyester Resins." *Polymer Process Engineering*, vol. 5, pp. 327-356, 1988.
33. Dalal, U. Personal communication. University of Delaware, Newark, DE.
34. Adler, D., L. P. Flora, and S. D. Senturia. "Electrical Conductivity in Disordered Systems." *Solid State Communication*, vol. 12, pp. 9-12, 1973.
35. Kirkpatrick, S. "Classical Transport in Disordered Media: Scaling and Effective Medium Theories." *Physical Review Letters*, vol. 27, pp. 1722-1725, 1971.
36. Kirkpatrick, S. "Percolation and Conduction." *Reviews of Modern Physics*, vol. 45, pp. 574-588, 1973.
37. Lobb, C. J., and D. J. Frank. "A Large-cell Renormalization Group Calculation of the Percolation Conduction Critical Exponent." *Journal of Physical Chemistry*, vol. 12, pp. L245-L248, 1979.

38. Straley, J. P. "Critical Exponents for the Conductivity of Random Resistor Lattices." *Physical Review*, vol. 15, pp. 5733-5737, 1977.
39. Watson, B. P., and P. L. Leath. "Conductivity in the Two-Dimensional Site Percolation Problem." *Physical Review B*, vol. 9, pp. 4893-4896, 1974.
40. Yuge, Y., and K. Onizuka. "Monte Carlo Experiment for the Two-Dimensional Site Percolation Network." *Journal of Physical Chemistry*, vol. 11, pp. L763-L765, 1978.
41. Last, B. J., and D. J. Thouless. "Percolation Theory and Electrical Conductivity." *Physical Review Letters*, vol. 27, pp. 1719-1721, 1971.
42. Rutgers, R. "Relative Viscosity of Suspensions of Rigid Spheres in Newtonian Liquids." *Rheologica Acta*, vol. 2, pp. 202-210, 1962.
43. Mooney, M. "The Viscosity of a Concentrated Suspension of Spherical Particles." *Journal of Colloid Science*, vol. 6, pp. 162-170, 1951.
44. Oliver, D. G., and S. G. Ward. "Relationship Between Relative Viscosity and Volume Concentration of Stable Suspension of Spherical Particles." *Nature*, vol. 171, p. 396, 1953.
45. Hadad, D. K. *Epoxy Resins Chemistry and Technology*. 2nd Edition, edited by C. A. May. New York, NY: Marcel Dekker, 1988.
46. Simpson, J. O., and S. A. Bidstrup. "Correlation Between Chain Segment and Ion Mobility in an Epoxy Resin System. A Free Volume Analysis." *Journal of Polymer Science. Part B, Polymer Physics*, vol. 31, pp. 609-618, 1993.
47. Bidstrup, S. A., and J. O. Simpson. "The Effect of Stoichiometry on Chain Segment and Ion Mobility in Partially Polymerized Epoxy Systems." *Journal of Polymer Science. Part B, Polymer Physics*, vol. 32, pp. 43-53, 1994.
48. Williams, M. L., R. F. Landel, and J. D. Ferry. "The Temperature Dependence of Relaxation Mechanisms in Amorphous Polymers and Other Glass-Forming Liquids." *Journal of American Chemical Society*, vol. 77, pp. 3701-3705, 1955.
49. Doolittle, A. K. "Studies in Newtonian Flow II. The Dependence of the Viscosity of Liquids on Free-Space." *Journal of Applied Physics*, vol. 22, pp. 1471-1475, 1951.
50. Doolittle, A. K. "Studies in Newtonian Flow III. The Dependence of the Viscosity of Liquids on Molecular Weight and Free-Space." *Journal of Applied Physics*, vol. 23, pp. 236-239, 1952.
51. Cohen, M. H., and D. Turnbull. "Molecular Transport in Liquids and Glasses." *Journal of Chemical Physics*, vol. 31, p. 1164, 1959.
52. Bueche, F. "Rate and Pressure Effects in Polymers and Other Glass Forming Substances." *Journal of Chemical Physics*, vol. 36, pp. 2940-2951, 1962.

53. Adam, G., and J. H. Gibbs. "On the Temperature Dependence of Cooperative Relaxation Properties in Glass-Forming Liquids." *Journal of Chemical Physics*, vol. 43, pp. 139-146, 1965.
54. Senturia, S. D., and N. F. Sheppard. "Dielectric Analysis of Thermoset Cure." *Advanced in Polymer Science*, vol. 80, pp. 1-47, 1986.
55. Gillham, J. K. "Formation and Properties of Thermosetting and High Tg Polymeric Materials." *Polymer Engineering and Science*, vol. 26, p. 1429, 1986.
56. Venditti, R. A., and J. K. Gillham. "Anomalous Behavior of Thermosetting Systems After Cure vs. Chemical Conversion: A Normalized Conversion-Temperature-Property Diagram." *Journal of Applied Polymer Science*, vol. 56, pp. 1687-1705, 1995.
57. Wang, X., and J. K. Gillham. "Tg-Temperature Property Diagram for Thermosetting Systems: Anomalous Behavior of Physical Properties vs. Extent of Cure." *Journal of Applied Polymer Science*, vol. 47, pp. 425-446, 1993.
58. Wisanrakkit, G., and J. K. Gillham. "The Glass Transition Temperature (Tg) as an Index of Chemical Conversion for a High-Tg Amine-Epoxy System: Chemical and Diffusion Controlled Reaction Kinetics." *Journal of Applied Polymer Science*, vol. 41, pp. 2885-2959, 1990.
59. Maffezzoli, A., A. Trivisano, M. Oplaicki, J. Mijovic, and J. M. Kenny. "Correlation Between Dielectric and Chemorheological Properties During Cure of Epoxy-Based Composites." *Journal of Materials Science*, vol. 29, pp. 800-808, 1994.
60. Kobayashi, Y., K. Haraya, S. Hattori, and T. Sasuga. "Evaluation of Polymer Free Volume by Positron Annihilation and Gas Diffusivity Measurements." *Polymer*, vol. 35, pp. 925-928, 1994.

INTENTIONALLY LEFT BLANK.

Appendix A. Dielectric Cure Monitoring

A.1 Basis of Dielectric Behavior

When a viscoelastic polymeric material containing permanent dipoles are placed in an alternating electric field the reorientation of dipoles upon the reversal of the electric field is not instantaneous. Consequently, when an alternating time-dependant voltage is applied to a parallel plate condenser, the corresponding time-dependent current will lag behind the applied voltage by a phase angle δ . Applying the phenomenological theory of linear dielectric relaxation behavior,^{1,2} it can be shown that the complex dielectric constant is given by

$$\epsilon^* = \epsilon_u + (\epsilon_r - \epsilon_u)/(1 + i\epsilon\tau) \quad (\text{A.1})$$

or

$$\epsilon^* = \epsilon' - i\epsilon'', \quad (\text{A.2})$$

where ϵ' = permittivity (real or storage component of the dielectric constant), and ϵ'' = loss factor (imaginary or loss component of the dielectric constant).

By using the parallel plate approximation,³ the capacitance of can be related to the permittivity and the loss factor to obtain:

$$\text{Dissipation} = \epsilon''/\epsilon'. \quad (\text{A.3})$$

The permittivity and loss factor can then be used to determine the material's average dipole relaxation time and the specific conductivity. The loss factor has two components, one associated with ionic conduction and the other associated with dipolar rotation:

$$\epsilon'' = \sigma/(\omega\epsilon_0) + \epsilon''(\text{dipolar}), \quad (\text{A.4})$$

where σ = specific conductivity, ω = angular frequency, ϵ_0 = permittivity of free space, and ϵ'' (dipolar) = dipolar contribution to the loss factor.

The specific conductivity is usually assumed to be a direct function of the loss component of the dielectric constant, when the loss factor exceeds 50:

$$\sigma = (\epsilon'')(\omega)(\epsilon_0). \quad (\text{A.5})$$

¹ Mccrum, N. G., B. E. Read, and G. Williams. *Anelastic and Dielectric Effects in Polymeric Solids*. New York, NY: Wiley, 1967.

² Ferry, J. D. *Viscoelastic Properties of Polymers*. Second Edition, New York, NY: Wiley, 1980.

³ May, C. A. *Interrelations Between Processing Structure and Properties of Polymeric Materials*. Amsterdam: Elsevier, 1984.

This is the region where the dipolar contribution to the loss factor for this system usually is less than 5% of the total observed signal. The dipolar relaxation time τ is given by the reciprocal of angular frequency corresponding to when the dipolar contribution to the loss factor reaches the maximum.

$$\tau = 1/\omega_{\max}, \quad (\text{A.6})$$

where τ = dipole relaxation time and ω_{\max} = angular frequency corresponding to when the dipolar contribution to the loss factor reaches the maximum.

A.2 Dielectric Measurements for On-line Cure Monitoring

The major limitation of dielectric techniques for in-situ monitoring of cure is the lack of both fundamental and phenomenological correlations between the dielectric signal and the processing parameters. Apart from the theoretical challenge, such information would be of considerable importance to the manufacturers of composites.

It must be noted that the dielectric behavior of a substance depends essentially on its structure and on the true electric field acting on it in the presence of an external macroscopic electric field. The available expressions for nonpolar materials when only electronic or atomic polarizations are observed can be well represented by the dielectric properties for gas and liquid states. On the other hand, the development of expressions relating the molecular structure and the dielectric constant for simple polar substances in the liquid state, such as water, is a difficult matter as a consequence of the effect of the local electric field, usually different from the macroscopic one. The prediction of the dielectric properties in the solid state is still more complex, not only as a consequence of the differences in the local and macroscopic electric field, but also because the dipoles are hindered in the motion. Reactive mixtures such as unsaturated polyester resin systems with many pendant polar groups and steric hinderances are much more complicated to model. As a result, the dielectric behavior have been correlated only qualitatively to fundamental processing parameters.^{4,5}

A.2.1 Ionic Resistivity

The determination of ionic resistivity with the currently available sensor instruments, is based upon the assumption that the free migrating ions are initially present in the resin owing to the contamination and other impurities such as Cl^- , which are unavoidable owing to the very nature of the synthesis of epoxies and, hence, vinyl-ester (VE) resins. Ionic resistivity depends on the ionic

⁴ Kranbuehl, D. E., S. E. Delos, and P. K. Jue. "Dielectric Properties of the Polymerization of an Aromatic Polyimide." *Polymer*, vol. 27, pp. 11-18, 1986.

⁵ Day, D. R. "Dielectric Determination of Cure State During Non-Isothermal Cure." *Polymer Engineering and Science*, vol. 29, pp. 334-338, 1989.

charge, q , number of ions, n , and on the mobility factor, m , sensitive to the structural changes of the matrix.

During cure, the ionic conductivity decreases owing to the reduction in the mobility of the ions as a result of cross linking and other related molecular events. The type and the concentration of the ions, as well as the effect that these two parameters exert on the dielectric measurements are not worthwhile quantifying, considering the large variety of resin systems, and the inevitable vicissitudes of the batch-to-batch characteristics. The isolation of ionic contribution to the dielectric signal occurs at different frequencies corresponding to different stages of the resin cure and it is more of an educated guess than an accurate representation of the actual contribution within the resin system. This also necessitates experiments performed at a series of frequencies until the right range is chanced upon.

A.2.2 Dielectric Constant and Dielectric Loss

Most of the research dealing with the dielectric constant and the dielectric loss has been devoted to the derivation of a fundamental expression for loss factor, which can then be used for correlating to describe the observed experimental results. Many difficulties arise from such an approach because in polymeric systems, the local internal electric field is not known. Its accurate determination is difficult, as the number of dipoles to the electric field varies as a function of the size of the segment to which the dipole is attached and the surroundings that hinder the dipole rotation to a different degree. This impedes any work directed towards relating the observed loss factor to the degree of reaction directly. Recently, Maffezzoli et al.⁶ were able to identify a frequency range in which the dielectric behavior was dominated by the disappearance of epoxy groups, allowing for a direct correlation between the dielectric signal and the degree of cure.

⁶ Maffezzoli, A., A. Trivisano, M. Oplaicki, J. Mijovic, and J. M. Kenny. "Correlation Between Dielectric and Chemorheological Properties During Cure of Epoxy-Based Composites." *Journal of Materials Science*, vol. 29, pp. 800-808, 1994.

INTENTIONALLY LEFT BLANK.

Appendix B. Calculation of the Volume Fraction of Microgels

The following calculation of the volume fraction of microgels assumes the following:

- All the reaction as observed by the Fourier-transform infrared (FTIR) goes into the formation of microgels.
- All microgels are of uniform spherical size of say diameter = 150nm.
- Density of monomers in the unreacted resin and that in the microgel remains the same.
- All vinyl-ester (VE) monomers are double-end reacted.

(1) Density of VE resin system = D_{Resin}

(2) Density of styrene (ST) monomer = D_{ST}

(3) Density of VE monomer = D_{VE}

(4) Volume of VE resin system = V_{Resin}

$$\text{Volume of VE monomers} = 0.52 * V_{\text{Resin}} * D_{\text{Resin}} / D_{\text{VE}} = V_{\text{VE}} \quad (\text{B.1})$$

$$\text{Volume of ST monomers} = 0.48 * V_{\text{Resin}} * D_{\text{Resin}} / D_{\text{ST}} = V_{\text{ST}} \quad (\text{B.2})$$

At time t:

- Degree of conversion of VE = α_{VE}
- Degree of conversion of ST = α_{ST}

$$\text{Volume of VE in microgels} = V_{\text{VE}} * \alpha_{\text{VE}} = V_{\text{VE Microgel}} \quad (\text{B.3})$$

$$\text{Volume of ST in microgels} = V_{\text{ST}} * \alpha_{\text{ST}} = V_{\text{ST Microgel}} \quad (\text{B.4})$$

$$\text{Volume of microgel} = 4 * \pi * R_{\text{Microgel}}^3 / 3 = V_{\text{Microgel}} \quad (\text{B.5})$$

$$\text{Number of microgels} = V_{\text{Microgel}} / (V_{\text{VE Microgel}} + V_{\text{ST Microgel}}) \quad (\text{B.6})$$

INTENTIONALLY LEFT BLANK.

Appendix C. Determination of L/A Ratio of Single Node Test Cell (SNTC)-3

A typical SNTC-3-type cell is shown in Figure C-1. Owing to the very nature of the placement of the electrodes, i.e., orthogonal placement, it presents a special problem in obtaining the conductivity data from the observed SMARTweave (SW) voltage. A typical single-node circuit diagram is given in Figure C-2. Applying basic Kirchoff's laws, one ends up with an expression for the Resistance of the resin as:

$$R_j = (10 \cdot R_{\text{sense}} / V_{\text{measured}}) - R_{\text{sense}}, \quad (\text{C.1})$$

where R_j is the resistance of the resin, R_{sense} is the sense resistance of value $10\text{M}\Omega$, and V_{measured} is the measured SMARTWeave (SW) voltage.

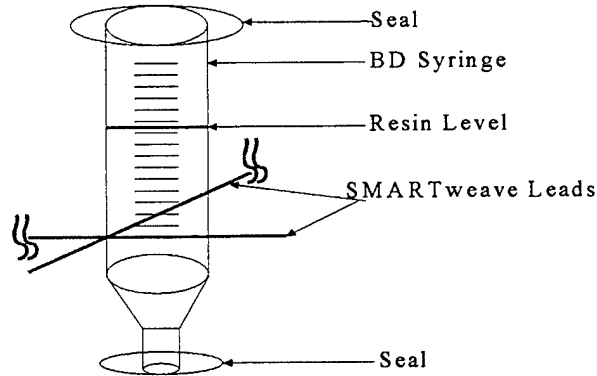


Figure C-1. SNTC-3 single node test cell.

From the resistance one can obtain the conductivity σ as:

$$\sigma = L / (R_j A), \quad (\text{C.2})$$

where L is the separation distance between the electrodes and A is the effective electrode surface area.

In case of parallel plate setup, this is essentially a straightforward problem. However, for the orthogonal set-up in single node test cell (SNTC)-3, the L/A ratio needs to be estimated indirectly.

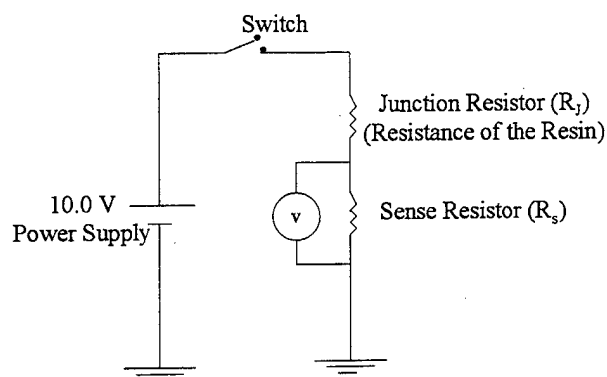


Figure C-2. Circuit diagram of a single node cell.

There are many different ways of determining the characteristic conductivity of a material. American Society for Testing and Materials (ASTM) standard D257-78¹ offers a variety of solutions for determining the DC conductivity of a material. One such method has been adopted for our purposes of DC conductivity measurements. The basic setup consists of two concentric cylinders sealed at one end made of aluminum. Figure C-3 shows the basic components and dimensions of the fabricated DC conductivity cell used in this study.

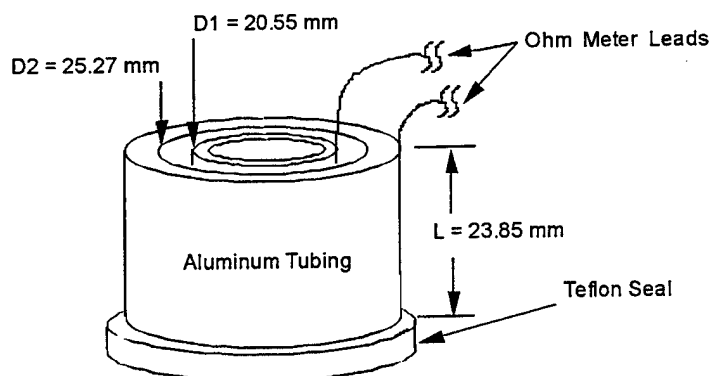


Figure C-3. Experimental cell for conductivity studies.

The outer and inner cylinders were machined out of aluminum and the seal was fabricated out of Teflon owing to its inertness.

Resistance values obtained using this setup can be converted into resistivity values by using the following equation:

$$\rho = 2\pi LR / (\ln(D_2/D_1)). \quad (C.3)$$

¹ American Society for Testing and Materials. "Test Method for Determining D-C Resistance or Conductance of Insulating Materials." ASTM D257-78, 1986.

The resistivity obtained can then be equated to the resistivity calculated using the resistance measured using SNTC-3 cell as follows:

$$\rho_{\text{SNTC-3}} = R_j A_{\text{SNTC-3}} / L_{\text{SNTC-3}}. \quad (\text{C.4})$$

This exercise was performed for different resin types at different temperatures. An average value of 172.45 was obtained for $(L/A)_{\text{SNTC-3}}$.

INTENTIONALLY LEFT BLANK.

Appendix D. Doping Results

D.1 Introduction

Vinyl-ester (VE) resins are inherently high resistance resins, i.e., they possess high resistivity. The source of ions in VE resins are primarily from the manufacturing step involving synthesis from epoxies, which are known to have chloride ions (Cl^-) as contaminants. Research work by England [4] has shown an increase in the ionic conductivity of VE with the addition of both cobalt naphthenate (CoNap) and Trigonox. This is due to the fact that CoNap and Trigonox dissociate on addition to VE resins.

The concentration of chloride ions are highly variable from one batch of VE resin to another. Also the SMARTweave (SW) signal obtained exhibited a low signal to noise (S/N) ratio. To improve the quality of observed direct current (DC) signal and to quantify the concentration of ions in the resin system, doping was adopted by England. Doping was achieved by introducing 0.1 weight-percent of an organic salt into the neat VE resin. England identified two such organic salts that favorably increase the observed DC signal on addition to the resin mixture: tetrabutyl ammonium acetate (TA) and tetra butyl ammonium iodide (TI). In his research work, England adopted the use of TA for doping. A cost analysis, however, indicated that replacing TA (\$3.50/g), with TI (\$0.25/g) is desirable from an economic point of view.

D.2 Cure Monitoring

Figure D-1 shows a comparison of an SW signal obtained using TI as a dopant against TA-doped 411-C-50 VE resin and undoped 411-C-50 resin mixture at an isothermal cure temperature of 40 °C. Figure D-2 presents the SW response of undoped resin on a different scale for better comparison. From Figure D-1, it is seen that the addition of dopants increases the SW signal by as much as a factor of 15. This translates into a better S/N ratio as observed from a comparison with Figure D-2 corresponding to undoped resin, where one sees a significant presence of noise.

As evident from Figure D-1, though the addition of dopants to the resin mixture increases the ionic conductivity, the SW profile of the curing resin remains largely unaltered. A comparison of Figures D-1 and D-2 reveals that the TA-doped resin mixture shows faster gelation (inflection point) and faster cutoff of the DC signal. However TI doped resin, follows more closely the behavior of undoped resin, highlighting another advantage to the use of TI over TA.

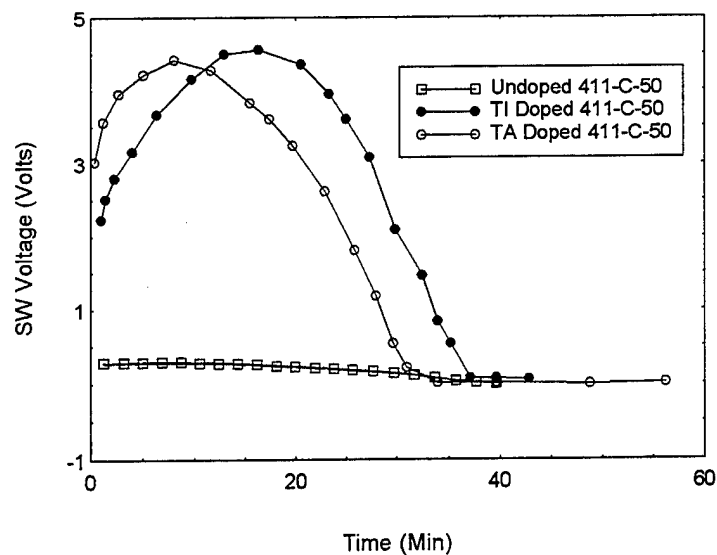


Figure D-1. Comparison of SW response of TI-doped 411-C-50 against TA- doped and undoped 411-C-50 at an isothermal cure temperature of 40 °C.

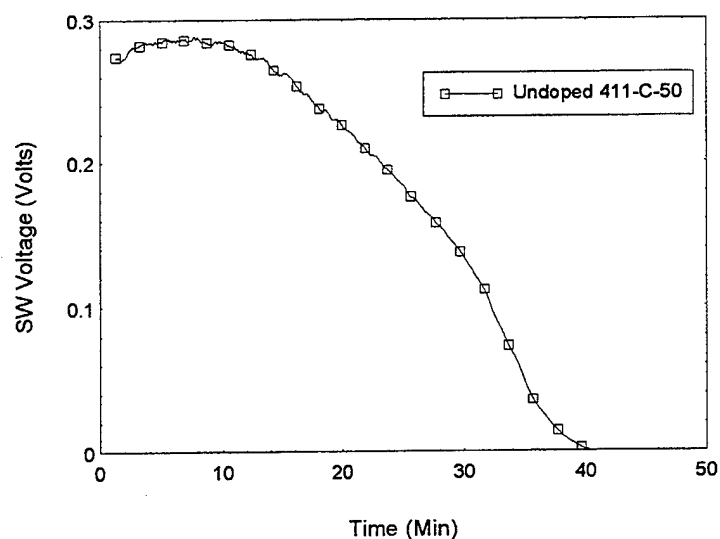


Figure D-2. SW response of undoped 411-C-50 at an isothermal cure temperature of 40 °C.

D.3 Cure Kinetics

One of the desirable qualities of dopants is that the addition of dopants to resin mixtures should not affect the rate of cure reaction. To investigate the effect of TI on the cure kinetics of the VE resin, infrared (IR) spectroscopy was performed on curing VE samples at an isothermal temperature of 40 °C. Figure D-3

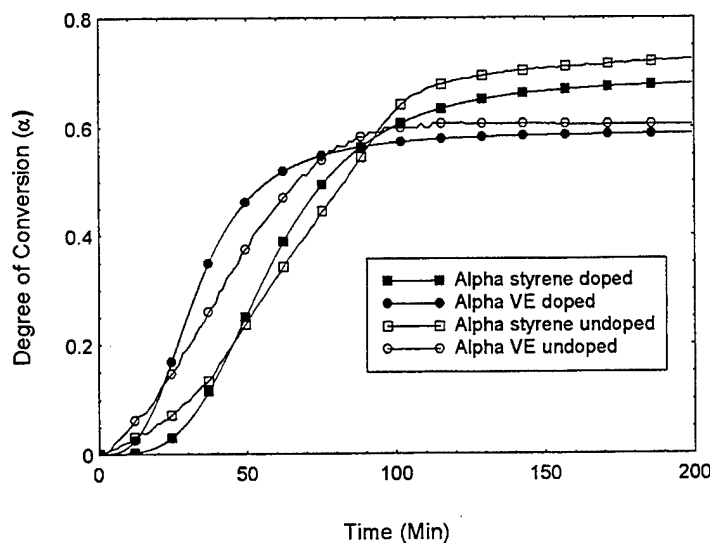


Figure D-3. Degree of conversion comparison between doped and undoped resin at 40 °C isothermal cure temperature.

presents the degree of conversions of VE and styrene monomers for both doped and undoped 411-C-50 resin mixtures. Figure D-3 reveals that the addition of TI to the curing resin mixture results in slower rates of monomer conversion and a lower maximum degree of conversion. Similar effect has been reported by England¹ for TA-doped resin mixtures. This suggests that the addition of dopants could potentially affect the network development during cure. Since one of the objectives of this research work is to gain an understanding of the network development during cure, dopants were not used for the remainder of this project.

¹ England, K. M. "Direct Current Sensing of Viscosity and Degree of Cure of Vinyl Ester Resins." Master's Thesis, University of Delaware, Newark, DE, 1997.

INTENTIONALLY LEFT BLANK.

Appendix E. Percolation Model

E.1 Introduction

Percolation theory is a mathematical theory which deals with disordered systems and give good application to the description of electrical conduction in disordered materials, such as conductor-insulator mixture. The conductivity of a composite material with spherical particles, of different electrical behavior (say insulator) can be predicted by a percolation model. Literature presents a number of efforts directed towards observing such a system.^{1,2,3,4}

In this study, an effort is made to describe the SMARTweave (SW) data based on the percolation model. The system under consideration is vinyl-ester (VE) resin undergoing cure, and the SW data corresponds to the drop in the observed conductivity with the proceeding of cure. This essentially presents a classical percolation problem in which regions (roughly spherical) of differing electrical behavior appear in a continuous medium in a random manner. In the system under consideration, the curing leads only to the formation of microgels, of a roughly spherical nature, which are assumed to have zero contribution towards the observed conductivity. With time, the number and hence the volume percentage of these dead zones (microgels) increase and this manifests itself as a decrease in the observed conductivity. Figure E-1 represents various stages of cure.

E.2 Theory

A percolation model was proposed first by Broadbent and Hammersley⁵ in 1957. Hammersley developed the theory further by successive papers on this approach. A detailed introduction and review of the applicability of percolation

¹ Abeles, B., H. L. Pinch, and J. I. Gittleman. "Percolation Conductivity in W-Al₂O₃ Granular Metal Films." *Physical Review Letters*, vol. 35, pp. 247-250, 1975.

² Deutscher, G., M. Rappaport, and Z. Ovadyan. "Random Percolation in Metal-Ge Mixtures." *Solid State Communication*, vol. 28, pp. 593-595, 1978.

³ Gurland, J. "The Fracture Strength of Sintered Tungsten Carbide-Cobalt Alloys in Relation to Composition and Particle Spacing." *Transactions of Metallurgical Society of AIME*, vol. 227, pp. 1146-1150, 1963.

⁴ Gurland, J. "An Estimate of Contact and Continuity of Dispersions in Opaque Samples." *Transactions of Metallurgical Society of AIME*, vol. 236, pp. 642-646, 1996.

⁵ Broadbent, S. R., and J. M. Hammersley. "Percolation Processes I. Crystals and Mazes." *Proceedings of Cambridge Philosophical Society*, vol. 53, pp. 629-641, 1957.

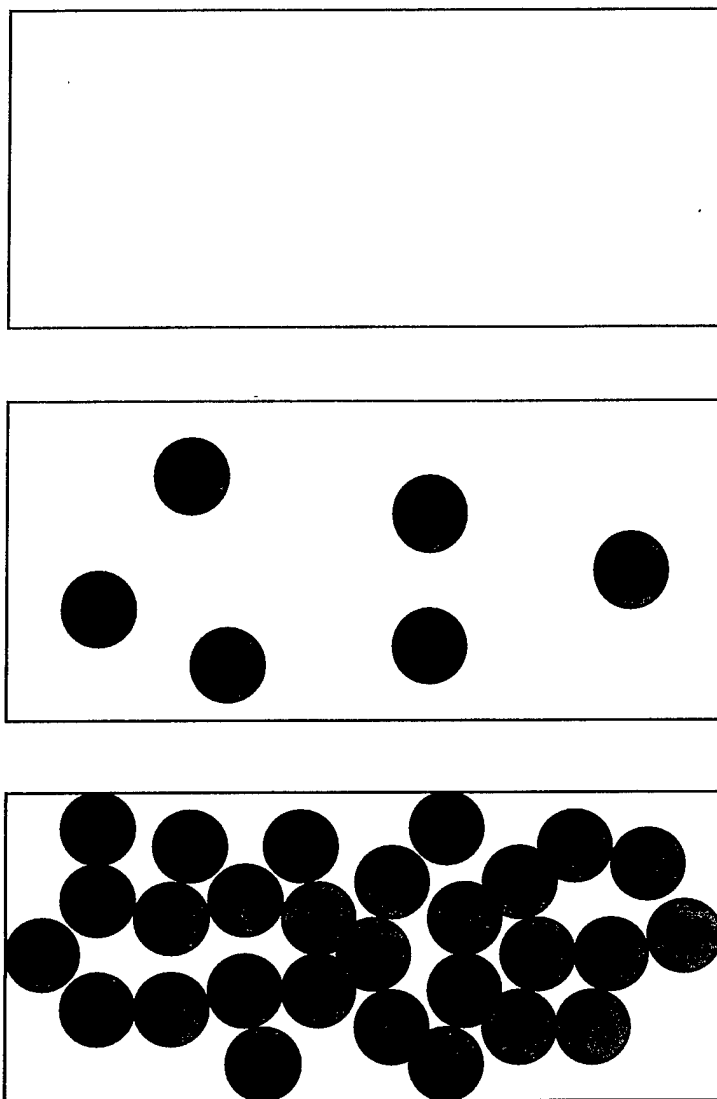


Figure E-1. Illustration of increasing volume contribution of the microgels with cure.

theory to a number of situations can be found in the 1963 review by Frisch and Hammersley,⁶ and in a 1971 article by Shante and Kirkpatrick.⁷

In brief, there are two types of percolation problems. If the occupancy of bonds is governed by a stochastic mechanism, the problem can be termed a "bond percolation problem," whereas if the problem is that of site, it is termed "a site percolation problem." A path between the two sites is said to exist if the two

⁶ Frisch, H. L., and J. M. Hammersley. *Journal of the Society of Industrial and Applied Mathematics*, vol. 11, p. 894, 1963.

⁷ Shante, V. K. S., and S. Kirkpatrick. "An Introduction to Percolation Theory." *Advances in Physics*, vol. 20, pp. 325-357, 1971.

sites are connected by a sequence of sites and bonds. Though there may be many paths between a given pair of sites, the sites are said to be connected if there exists at least one path between them. This is known as "pair connectedness," and its probability plays a significant role in many applications. The presence of the path, for example, allows the flow of charges between the two sites which are connected by the path. A set of occupied sites connected to one another through bonds is called a "cluster." When the probability of occupied sites P_s or that of occupied bonds P_b increases so do the cluster size. At a critical value of P_b or P_s , the cluster size becomes infinite. At this stage, the system is said to be in a percolating stage. A detailed description and applicability are discussed elsewhere.^{2,8}

Table E-1 gives the various lattices and the corresponding critical P_b (P_{cb}) and P_s (P_{cs}).

Table E-1. Percolation thresholds.

Lattice	d	z	Monte Carlo		Series Expansion	
			P_{cb}	P_{cs}	P_{cb}	P_{cs}
Honeycomb	2	3	0.688	0.64	0.698	0.653
Square	2	4	0.581	0.498	0.593	0.5
Triangular	2	4	0.655	0.435	0.6527	—
Simple Cubic	3	6	0.325	0.254	0.310	0.247
Diamond	3	4	0.436	0.390	0.428	0.388
Body-Centered Cubic (BCC)	3	8	—	—	0.245	0.178
Face-Centered Cubic (FCC)	3	12	0.199	0.125	0.198	0.119

E.3 Percolation and Conduction

Electrical conductivity in disordered systems akin to that present in our resin system has been studied extensively.^{2-4,9} Gurland⁴ studied the system composed of Bakelite and silver. The system exhibited a strong and abrupt transition in its conducting behavior at a volume-percent of 30-40 (silver). In 1975, Abeles et al.¹

⁸ Malliaris, A., and D. T. Turner. "Influence of Particle Size on the Electrical Resistivity of Compacted Mixture of Polymeric and Metallic Powders." *Journal of Applied Physics*, vol 42, pp. 614-618, 1971.

⁹ Hammersley, J. M., and K. W. Morton. "Poor Man's Monte Carlo." *Journal of Royal Statistical Society. B*, vol. 16, pp. 23-38, 1954.

studied a composite of W-Al₂O₃ exhibiting a sharp transition between a conducting material to being an insulator below a critical volume fraction of W of 0.47. A study of a nickel-polyvinylchloride (PVC) mixture by Mallaris and Turner⁸ deals with percolating situation, very similar to that observed in VE resin systems. The study successfully applied percolation principles to describe the observed conductivity, as well as catalogued a detailed study on the influence of particle size on the observed electrical resistivity of the mixture.

E.4 Evidence of Percolation in VE system

A key feature that sets apart a percolating system is the abrupt transition of, say, electrical behavior with change in the volume contribution of one of the constituents. This seems to be true in the case of the VE resin system, too, as illustrated by experimental results presented in Figures E-2 and E-3. These figures illustrate the convergence of the curves in the region of acute conductivity transition to a narrow range of volume fraction (of microgels). Based on the success of percolation model in describing systems similar to the VE systems and primarily due to the fact that the conductivity of VE follows the expected trends of a percolation model, one can reasonably expect to model the VE system based on percolation.

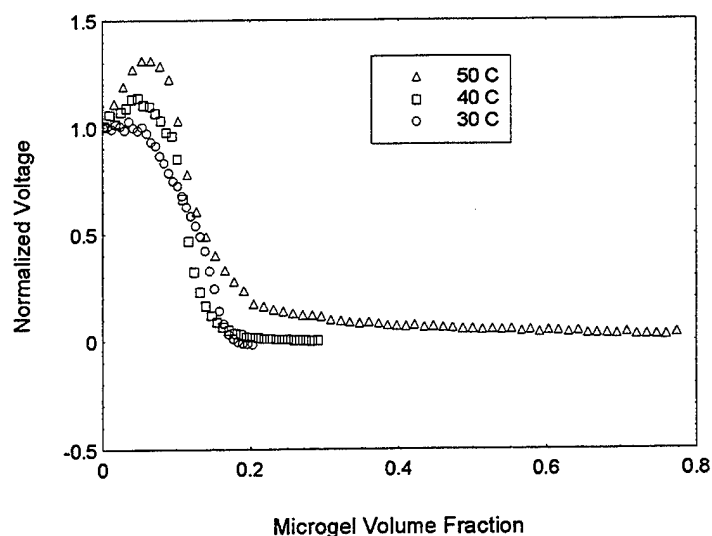


Figure E-2. Normalized DC signal vs. microgel volume fraction of Derakane 411-C-50 at different isothermal cure temperatures.

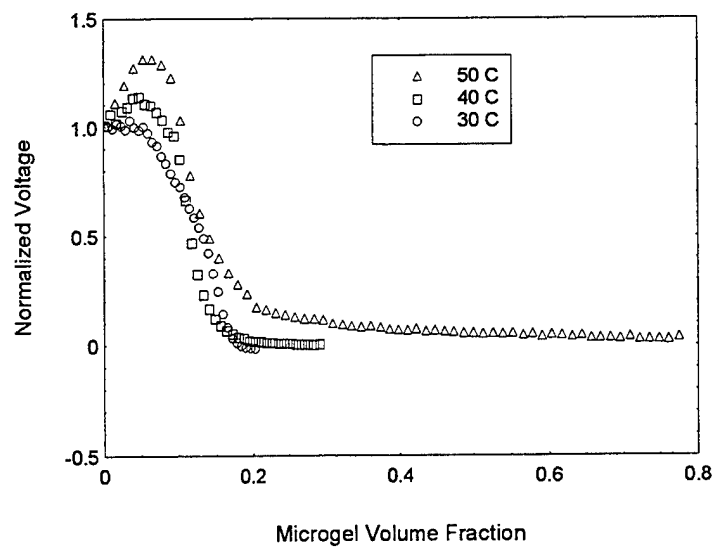


Figure E-3. Normalized DC signal vs. microgel volume fraction of Derakane 411-C-50 at different isothermal cure temperatures.

INTENTIONALLY LEFT BLANK.

Appendix F. Analyzing Diffusion in the Pregel and Postgel Stage

F.1 Pregel Stage

Diffusion is a direct result of the Brownian motion of particles (molecular or ionic species) in the system. The diffusion processes tend to have all the species uniformly distributed in the system. In the presence of an electric field, there exists another transport process as a way of migration of ionic species towards one of the two electrodes.

Einstein's relationship between the mobility of ions and the ionic diffusion coefficient is given as follows in Bockris.¹

$$\mu_i = Q_i D_i / K_B T, \quad (F.1)$$

where μ_i is the mobility of the ions, D_i is the diffusion coefficient of ions, Q_i is the charge carried by each ion, and K_B is Boltzmann's constant. If only one type of ion is considered, the ionic conductivity is given by

$$\sigma = Q_i \mu_i N_i, \quad (F.2)$$

where σ is the ionic conductivity and N is the number of ions per unit volume. Thus for the isothermal cure without any generation of ions, the ionic conductivity is proportional to the diffusion coefficient of ions.

According to the Stokes-Einstein relation,

$$D_i = K_B T / 6\pi\eta R, \quad (F.3)$$

where D_i is the diffusion coefficient of ion, η is the viscosity, and R is the radius of the particle. Combining equations F.1-F.3, one can see that the ionic conductivity is inversely proportional to the macroscopic viscosity. However in case of vinyl-ester (VE) resin systems studied in this work does not exactly fall under this relationship. But due to the universality of the application of diffusion modeling and owing to limited success of ionic conductivity modeling based on the above relationships applied to VE 411-C-50, it is worthwhile to proceed with diffusion modeling based on the above relationship.

More importantly, equation F.4 establishes a direct relationship between the size of a particle and its diffusion coefficient. Therefore, the diffusion coefficient of

¹ Bockris, J. O. M., and A. K. N. Reddy. *Modern Electrochemistry*. New York, NY: Plenum, 1970.

ions and the diffusion coefficient of the monomer may be correlated through their sizes as below:

$$D_m = D_i K_2 = K_2 \sigma / K_1, \quad (F.4)$$

where D_m is the diffusion coefficient of monomer, K_1 is given by $Q_i 2 N_i / K_B T$, and K_2 is the ratio of the size of ions to that of the monomer.

The diffusion coefficient of a particle is by definition

$$D_p = \langle \delta^2 \rangle / 6t, \quad (F.5)$$

where $\langle \delta^2 \rangle$ is the mean square displacement that the molecule as a whole undergoes over a time period, t . By evaluating the total mean-square displacement of all the monomer units in the system during the same time period, the overall diffusion coefficient, or the average diffusion coefficient of monomer unit, is given by:

$$D = D_m X_n^{-1}, \quad (F.6)$$

where X_n is the number-average degree of polymerization. Consequently, before gelation, the overall diffusion coefficient can be estimated using the following diffusion model by substituting equation F.4 into equation F.6:

$$D = K_2 \sigma X_n^{-1} / K_1. \quad (F.7)$$

F.2 Postgel Stage

Since a scaling relationship between the diffusion of the gel and the diffusion of the gel and the diffusion of free chains is not known to exist, a different model based on dipolar relaxation time has been proposed. The ionic conductivity is directly related to the mobility of the ionic species, while the dipole relaxation time is a direct indicator of the mobility of the molecular species.

The model that describes the free volume dependence of diffusivity is given by Kumins:²

$$D = D_0 \exp(-b_D v^* / v_f), \quad (F.8)$$

where v_f is the average free volume and v^* is the average close-packed-sphere volume or the critical free volume needed for a segmental jump to take place.

For the dipole relaxation time, the free volume model is given by

$$\Gamma = \Gamma_0 \exp(-b_\Gamma v / v_f), \quad (F.9)$$

² Kumins, C. A. and T. K. Kwei. *Diffusion in Polymers*. Edited by J. Crank, and G. S. Park, New York, NY: Academic Press, 1968.

where Γ is the dipole relaxation time, Γ_0 is a constant, b is a constant that includes the critical free volume for dipole relaxation, and v ($=v^* + v_f$) is the average free volume per chain segment.

Combining the equations F.8 and F.9, one ends with

$$D\Gamma^n = K_3, \quad (F.10)$$

where n ($=b_D/b_T$) is a constant independent of conversion and temperature and K_3 is a constant.

Rewriting equation F.10 yields

$$\text{Log } D = -n \text{ Log } \Gamma + \text{Log } K_3. \quad (F.11)$$

Since equation F.11 holds for even in case of pregel stage, substitution of expression of pregel D in equation F.11 yields:

$$\text{Log } (\sigma X_n^{-1}) = -n \text{ Log } \Gamma + \text{Log } K_3', \quad (F.12)$$

where K_3' ($=K_3 K_1/K_2$) depends only on the temperature. From relation F.12, one can obtain the power law index that can then be subsequently used for diffusion modeling in the postgel stage.

Thus, the overall diffusion coefficient may be determined using equation F.7 in the pregel stage and equation F.10 in the postgel stage. In principle, however, equation F.10 can be used both in the pregel and postgel stage. However, owing to the difficulty in isolating the ionic contribution from the dipolar contribution in the pregel stage, equation F.7 presents itself as a more reliable model for diffusion behavior.

INTENTIONALLY LEFT BLANK.

Appendix G. Differential Scanning Calorimeter (DSC)-Based Free Volume Modeling

G.1 Introduction

Section 6 examined free volume modeling of ionic conductivity and viscosity development during cure, based on T_g - α relationship. The degree of cure α was obtained using Fourier-transform infrared (FTIR) for the same. This appendix provides information on the development of free volume model, for degree of conversion estimated using DSC. For VE 411-C-50, the degree of conversion as obtained using DSC is different from FTIR data. This makes it necessary for explicit estimation of the Williams, Landel, and Ferry (WLF) parameters required for describing conductivity and viscosity.

G.2 Cure Kinetic Model

The cure kinetic expression corresponding to degree of conversion determined by DSC is given by:

$$d\alpha/dt = (K_1 + K_2\alpha^m)(\alpha_{\max} - \alpha)^n. \quad (G.1)$$

The autocatalytic parameters for equation 13 are presented in Table G-1.

Table G-1. T_g - α model parameters.

Temperature (K)	$0 < \alpha < \alpha_{vit}$			$\alpha_{vit} < \alpha < 1$		
	$(C_{pr})_1$	$(T_{g0})_1$	$(T_g^\infty)_1$	$(C_{pr})_2$	$(T_{g0})_2$	$(T_g^\infty)_2$
293	150	248.15	294.15	0.15	289.15	398.15
303	100	248.15	308.15	0.15	303.15	398.15
313	35	248.15	330.15	0.15	319.15	398.15

G.3 T_g - α Model

Linear relationships of the form $T_g = T_{g0} + K\alpha$ have usually been used in the literature for the T_g - α model. However in this study, the T_g - α model developed by Stone¹ would be used.

¹ Stone, M. A. "Thermo-chemical and Thermo-mechanical Response of Reacting Polymers." CCM Report No. 97-13, University of Delaware, Center for Composite Materials, Newark, DE, 1997.

Equation G.2 presents the Venditti's relationship between T_g and α :

$$\ln(T_g) = ((1 - \alpha)\ln(T_g) + (C_{pr}) \alpha \ln(T_g^{\infty})) / ((1 - \alpha) + (C_{pr}) \alpha). \quad (G.2)$$

The model parameters corresponding to the degree of conversion obtained using DSC are presented in Table G-1.¹

G.4 Conductivity Model

The WLF equation used for the modeling of ionic conductivity is given by equation G.3 and the estimated WLF constants are given in Table G-2.

$$\log(\text{Cond}_T / \text{Cond}_{T_g}) = C_1(T - T_g) / ((C_2 + C_3 T_g) + (T - T_g)), \quad (G.3)$$

and

$$\log(\text{Cond}_{T_g}) = C_4.$$

Table G-2. WLF parameters for conductivity model.

Temperature (K)	C_1	C_2	C_3	C_4
303	1.1696	9.5453	-0.026298	-7.3974
313	0.24118	8.5876	-0.020983	-6.3851

Figures G-1 and G-2 illustrate the free volume model comparison with the experimental data.

G.5 Viscosity Model

Equation G.4 gives the WLF relationship used for describing the viscosity behavior. Table G-3 gives the estimated values of the WLF constants. A value of 15 was chosen for $\log(\eta_{T_g})$ value.² Figures G-3 and G-4 illustrate the comparison of the free volume model to the experimental data.

$$\log(\eta_T / \eta_{T_g}) = C_1(T - T_g) / ((C_2 + C_3 T_g) + (T - T_g)), \quad (G.4)$$

and

$$\log(\eta_{T_g}) = C_4 = 15.$$

² Maffezzoli, A., A. Trivisano, M. Oplaicki, J. Mijovic, and J. M. Kenny. "Correlation Between Dielectric and Chemorheological Properties During Cure of Epoxy-Based Composites." *Journal of Materials Science*, vol. 29, pp. 800-808, 1994.

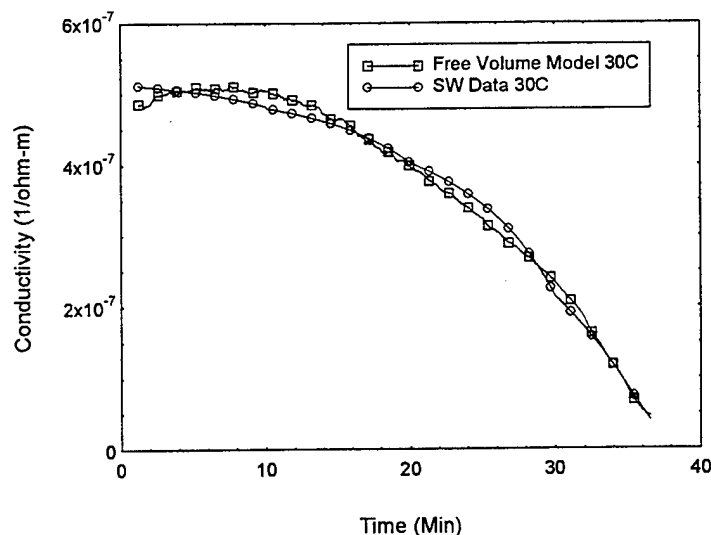


Figure G-1. SMARTweave (SW) behavior prediction using free volume theory at 30 °C.

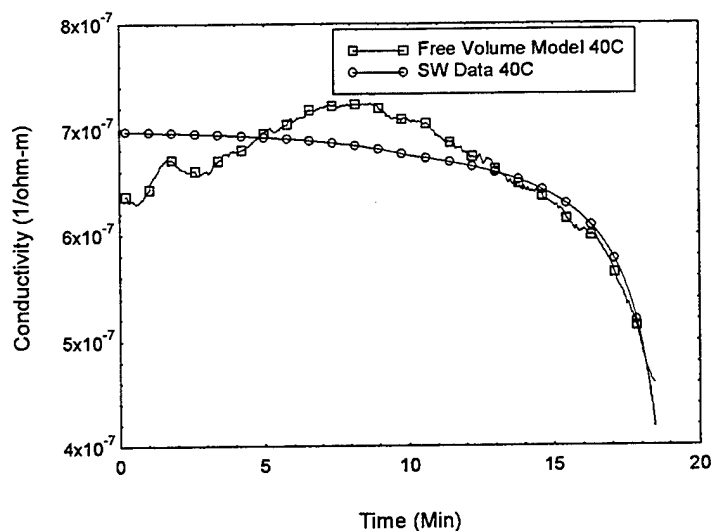


Figure G-2. SW behavior prediction using free volume theory at 40 °C.

The estimation of the WLF constants for both ionic conductivity and viscosity models, presents an elegant way of “sensing” viscosity and degree of cure using SW signal as the model input. Figure G-5 illustrates the model input and model predictions, i.e., viscosity and degree of cure. From Figure G-5, it is seen that the model input (SW signal) is used to generate the corresponding T_g data. This in turn is used to yield predictions of viscosity and degree of cure. Figures G-6 and G-7 illustrate the predictive capability of the free volume model in estimating the macroscopic viscosity using DC SW signal as the model input, while Figures G-8 and G-9 presents the degree of cure as predicted by the free volume model.

Table G-3. WLF parameters for viscosity modeling.

Temperature (K)	C_1	C_2	C_3	C_4
303	-13.505	7.2285	-0.020029	15
313	-13.347	7.5213	-0.021285	15

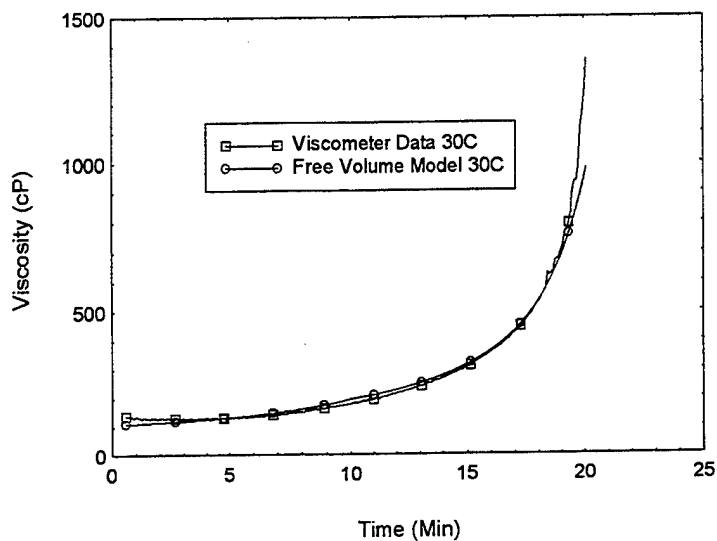


Figure G-3. Viscosity prediction using free volume theory at 30 °C.

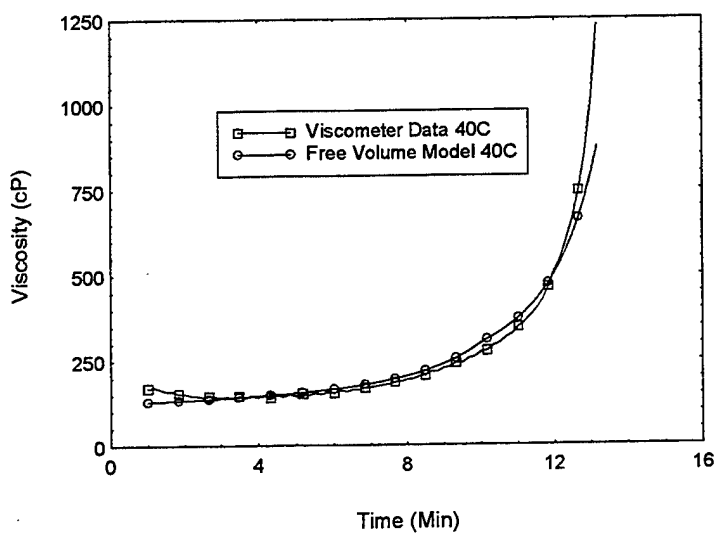


Figure G-4. Viscosity prediction using free volume theory at 40 °C.

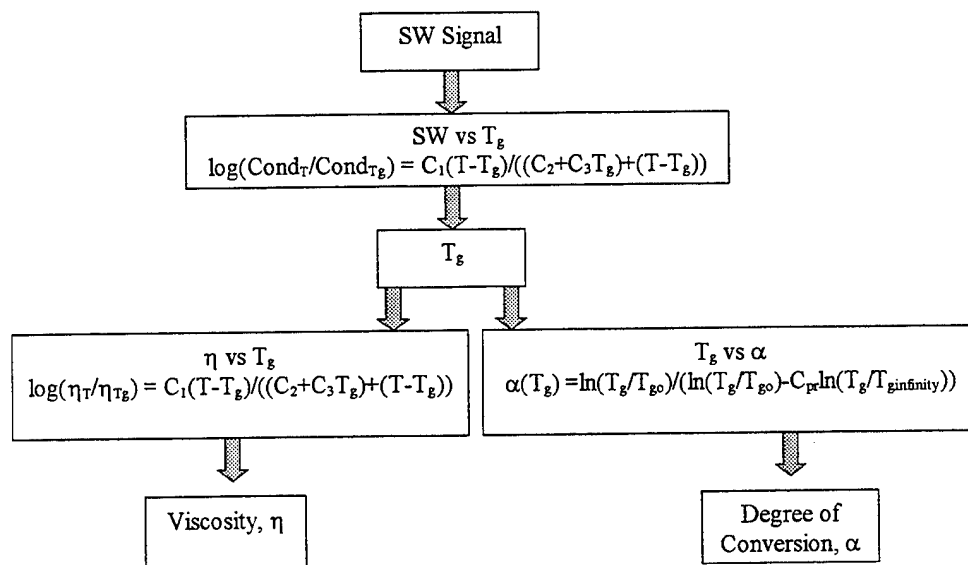


Figure G-5. Schematic of viscosity and cure sensing using SW signal as the model input.

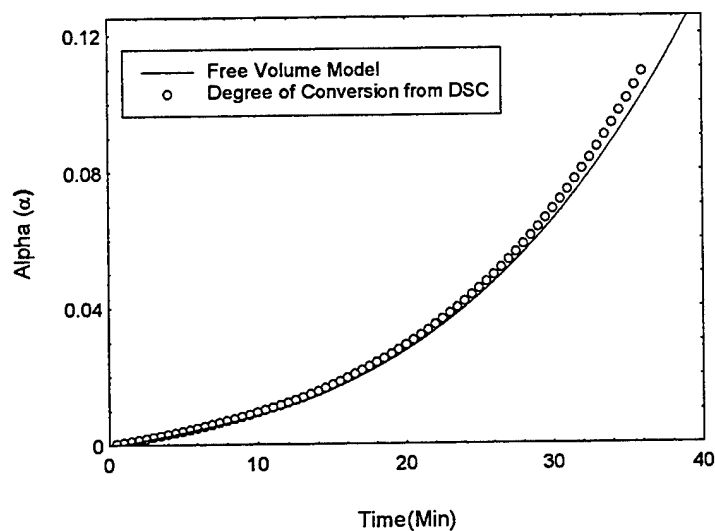


Figure G-6. Degree of cure prediction from SW data using free volume theory at 30 °C.

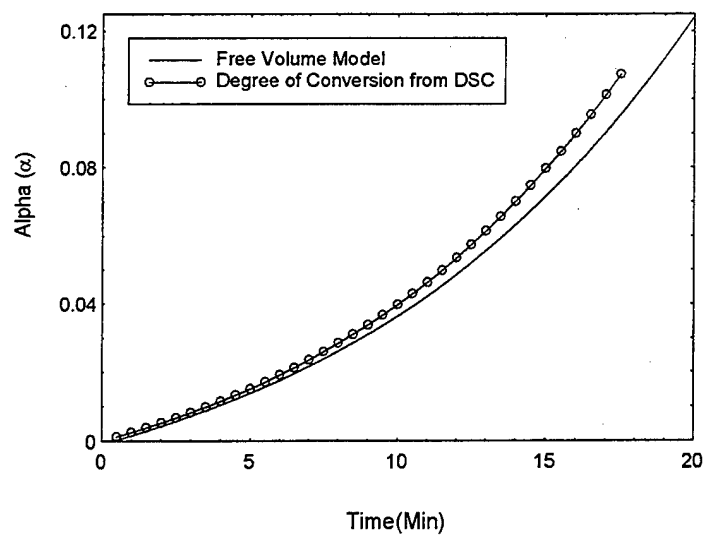


Figure G-7. Degree of cure prediction from SW data using free volume theory at 40 °C.

<u>NO. OF COPIES</u>	<u>ORGANIZATION</u>	<u>NO. OF COPIES</u>	<u>ORGANIZATION</u>
2	DEFENSE TECHNICAL INFORMATION CENTER DTIC DDA 8725 JOHN J KINGMAN RD STE 0944 FT BELVOIR VA 22060-6218	1	DIRECTOR US ARMY RESEARCH LAB AMSRL D D R SMITH 2800 POWDER MILL RD ADELPHI MD 20783-1197
1	HQDA DAMO FDT 400 ARMY PENTAGON WASHINGTON DC 20310-0460	1	DIRECTOR US ARMY RESEARCH LAB AMSRL DD 2800 POWDER MILL RD ADELPHI MD 20783-1197
1	OSD OUSD(A&T)/ODDDR&E(R) R J TREW THE PENTAGON WASHINGTON DC 20301-7100	1	DIRECTOR US ARMY RESEARCH LAB AMSRL CI AI R (RECORDS MGMT) 2800 POWDER MILL RD ADELPHI MD 20783-1145
1	DPTY CG FOR RDA US ARMY MATERIEL CMD AMCRDA 5001 EISENHOWER AVE ALEXANDRIA VA 22333-0001	3	DIRECTOR US ARMY RESEARCH LAB AMSRL CI LL 2800 POWDER MILL RD ADELPHI MD 20783-1145
1	INST FOR ADVNCD TCHNLGY THE UNIV OF TEXAS AT AUSTIN PO BOX 202797 AUSTIN TX 78720-2797	1	DIRECTOR US ARMY RESEARCH LAB AMSRL CI AP 2800 POWDER MILL RD ADELPHI MD 20783-1197
1	DARPA B KASPAR 3701 N FAIRFAX DR ARLINGTON VA 22203-1714		
1	US MILITARY ACADEMY MATH SCI CTR OF EXCELLENCE MADN MATH MAJ HUBER THAYER HALL WEST POINT NY 10996-1786		
			<u>ABERDEEN PROVING GROUND</u>
		4	DIR USARL AMSRL CI LP (BLDG 305)

<u>NO. OF COPIES</u>	<u>ORGANIZATION</u>
1	DIRECTOR US ARMY RESEARCH LAB AMSRL CP CA D SNIDER 2800 POWDER MILL RD ADELPHI MD 20783-1145
1	DIRECTOR US ARMY RESEARCH LAB AMSRL OP SD TA 2800 POWDER MILL RD ADELPHI MD 20783-1145
3	DIRECTOR US ARMY RESEARCH LAB AMSRL OP SD TL 2800 POWDER MILL RD ADELPHI MD 20783-1145
1	DIRECTOR US ARMY RESEARCH LAB AMSRL OP SD TP 2800 POWDER MILL RD ADELPHI MD 20783-1145
1	DIRECTOR DA OASARDA SARD SO 103 ARMY PENTAGON WASHINGTON DC 20310-0103
1	DPTY ASST SECY FOR R&T SARD TT THE PENTAGON RM 3EA79 WASHINGTON DC 20301-7100
1	COMMANDER US ARMY MATERIEL CMD AMXMI INT 5001 EISENHOWER AVE ALEXANDRIA VA 22333-0001
2	COMMANDER US ARMY ARDEC AMSTA AR AE WW E BAKER J PEARSON PICATINNY ARSENAL NJ 07806-5000

<u>NO. OF COPIES</u>	<u>ORGANIZATION</u>
1	COMMANDER US ARMY ARDEC AMSTA AR TD C SPINELLI PICATINNY ARSENAL NJ 07806-5000
1	COMMANDER US ARMY ARDEC AMSTA AR FSE PICATINNY ARSENAL NJ 07806-5000
6	COMMANDER US ARMY ARDEC AMSTA AR CCH A W ANDREWS S MUSALLI R CARR M LUCIANO E LOGSDEN T LOUZEIRO PICATINNY ARSENAL NJ 07806-5000
4	COMMANDER US ARMY ARDEC AMSTA AR CC G PAYNE J GEHBAUER C BAULIEU H OPAT PICATINNY ARSENAL NJ 07806-5000
1	COMMANDER US ARMY ARDEC AMSTA AR CCH P J LUTZ PICATINNY ARSENAL NJ 07806-5000
1	COMMANDER US ARMY ARDEC AMSTA AR FSF T C LIVECCHIA PICATINNY ARSENAL NJ 07806-5000

<u>NO. OF COPIES</u>	<u>ORGANIZATION</u>	<u>NO. OF COPIES</u>	<u>ORGANIZATION</u>
1	COMMANDER US ARMY ARDEC AMSTA AR QAC T C C PATEL PICATINNY ARSENAL NJ 07806-5000	9	COMMANDER US ARMY ARDEC AMSTA AR CCH B P DONADIA F DONLON P VALENTI C KNUTSON G EUSTICE S PATEL G WAGNECZ R SAYER F CHANG PICATINNY ARSENAL NJ 07806-5000
1	COMMANDER US ARMY ARDEC AMSTA AR M D DEMELLA PICATINNY ARSENAL NJ 07806-5000		
3	COMMANDER US ARMY ARDEC AMSTA AR FSA A WARNASH B MACHAK M CHIEFA PICATINNY ARSENAL NJ 07806-5000	6	COMMANDER US ARMY ARDEC AMSTA AR CCL F PUZYCKI R MCHUGH D CONWAY E JAROSZEWSKI R SCHLENNER M CLUNE PICATINNY ARSENAL NJ 07806-5000
2	COMMANDER US ARMY ARDEC AMSTA AR FSP G M SCHIKSNIS D CARLUCCI PICATINNY ARSENAL NJ 07806-5000	1	COMMANDER US ARMY ARDEC AMSTA AR SRE D YEE PICATINNY ARSENAL NJ 07806-5000
1	COMMANDER US ARMY ARDEC AMSTA AR FSP A P KISATSKY PICATINNY ARSENAL NJ 07806-5000	1	COMMANDER US ARMY ARDEC AMSTA AR WET T SACHAR BLDG 172 PICATINNY ARSENAL NJ 07806-5000
2	COMMANDER US ARMY ARDEC AMSTA AR CCH C H CHANIN S CHICO PICATINNY ARSENAL NJ 07806-5000	1	COMMANDER US ARMY ARDEC AMSTA ASF PICATINNY ARSENAL NJ 07806-5000
1	COMMANDER US ARMY ARDEC AMSTA AR QAC T D RIGOGLIOSO PICATINNY ARSENAL NJ 07806-5000		

<u>NO. OF COPIES</u>	<u>ORGANIZATION</u>
1	US ARMY ARDEC INTELLIGENCE SPECIALIST AMSTA AR WEL F M GUERRIERE PICATINNY ARSENAL NJ 07806-5000
11	PM TMAS SFAE GSSC TMA R MORRIS C KIMKER D GUZOWICZ E KOPACZ R ROESER R DARCY R MCDANOLDS L D ULISSE C ROLLER J MCGREEN B PATTEN PICATINNY ARSENAL NJ 07806-5000
2	PEO FIELD ARTILLERY SYS SFAE FAS PM H GOLDMAN T MCWILLIAMS PICATINNY ARSENAL NJ 07806-5000
1	COMMANDER US ARMY TACOM PM ABRAMS SFAE ASM AB 6501 ELEVEN MILE RD WARREN MI 48397-5000
1	COMMANDER US ARMY ARDEC PRODUCTION BASE MODERN ACTY AMSMC PBM K PICATINNY ARSENAL NJ 07806-5000
1	COMMANDER US ARMY TACOM PM BFVS SFAE ASM BV 6501 ELEVEN MILE RD WARREN MI 48397-5000

<u>NO. OF COPIES</u>	<u>ORGANIZATION</u>
6	PM SADARM SFAE GCSS SD COL B ELLIS M DEVINE R KOWALSKI W DEMASSI J PRITCHARD S HROWNACK PICATINNY ARSENAL NJ 07806-5000
3	COMMANDER US ARMY TACOM PM TACTICAL VEHICLES SFAE TVL SFAE TVM SFAE TVH 6501 ELEVEN MILE RD WARREN MI 48397-5000
1	COMMANDER US ARMY TACOM PM AFAS SFAE ASM AF 6501 ELEVEN MILE RD WARREN MI 48397-5000
1	COMMANDER US ARMY TACOM PM RDT&E SFAE GCSS W AB J GODELL 6501 ELEVEN MILE RD WARREN MI 48397-5000
1	COMMANDER US ARMY TACOM PM SURVIVABLE SYSTEMS SFAE GCSS W GSI H M RYZYI 6501 ELEVEN MILE RD WARREN MI 48397-5000
2	COMMANDER US ARMY TACOM PM SURV SYS SFAE ASM SS T DEAN SFAE GCSS W GSI M D COCHRAN 6501 ELEVEN MILE RD WARREN MI 48397-5000

<u>NO. OF COPIES</u>	<u>ORGANIZATION</u>	<u>NO. OF COPIES</u>	<u>ORGANIZATION</u>
1	COMMANDER US ARMY TACOM PM BFV SFAE GCSS W BV S DAVIS 6501 ELEVEN MILE RD WARREN MI 48397-5000	14	COMMANDER US ARMY TACOM AMSTA TR R J CHAPIN R MCCLELLAND D THOMAS J BENNETT D HANSEN AMSTA JSK S GOODMAN J FLORENCE K IYER J THOMSON AMSTA TR D D OSTBERG L HINOJOSA B RAJU AMSTA CS SF H HUTCHINSON F SCHWARZ WARREN MI 48397-5000
1	COMMANDER US ARMY TACOM PM LIGHT TACTICAL VHCLS AMSTA TR S A J MILLS MS 209 6501 ELEVEN MILE RD WARREN MI 48397-5000	1	COMMANDER WATERVLIET ARSENAL SMCWV SPM T MCCLOSKEY BLDG 253 WATERVLIET NY 12189-4050
1	COMMANDER US ARMY TACOM PM GROUND SYSTEMS INTEGRATION SFAE GCSS W GSI R LABATILLE 6501 ELEVEN MILE RD WARREN MI 48397-5000	3	ARMOR SCHOOL ATZK TD R BAUEN J BERG A POMEY FT KNOX KY 40121
1	COMMANDER US ARMY TACOM CHIEF ABRAMS TESTING SFAE GCSS W AB QT T KRASKIEWICZ 6501 ELEVEN MILE RD WARREN MI 48397-5000	10	BENET LABORATORIES AMSTA AR CCB R FISCELLA G D ANDREA M SCAVULO G SPENCER P WHEELER K MINER J VASILAKIS G FRIAR R HASENBEIN AMSTA CCB R S SOPOK WATERVLIET NY 12189-4050
1	COMMANDER US ARMY TACOM AMSTA SF WARREN MI 48397-5000		
1	COMMANDER WATERVLIET ARSENAL SMCWV QAE Q B VANINA BLDG 44 WATERVLIET NY 12189-4050		
2	TSM ABRAMS ATZK TS S JABURG W MEINSHAUSEN FT KNOX KY 40121		

<u>NO. OF COPIES</u>	<u>ORGANIZATION</u>
2	HQ IOC TANK AMMUNITION TEAM AMSIO SMT R CRAWFORD W HARRIS ROCK ISLAND IL 61299-6000
1	DIRECTOR US ARMY AMCOM SFAE AV RAM TV D CALDWELL BLDG 5300 REDSTONE ARSENAL AL 35898
2	COMMANDER US ARMY AMCOM AVIATION APPLIED TECH DIR J SCHUCK FT EUSTIS VA 23604-5577
1	US ARMY CERL R LAMPO 2902 NEWMARK DR CHAMPAIGN IL 61822
2	US ARMY CORPS OF ENGINEERS CERD C T LIU CEW ET T TAN 20 MASS AVE NW WASHINGTON DC 20314
4	DIRECTOR US ARMY CECOM NIGHT VISION & ELECTRONIC SENSORS DIR AMSEL RD NV CM CCD R ADAMS R MCLEAN A YINGST AMSEL RD NV VISP E JACOBS 10221 BURBECK RD FT BELVOIR VA 22060-5806

<u>NO. OF COPIES</u>	<u>ORGANIZATION</u>
1	US ARMY COLD REGIONS RSCH & ENGRNG LAB P DUTTA 72 LYME RD HANOVER NH 03755
1	SYSTEM MNGR ABRAMS ATZK TS LTC J H NUNN BLDG 1002 RM 110 FT KNOX KY 40121
1	CHIEF USAIC ATZB COM LTC T J CUMMINGS FT BENNING GA 31905-5800
1	USA SBCCOM PM SOLDIER SPT AMSSB PM RSS A J CONNORS KANSAS ST. NATICK, MA 01760-5057
8	DIRECTOR US ARMY NATIONAL GROUND INTELLIGENCE CTR D LEITER M HOLTUS M WOLFE S MINGLEDORF J GASTON W GSTATTENBAUER R WARNER J CRIDER 220 SEVENTH ST NE CHARLOTTESVILLE VA 22091
1	NSWC DAHLGREN DIV CODE G06 DAHLGREN VA 22448
1	NSWC TECH LIBRARY CODE 323 17320 DAHLGREN RD DAHLGREN VA 22448

<u>NO. OF COPIES</u>	<u>ORGANIZATION</u>	<u>NO. OF COPIES</u>	<u>ORGANIZATION</u>
6	US ARMY SBCCOM SOLDIER SYSTEMS CENTER BALLISTICS TEAM J WARD MARINE CORPS TEAM J MACKIEWICZ BUS AREA ADVOCACY TEAM W HASKELL SSCNC WST W NYKVIST T MERRILL S BEAUDOIN KANSAS ST NATICK MA 01760-5019	2	NSWC U SORATHIA C WILLIAMS CD 6551 9500 MACARTHUR BLVD WEST BETHESDA MD 20817
		1	DAVID TAYLOR RESEARCH CTR SHIP STRUCTURES & PROTECTION DEPT CODE 1702 BETHESDA MD 20084
		2	DAVID TAYLOR RESEARCH CTR R ROCKWELL W PHYLLAIER BETHESDA MD 20054-5000
9	US ARMY RESEARCH OFC A CROWSON J CHANDRA H EVERETT J PRATER R SINGLETON G ANDERSON D STEPP D KISEROW J CHANG PO BOX 12211 RESEARCH TRIANGLE PARK NC 27709-2211	1	OFC OF NAVAL RESEARCH D SIEGEL CODE 351 800 N QUINCY ST ARLINGTON VA 22217-5660
		8	NSWC J FRANCIS CODE G30 D WILSON CODE G32 R D COOPER CODE G32 J FRAYSSE CODE G33 E ROWE CODE G33 T DURAN CODE G33 L DE SIMONE CODE G33 R HUBBARD CODE G33 DAHLGREN VA 22448
3	NAVAL RESEARCH LAB I WOLOCK CODE 6383 R BADALIANCE CODE 6304 L GAUSE WASHINGTON DC 20375	1	NAVAL SEA SYSTEMS CMD D LIESE 2531 JEFFERSON DAVIS HWY ARLINGTON VA 22242-5160
1	NSWC CRANE DIVISION M JOHNSON CODE 20H4 LOUISVILLE KY 40214-5245	1	NSWC M LACY CODE B02 17320 DAHLGREN RD DAHLGREN VA 22448
2	COMMANDER NSWC CARDEROCK DIVISION R PETERSON CODE 2020 M CRITCHFIELD CODE 1730 BETHESDA MD 20084	1	OFC OF NAVAL RES J KELLY 800 NORTH QUINCEY ST ARLINGTON VA 22217-5000

<u>NO. OF COPIES</u>	<u>ORGANIZATION</u>	<u>NO. OF COPIES</u>	<u>ORGANIZATION</u>
2	NSWC CARDEROCK DIVISION R CRANE CODE 2802 C WILLIAMS CODE 6553 3A LEGGETT CIR BETHESDA MD 20054-5000	1	WATERWAYS EXPERIMENT D SCOTT 3909 HALLS FERRY RD SC C VICKSBURG MS 39180
1	EXPEDITIONARY WARFARE DIV N85 F SHOUP 2000 NAVY PENTAGON WASHINGTON DC 20350-2000	3	DARPA M VANFOSSSEN S WAX L CHRISTODOULOU 3701 N FAIRFAX DR ARLINGTON VA 22203-1714
1	AFRL MLBC 2941 P ST RM 136 WPAFB OH 45433-7750	2	FAA TECH CENTER D OPLINGER AAR 431 P SHYPRYKEVICH AAR 431 ATLANTIC CITY NJ 08405
1	AFRL MLSS R THOMSON 2179 12TH ST RM 122 WPAFB OH 45433-7718	2	SERDP PROGRAM OFC PM P2 C PELLERIN B SMITH 901 N STUART ST STE 303 ARLINGTON VA 22203
2	AFRL F ABRAMS J BROWN BLDG 653 2977 P ST STE 6 WPAFB OH 45433-7739	1	FAA MIL HDBK 17 CHAIR L ILCEWICZ 1601 LIND AVE SW ANM 115N RESTON VA 98055
1	AFRL MLS OL L COULTER 7278 4TH ST BLDG 100 BAY D HILL AFB UT 84056-5205	1	US DEPT OF ENERGY OFC OF ENVIRONMENTAL MANAGEMENT P RITZCOVAN 19901 GERMANTOWN RD GERMANTOWN MD 20874-1928
1	OSD JOINT CCD TEST FORCE OSD JCCD R WILLIAMS 3909 HALLS FERRY RD VICKSBURG MS 29180-6199	1	DIRECTOR LLNL F ADDESSIO MS B216 PO BOX 1633 LOS ALAMOS NM 87545
1	DEFENSE NUCLEAR AGENCY INNOVATIVE CONCEPTS DIV 6801 TELEGRAPH RD ALEXANDRIA VA 22310-3398	1	OAK RIDGE NATIONAL LABORATORY R M DAVIS PO BOX 2008 OAK RIDGE TN 37831-6195

<u>NO. OF COPIES</u>	<u>ORGANIZATION</u>	<u>NO. OF COPIES</u>	<u>ORGANIZATION</u>
5	DIRECTOR LLNL R CHRISTENSEN S DETERESA F MAGNESS M FINGER MS 313 M MURPHY L 282 PO BOX 808 LIVERMORE CA 94550	3	DIRECTOR SANDIA NATIONAL LABS APPLIED MECHANICS DEPT DIV 8241 J HANDROCK Y R KAN J LAUFFER PO BOX 969 LIVERMORE CA 94550-0096
1	OAK RIDGE NATIONAL LABORATORY C EBERLE MS 8048 PO BOX 2009 OAK RIDGE TN 37831	3	NASA LANGLEY RSCH CTR AMSRL VS W ELBER MS 266 F BARTLETT JR MS 266 G FARLEY MS 266 HAMPTON VA 23681-0001
1	OAK RIDGE NATIONAL LABORATORY C D WARREN MS 8039 PO BOX 2009 OAK RIDGE TN 37922	1	FHWA E MUNLEY 6300 GEORGETOWN PIKE MCLEAN VA 22101
7	NIST R PARNAS J DUNKERS M VANLANDINGHAM MS 8621 J CHIN MS 8621 D HUNSTON MS 8543 J MARTIN MS 8621 D DUTHINH MS 8611 100 BUREAU DR GAITHERSBURG MD 20899	1	CENTRAL INTLLGNC AGENCY OTI WDAG GT W L WALTMAN PO BOX 1925 WASHINGTON DC 20505
1	HYDROGEOLOGIC INC SERDP ESTCP SPT OFC S WALSH 1155 HERNDON PKWY STE 900 HERNDON VA 20170	1	MARINE CORPS INTLLGNC ACTVTY D KOSITZKE 3300 RUSSELL RD STE 250 QUANTICO VA 22134-5011
1	NASA LANGLEY RSCH CTR T GATES MS 188E HAMPTON VA 23661-3400	1	DIRECTOR NATIONAL GRND INTLLGNC CTR IANG TMT 220 SEVENTH ST NE CHARLOTTESVILLE VA 22902-5396
1	USDOT FEDERAL RAILRD M FATEH RDV 31 WASHINGTON DC 20590	1	DIRECTOR DEFENSE INTLLGNC AGENCY TA 5 K CRELLING WASHINGTON DC 20310

<u>NO. OF COPIES</u>	<u>ORGANIZATION</u>	<u>NO. OF COPIES</u>	<u>ORGANIZATION</u>
1	GRAPHITE MASTERS INC J WILLIS 3815 MEDFORD ST LOS ANGELES CA 90063-1900	1	SIOUX MFG B KRIEL PO BOX 400 FT TOTTEN ND 58335
1	ADVANCED GLASS FIBER YARNS T COLLINS 281 SPRING RUN LANE STE A DOWNINGTON PA 19335	2	PROTECTION MATERIALS INC M MILLER F CRILLEY 14000 NW 58 CT MIAMI LAKES FL 33014
1	COMPOSITE MATERIALS INC D SHORTT 19105 63 AVE NE PO BOX 25 ARLINGTON WA 98223	3	FOSTER MILLER J J GASSNER M ROYLANCE W ZUKAS 195 BEAR HILL RD WALTHAM MA 02354-1196
1	COMPOSITE MATERIALS INC R HOLLAND 11 JEWEL CT ORINDA CA 94563	1	ROM DEVELOPMENT CORP R O MEARA 136 SWINEBURNE ROW BRICK MARKET PLACE NEWPORT RI 02840
1	COMPOSITE MATERIALS INC C RILEY 14530 S ANSON AVE SANTA FE SPRINGS CA 90670	2	TEXTRON SYSTEMS T FOLTZ M TREASURE 201 LOWELL ST WILMINGTON MA 08870-2941
2	COMPOSIX D BLAKE L DIXON 120 O NEILL DR HEBRUN OHIO 43025	1	JPS GLASS L CARTER PO BOX 260 SLATER RD SLATER SC 29683
4	CYTEC FIBERITE R DUNNE D KOHLI M GILLIO R MAYHEW 1300 REVOLUTION ST HAVRE DE GRACE MD 21078	1	O GARA HESS & EISENHARDT M GILLESPIE 9113 LESAINTE DR FAIRFIELD OH 45014
2	SIMULA J COLTMAN R HUYETT 10016 S 51ST ST PHOENIX AZ 85044	2	MILLIKEN RSCH CORP H KUHN M MACLEOD PO BOX 1926 SPARTANBURG SC 29303

<u>NO. OF COPIES</u>	<u>ORGANIZATION</u>	<u>NO. OF COPIES</u>	<u>ORGANIZATION</u>
1	CONNEAUGHT INDUSTRIES INC J SANTOS PO BOX 1425 COVENTRY RI 02816	1	SAIC G CHRYSSOMALLIS 3800 W 80TH ST STE 1090 BLOOMINGTON MN 55431
1	PROJECTILE TECHNOLOGY INC 515 GILES ST HAVRE DE GRACE MD 21078	1	AAI CORPORATION T G STASTNY PO BOX 126 HUNT VALLEY MD 21030-0126
2	BATTELLE NATICK OPNS J CONNORS B HALPIN 209 W CENTRAL ST STE 302 NATICK MA 01760	1	APPLIED COMPOSITES W GRISCH 333 NORTH SIXTH ST ST CHARLES IL 60174
1	ARMTEC DEFENSE PRODUCTS S DYER 85 901 AVE 53 PO BOX 848 COACHELLA CA 92236	3	ALLIANT TECHSYSTEMS INC J CONDON E LYNAM J GERHARD WV01 16 STATE RT 956 PO BOX 210 ROCKET CENTER WV 26726-0210
1	GLCC INC J RAY 103 TRADE ZONE DR STE 26C WEST COLUMBIA SC 29170	1	CUSTOM ANALYTICAL ENG SYS INC A ALEXANDER 13000 TENSOR LANE NE FLINTSTONE MD 21530
3	PACIFIC NORTHWEST LAB M SMITH G VAN ARSDALE R SHIPPELL PO BOX 999 RICHLAND WA 99352	1	OFC DEPUTY UNDER SEC DEFNS J THOMPSON 1745 JEFFERSON DAVIS HWY CRYSTAL SQ 4 STE 501ARLINGTON VA 22202
2	AMOCO PERFORMANCE PRODUCTS M MICHNO JR J BANISAUUKAS 4500 MCGINNIS FERRY RD ALPHARETTA GA 30202-3944	1	LORAL VOUGHT SYSTEMS K COOK 1701 W MARSHALL DR GRAND PRAIRIE TX 75051
1	SAIC M PALMER 1410 SPRING HILL RD STE 400 MS SH4 5 MCLEAN VA 22102	1	GKN AEROSPACE D OLDS 15 STERLING DR WALLINGFORD CT 06492

<u>NO. OF COPIES</u>	<u>ORGANIZATION</u>	<u>NO. OF COPIES</u>	<u>ORGANIZATION</u>
8	ALLIANT TECHSYSTEMS INC C CANDLAND MN11 2830 C AAKHUS MN11 2830 B SEE MN11 2439 N VLAHAKUS MN11 2145 R DOHRN MN11 2830 S HAGLUND MN11 2439 M HISSONG MN11 2830 D KAMDAR MN11 2830 600 SECOND ST NE HOPKINS MN 55343-8367	1	OLIN CORPORATION L WHITMORE 10101 NINTH ST NORTH ST PETERSBURG FL 33702
3	HEXCEL INC R BOE F POLICELLI J POESCH PO BOX 98 MAGNA UT 84044	5	SIKORSKY AIRCRAFT G JACARUSO T CARSTENSAN B KAY S GARBO MS S330A J ADELMANN 6900 MAIN ST PO BOX 9729 STRATFORD CT 06497-9729
5	AEROJET GEN CORP D PILLASCH T COULTER C FLYNN D RUBAREZUL M GREINER 1100 WEST HOLLYVALE ST AZUSA CA 91702-0296	1	PRATT & WHITNEY C WATSON 400 MAIN ST MS 114 37 EAST HARTFORD CT 06108
1	HERCULES INC HERCULES PLAZA WILMINGTON DE 19894	1	AEROSPACE CORP G HAWKINS M4 945 2350 E EL SEGUNDO BLVD EL SEGUNDO CA 90245
1	BRIGS COMPANY J BACKOFEN 2668 PETERBOROUGH ST HERNDON VA 22071-2443	2	CYTEC FIBERITE M LIN W WEB 1440 N KRAEMER BLVD ANAHEIM CA 92806
1	ZERNOW TECHNICAL SERVICES L ZERNOW 425 W BONITA AVE STE 208 SAN DIMAS CA 91773	1	HEXCEL T BITZER 11711 DUBLIN BLVD DUBLIN CA 94568
2	OLIN CORPORATION FLINCHBAUGH DIV E STEINER B STEWART PO BOX 127 RED LION PA 17356	1	BOEING R BOHLMANN PO BOX 516 MC 5021322 ST LOUIS MO 63166-0516
		2	BOEING DFNSE & SPACE GP W HAMMOND S 4X55 J RUSSELL S 4X55 PO BOX 3707 SEATTLE WA 98124-2207
		2	BOEING ROTORCRAFT P MINGURT P HANDEL 800 B PUTNAM BLVD WALLINGFORD PA 19086

<u>NO. OF COPIES</u>	<u>ORGANIZATION</u>
1	BOEING DOUGLAS PRODUCTS DIV L J HART SMITH 3855 LAKEWOOD BLVD D800 0019 LONG BEACH CA 90846-0001
1	LOCKHEED MARTIN S REEVE 8650 COBB DR D 73 62 MZ 0648 MARIETTA GA 30063-0648
1	LOCKHEED MARTIN SKUNK WORKS D FORTNEY 1011 LOCKHEED WAY PALMDALE CA 93599-2502
1	LOCKHEED MARTIN R FIELDS 1195 IRWIN CT WINTER SPRINGS FL 32708
1	MATERIALS SCIENCES CORP B W ROSEN 500 OFC CENTER DR STE 250 FT WASHINGTON PA 19034
1	NORTHROP GRUMMAN CORP ELECTRONIC SENSORS & SYSTEMS DIV E SCHOCH MS V 16 1745A W NURSERY RD LINTHICUM MD 21090
2	NORTHROP GRUMMAN ENVIRONMENTAL PROGRAMS R OSTERMAN A YEN 8900 E WASHINGTON BLVD PICO RIVERA CA 90660
1	UDLP D MARTIN PO BOX 359 SANTA CLARA CA 95052

<u>NO. OF COPIES</u>	<u>ORGANIZATION</u>
1	UDLP G THOMAS PO BOX 58123 SANTA CLARA CA 95052
2	UDLP R BARRETT MAIL DROP M53 V HORVATICH MAIL DROP M53 328 W BROKAW RD SANTA CLARA CA 95052-0359
4	UDLP R BRYNSVOLD P JANKE MS 170 4800 EAST RIVER RD MINNEAPOLIS MN 55421-1498
3	UDLP GROUND SYSTEMS DIV M PEDRAZZI MAIL DROP N09 A LEE MAIL DROP N11 M MACLEAN MAIL DROP N06 1205 COLEMAN AVE SANTA CLARA CA 95052
1	GDLS DIVISION D BARTLE PO BOX 1901 WARREN MI 48090
2	GDLS D REES M PASIK PO BOX 2074 WARREN MI 48090-2074
1	GDLS MUSKEGON OPERATIONS W SOMMERS JR 76 GETTY ST MUSKEGON MI 49442
1	IIT RESEARCH CENTER D ROSE 201 MILL ST ROME NY 13440-6916

<u>NO. OF COPIES</u>	<u>ORGANIZATION</u>	<u>NO. OF COPIES</u>	<u>ORGANIZATION</u>
1	GENERAL DYNAMICS AMPHIBIOUS SYS SURVIVABILITY LEAD G WALKER 991 ANNAPOLIS WAY WOODBIDGE VA 22191	1	GA TECH RSCH INST GA INST OF TCHNLGY P FRIEDERICH ATLANTA GA 30392
6	INST FOR ADVANCED TECH H FAIR I MCNAB P SULLIVAN S BLESS W REINECKE C PERSAD 3925 W BRAKER LN STE 400 AUSTIN TX 78759-5316	1	MICHIGAN ST UNIV MSM DEPT R AVERILL 3515 EB EAST LANSING MI 48824-1226
2	CIVIL ENGRRSCH FOUNDATION PRESIDENT H BERNSTEIN R BELLE 1015 15TH ST NW STE 600 WASHINGTON DC 20005	1	UNIV OF KENTUCKY L PENN 763 ANDERSON HALL LEXINGTON KY 40506-0046
1	ARROW TECH ASSO 1233 SHELBURNE RD STE D 8 SOUTH BURLINGTON VT 05403-7700	1	UNIV OF WYOMING D ADAMS PO BOX 3295 LARAMIE WY 82071
1	R EICHELBERGER CONSULTANT 409 W CATHERINE ST BEL AIR MD 21014-3613	1	UNIV OF UTAH DEPT OF MECH & INDUSTRIAL ENGR S SWANSON SALT LAKE CITY UT 84112
1	UCLA MANE DEPT ENGRIV H T HAHN LOS ANGELES CA 90024-1597	2	PENN STATE UNIV R MCNITT C BAKIS 212 EARTH ENGR SCIENCES BLDG UNIVERSITY PARK PA 16802
2	UNIV OF DAYTON RESEARCH INST R Y KIM A K ROY 300 COLLEGE PARK AVE DAYTON OH 45469-0168	1	PENN STATE UNIV R S ENGEL 245 HAMMOND BLDG UNIVERSITY PARK PA 16801
1	MIT P LAGACE 77 MASS AVE CAMBRIDGE MA 01887	1	PURDUE UNIV SCHOOL OF AERO & ASTRO C T SUN W LAFAYETTE IN 47907-1282
		1	STANFORD UNIV DEPT OF AERONAUTICS & AEROBALLISTICS S TSAI DURANT BLDG STANFORD CA 94305

<u>NO. OF COPIES</u>	<u>ORGANIZATION</u>	<u>NO. OF COPIES</u>	<u>ORGANIZATION</u>
1	UNIV OF DAYTON J M WHITNEY COLLEGE PARK AVE DAYTON OH 45469-0240	1	UNIV OF MARYLAND DEPT OF AEROSPACE ENGNRNG A J VIZZINI COLLEGE PARK MD 20742
7	UNIV OF DELAWARE CTR FOR COMPOSITE MTRLs J GILLESPIE M SANTARE G PALMESE S YARLAGADDA S ADVANI D HEIDER D KUKICH 201 SPENCER LABORATORY NEWARK DE 19716	1	DREXEL UNIV A S D WANG 32ND & CHESTNUT ST PHILADELPHIA PA 19104
1	DEPT OF MATERIALS SCIENCE & ENGINEERING UNIVERSITY OF ILLINOIS AT URBANA CHAMPAIGN J ECONOMY 1304 WEST GREEN ST URBANA IL 61801	1	SOUTHWEST RSCH INST ENGR & MATL SCIENCES DIV J RIEGEL 6220 CULEBRA RD PO DRAWER 28510 SAN ANTONIO TX 78228-0510
1	NORTH CAROLINA STATE UNIV CIVIL ENGINEERING DEPT W RASDORF PO BOX 7908 RALEIGH NC 27696-7908	<u>ABERDEEN PROVING GROUND</u>	
3	THE UNIV OF TEXAS AT AUSTIN CTR FOR ELECTROMECHANICS J PRICE A WALLS J KITZMILLER 10100 BURNET RD AUSTIN TX 78758-4497	1	US ARMY MATERIEL SYSTEMS ANALYSIS P DIETZ 392 HOPKINS RD AMXSY TD APG MD 21005-5071
3	VA POLYTECHNICAL INST & STATE UNIV DEPT OF ESM M W HYER K REIFSNIDER R JONES BLACKSBURG VA 24061-0219	1	DIRECTOR US ARMY RESEARCH LAB AMSRL OP AP L APG MD 21005-5066
		106	DIR USARL AMSRL CI AMSRL CI H W STUREK AMSRL CI S A MARK AMSRL CS IO FI M ADAMSON AMSRL SL B J SMITH AMSRL SL BA AMSRL SL BL D BELY R HENRY AMSRL SL BG AMSRL SL I AMSRL WM B A HORST E SCHMIDT

NO. OF
COPIES ORGANIZATION

ABERDEEN PROVING GROUND (CONT)

AMSRL WM BA
F BRANDON
AMSRL WM BC
P PLOSTINS
D LYON
J NEWILL
S WILKERSON
A ZIELINSKI
AMSRL WM BD
B FORCH
R FIFER
R PESCE RODRIGUEZ
B RICE
AMSRL WM BE
C LEVERITT
D KOOKER
AMSRL WM BR
C SHOEMAKER
J BORNSTEIN
AMSRL WM M
D VIECHNICKI
G HAGNAUER
J MCCAULEY
B TANNER
AMSRL WM MA
R SHUFORD
P TOUCHET
N BECK TAN
AMSRL WM MA
D FLANAGAN
L GHIORSE
D HARRIS
S MCKNIGHT
P MOY
P PATTERSON
G RODRIGUEZ
A TEETS
R YIN
AMSRL WM MB
B FINK
J BENDER
T BLANAS
T BOGETTI
R BOSSOLI
L BURTON
K BOYD
S CORNELISON
P DEHMER
R DOOLEY
W DRYSDALE
G GAZONAS
S GHIORSE

NO. OF
COPIES ORGANIZATION

ABERDEEN PROVING GROUND (CONT)

D GRANVILLE
D HOPKINS
C HOPPEL
D HENRY
R KASTE
M KLUSEWITZ
M LEADORE
R LIEB
E RIGAS
J SANDS
D SPAGNUOLO
W SPURGEON
J TZENG
E WETZEL
AMSRL WM MB ALC
A FRYDMAN
AMRSL WM MC
J BEATTY
E CHIN
J MONTGOMERY
A WERECZCAK
J LASALVIA
J WELLS
AMSRL WM MD
W ROY
S WALSH
AMSRL WM T
B BURNS
AMSRL WM TA
W GILLICH
T HAVEL
J RUNYEON
M BURKINS
E HORWATH
B GOOCH
W BRUCHEY
AMSRL WM TC
R COATES
AMSRL WM TD
A DAS GUPTA
T HADUCH
T MOYNIHAN
F GREGORY
A RAJENDRAN
M RAFTENBERG
M BOTELER
T WEERASOORIYA
D DANDEKAR
A DIETRICH
AMSRL WM TE
A NIILER
J POWELL

NO. OF
COPIES ORGANIZATION

ABERDEEN PROVING GROUND (CONT)

AMSRL SS SD
H WALLACE
AMSRL SS SE R
R CHASE
AMSRL SS SE DS
R REYZER
R ATKINSON
AMSRL SE L
R WEINRAUB
J DESMOND
D WOODBURY

<u>NO. OF COPIES</u>	<u>ORGANIZATION</u>	<u>NO. OF COPIES</u>	<u>ORGANIZATION</u>
1	LTD R MARTIN MERL TAMWORTH RD HERTFORD SG13 7DG UK	1	SWISS FEDERAL ARMAMENTS WKS W LANZ ALLMENDSTRASSE 86 3602 THUN SWITZERLAND
1	SMC SCOTLAND P W LAY DERA ROSYTH ROSYTH ROYAL DOCKYARD DUNFERMLINE FIFE KY 11 2XR UK	1	ISRAEL INST OF TECHNOLOGY S BODNER FACULTY OF MECHANICAL ENGR HAIFA 3200 ISRAEL
1	CIVIL AVIATION ADMINSTRATION T GOTTESMAN PO BOX 8 BEN GURION INTERNL AIRPORT LOD 70150 ISRAEL	1	DSTO MATERIALS RESEARCH LAB NAVAL PLATFORM VULNERABILITY SHIP STRUCTURES & MTRLS DIV N BURMAN PO BOX 50 ASCOT VALE VICTORIA AUSTRALIA 3032
1	AEROSPATIALE S ANDRE A BTE CC RTE MD132 316 ROUTE DE BAYONNE TOULOUSE 31060 FRANCE	1	ECOLE ROYAL MILITAIRE E CELENS AVE DE LA RENAISSANCE 30 1040 BRUXELLE BELGIQUE
3	DRA FORT HALSTEAD P N JONES M HINTON SEVEN OAKS KENT TN 147BP UK	1	DEF RES ESTABLISHMENT VALCARTIER A DUPUIS 2459 BOULEVARD PIE XI NORTH VALCARTIER QUEBEC CANADA PO BOX 8800 COURCELETTE GOA IRO QUEBEC CANADA
1	DEFENSE RESEARCH ESTAB VALCARTIER F LESAGE COURCELETTE QUEBEC COA IRO CANADA		
2	ROYAL MILITARY COLLEGE OF SCIENCE SHRIVENHAM D BULMAN B LAWTON SWINDON WILTS SN6 8LA UK	1	ECOLE POLYTECH J MANSON DMX LTC CH 1015 LAUSANNE SWITZERLAND

<u>NO. OF COPIES</u>	<u>ORGANIZATION</u>	<u>NO. OF COPIES</u>	<u>ORGANIZATION</u>
1	INSTITUT FRANCO ALLEMAND DE RECHERCHES DE SAINT LOUIS DE M GIRAUD 5 RUE DU GENERAL CASSAGNOU BOITE POSTALE 34 F 68301 SAINT LOUIS CEDEX FRANCE	1	TNO DEFENSE RESEARCH I H PASMAN POSTBUS 6006 2600 JA DELFT THE NETHERLANDS
1	TNO PRINS MAURITS LABORATORY R IJSSELSTEIN LANGE KLEIWEG 137 PO BOX 45 2280 AA RIJSWIJK THE NETHERLANDS	1	B HIRSCH TACHKEMONY ST 6 NETAMUA 42611 ISRAEL
2	FOA NATL DEFENSE RESEARCH ESTAB DIR DEPT OF WEAPONS & PROTECTION B JANZON R HOLMLIN S 172 90 STOCKHOLM SWEDEN	1	DEUTSCHE AEROSPACE AG DYNAMICS SYSTEMS M HELD PO BOX 1340 D 86523 SCHROBENHAUSEN GERMANY
2	DEFENSE TECH & PROC AGENCY GROUND I CREWTHERR GENERAL HERZOG HAUS 3602 THUN SWITZERLAND		
1	MINISTRY OF DEFENCE RAFAEL ARMAMENT DEVELOPMENT AUTH M MAYSELESS PO BOX 2250 HAIFA 31021 ISRAEL		
1	DYNAMEC RESEARCH AB AKE PERSSON BOX 201 SE 151 23 SODERTALJE SWEDEN		

INTENTIONALLY LEFT BLANK.

REPORT DOCUMENTATION PAGE			Form Approved OMB No. 0704-0188	
Public reporting burden for this collection of information is estimated to average 1 hour per response, including the time for reviewing instructions, searching existing data sources, gathering and maintaining the data needed, and completing and reviewing the collection of information. Send comments regarding this burden estimate or any other aspect of this collection of information, including suggestions for reducing this burden, to Washington Headquarters Services, Directorate for Information Operations and Reports, 1215 Jefferson Davis Highway, Suite 1204, Arlington, VA 22202-4302, and to the Office of Management and Budget, Paperwork Reduction Project (0704-0188), Washington, DC 20503.				
1. AGENCY USE ONLY (Leave blank)		2. REPORT DATE March 2001		3. REPORT TYPE AND DATES COVERED Final, May 1997-May 2000
4. TITLE AND SUBTITLE Vinyl-Ester (VE) Cure Characterization Via Direct Current Sensors			5. FUNDING NUMBERS AH42	
6. AUTHOR(S) Bruce K. Fink, Mahendra B. Dorairaj,* and John W. Gillespie, Jr.*				
7. PERFORMING ORGANIZATION NAME(S) AND ADDRESS(ES) U.S. Army Research Laboratory ATTN: AMSRL-WM-MB Aberdeen Proving Ground, MD 21005-5069			8. PERFORMING ORGANIZATION REPORT NUMBER ARL-TR-2441	
9. SPONSORING/MONITORING AGENCY NAME(S) AND ADDRESS(ES)			10. SPONSORING/MONITORING AGENCY REPORT NUMBER	
11. SUPPLEMENTARY NOTES *University of Delaware, Center for Composite Materials, Newark, DE 19716				
12a. DISTRIBUTION/AVAILABILITY STATEMENT Approved for public release; distribution is unlimited.			12b. DISTRIBUTION CODE	
13. ABSTRACT (Maximum 200 words) High-performance thermosetting composites typically consist of a high-modulus fibrous material embedded in a thermosetting polymer matrix. The behavior of the resulting composite depends on the properties of the reinforcement, the interphase, and the matrix. Vinyl-ester (VE) resins are relatively low-cost matrix resins used in liquid molding of large structures such as contiguous vehicle hulls. In liquid-molding processes, quality-control sensors can ensure resin impregnation of the preform and cure of the resin after infiltration. For these purposes, SMARTweave (SW), based on direct current (DC) sensing, is used as an in-situ flow-front detection and cure-monitoring system. SW measures change in the ionic conductivity with cure, which can then be related to the material properties like viscosity and degree of cure. This enables in-situ measurement of degree of cure and viscosity development during cure from SW measurements. This report builds on previous modeling work that assumed a direct dependence of DC resistance on the resin viscosity, limiting the use of such models beyond gelation. This report presents a continuum model based on free volume theory to describe ionic conductivity through gelation to vitrification.				
14. SUBJECT TERMS composite material, vinyl ester, SMARTweave, cure kinetics			15. NUMBER OF PAGES 145	
			16. PRICE CODE	
17. SECURITY CLASSIFICATION OF REPORT UNCLASSIFIED	18. SECURITY CLASSIFICATION OF THIS PAGE UNCLASSIFIED	19. SECURITY CLASSIFICATION OF ABSTRACT UNCLASSIFIED	20. LIMITATION OF ABSTRACT UL	

INTENTIONALLY LEFT BLANK.

USER EVALUATION SHEET/CHANGE OF ADDRESS

This Laboratory undertakes a continuing effort to improve the quality of the reports it publishes. Your comments/answers to the items/questions below will aid us in our efforts.

1. ARL Report Number/Author ARL-TR-2441 (Fink) Date of Report March 2001
2. Date Report Received _____
3. Does this report satisfy a need? (Comment on purpose, related project, or other area of interest for which the report will be used.) _____

4. Specifically, how is the report being used? (Information source, design data, procedure, source of ideas, etc.) _____

5. Has the information in this report led to any quantitative savings as far as man-hours or dollars saved, operating costs avoided, or efficiencies achieved, etc? If so, please elaborate. _____

6. General Comments. What do you think should be changed to improve future reports? (Indicate changes to organization, technical content, format, etc.) _____

CURRENT
ADDRESS

Organization

Name

E-mail Name

Street or P.O. Box No.

City, State, Zip Code

7. If indicating a Change of Address or Address Correction, please provide the Current or Correct address above and the Old or Incorrect address below.

OLD
ADDRESS

Organization

Name

Street or P.O. Box No.

City, State, Zip Code

(Remove this sheet, fold as indicated, tape closed, and mail.)
(DO NOT STAPLE)

DEPARTMENT OF THE ARMY

OFFICIAL BUSINESS

BUSINESS REPLY MAIL

FIRST CLASS PERMIT NO 0001,APG,MD

POSTAGE WILL BE PAID BY ADDRESSEE

DIRECTOR
US ARMY RESEARCH LABORATORY
ATTN AMSRL WM MB
ABERDEEN PROVING GROUND MD 21005-5069

NO POSTAGE
NECESSARY
IF MAILED
IN THE
UNITED STATES